Daniela Eletto

UNIVERSITÀ DI SALERNO
DIPARTIMENTO DI SCIENZE FARMACEUTICHE E BIOMEDICHE

Dottorato di Ricerca in Scienze Farmaceutiche
X-Ciclo NS
2008-2011

Study of bio-molecular interactions: a) Mapping of the interaction between STAT1 and flavonoids b) Role of PDIA6-BiP complex in the regulation of the unfolded protein response

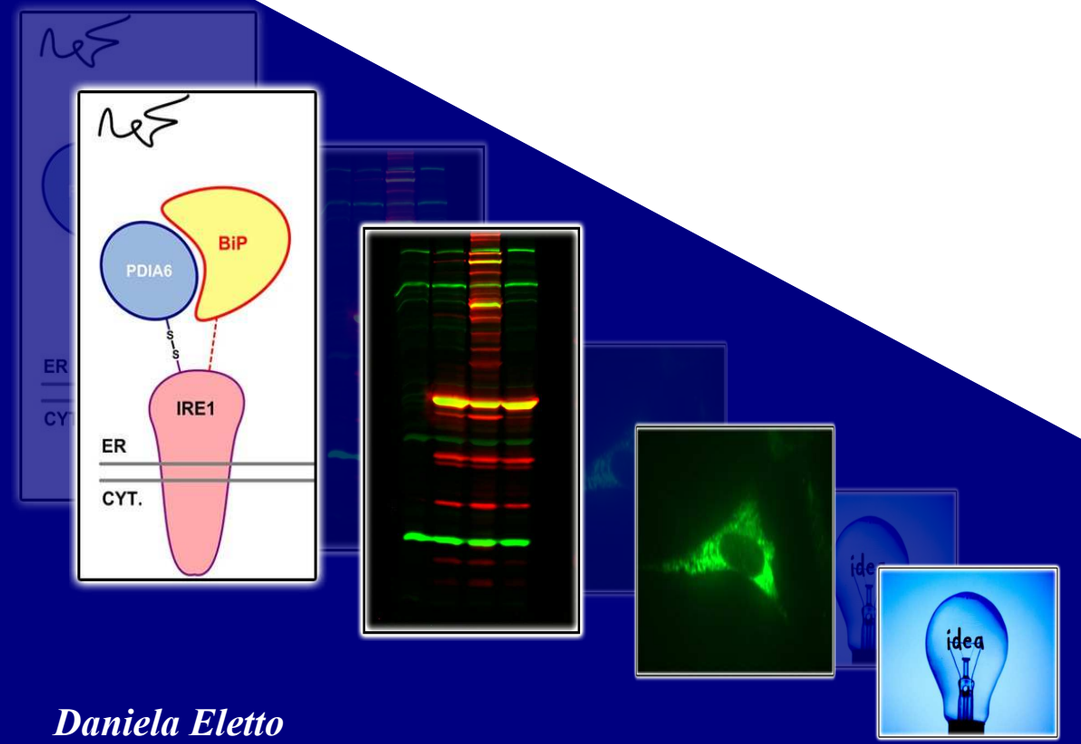

Dipartimento di Scienze Farmaceutiche e Biomediche
Via Ponte Don Melillo 84084
Fisciano, Salerno

Study of bio-molecular interactions

Daniela Eletto

UNIVERSITÀ DEGLI STUDI DI SALERNO

DIPARTIMENTO DI SCIENZE FARMACEUTICHE E BIOMEDICHE

Dottorato di Ricerca in Scienze Farmaceutiche

X-CICLO NUOVA SERIE

2008-2011

Study of bio-molecular interactions: a) Mapping of the interaction between STAT1 and flavonoids b) Role of PDIA6-BiP complex in the regulation of the unfolded protein response

Tutor
Prof. Cosimo Pizza

PhD Student
Daniela Eletto

Coordinator
Prof.ssa Nunziatina De Tommasi

I was thinking about the good old times
And all the people who helped me survive
Now who the hell knows where I'd be
Without the branches of my family tree

I was thinking about the friends who cared
And all the times that we shared
And if I had the strength to be what I could be
Love and respect to the branches of my tree

Don't forget your roots

Table of Contents

b) PDIA6-BiP complex: role in the regulation of the unfolded protein response

Abstracts

a) Mapping of the interaction between STAT1 and flavonoids

An experimental approach is described, in the first part of this Ph.D. work, for determining protein-small molecule non-covalent ligand binding sites and protein conformational changes induced by ligand binding. The methodology utilizes a combination of multiple technical approaches: limited proteolysis, MALDI TOF MS, circular dichroism and Surface Plasmon Resonance (SPR) to determine the binding sites in signal transducer and activator of transcription 1, STAT1 (87kDa)-flavonoid (Epigallocatechin-3-gallate, Myricetin and Delphinidin, about 500 Da) non-covalent complex. Comparing relative ion abundances of peptides released from the limited proteolysis of STAT1 and the STAT1-flavonoid complex after 0, 5, 15 and 30 minutes of digestion revealed that the binding of flavonoid induced a significant change in surface topology of STAT1. An increase in ion abundance and a different peptide profile suggest that the flavonoids obstruct the access of the proteases to one or both termini of specific peptides, identifying flavonoids binding region. Taken together, MALDI MS and SPR data led us to assume that the binding sites are close to Tyrosine 701 and that the flavonoids probably act disturbing the phosphorylation of TYR701 and the following dimerization and activation of STAT1.

b) PDIA6-BiP complex: role in the regulation of the unfolded protein response

The unfolded proteins response (UPR) induced in many experimental settings is an extremely strong response that usually leads to cell death rather than to restoration of the ER homeostasis. Because the outcome of UPR signaling determines cell fate, a key unresolved molecular question is how UPR signaling is attenuated. Indeed, it is often under-appreciated that UPR signaling in response to stress is transient and is attenuated. Recently it has been proved that yeast UPR matches its output to the magnitude of the stress by regulating the duration of IRE1 signaling. An ER protein, knows as binding immunoglobulin protein (BiP), binding to UPR sensors regulates their deactivation. Our idea, described in the second part of this Ph.D. work, is that there is another luminal ER factor, which interacts with the UPR sensors and is involved in attenuation of their activities. This factor is protein disulphide isomerase 6, PDIA6 (also known as P5), a poorly understood member of the protein disulfide isomerase (PDI) family, whose absence, according to our data, confers hypersensitivity to ER stress because one of its main action is tied to the sensing of UPR, rather than to the consequences of UPR signaling. We thought that PDIA6 uses its protein disulfide isomerase activity to interact specifically with UPR sensors in the ER lumen and attenuate their activities, thus regulating the duration of ER stress signaling.

MAPPING OF THE INTERACTION BETWEEN STAT1 AND FLAVONOIDS

INTRODUCTION

-CHAPTER 1-

Probing of non-covalent interactions: from Mass Spectrometry to Surface Plasmon Resonance

Non-covalent ProteinLigand Complexes:

1.1 Limited Proteolysis
1.2 Circular Dichroism
1.3 Surface Plasmon Resonance

1.1 Limited Proteolysis/Mass Spectrometry

In the last two decades, chemical strategy coupled with mass spectrometry has emerged as a powerful approach in structural proteomics research [1]. The availability of chemical strategies, in combination with sensitive and accurate mass spectrometric techniques have allowed the exploration of protein structure, protein conformational dynamics and the determination of protein-protein or protein-ligand interactions in solution.

Understanding where small molecules bind to proteins and how the binding affects the protein structure is the key to the development of high affinity ligands for the purpose of immunoassay detection technologies or drug discovery. Non-covalent complexes formed between biomolecules such as proteins, small molecules, DNA, RNA, and metal ions play a central role in many important biochemical processes such as gene transcription, cell signaling, and ion transport. Knowing molecular dynamics and the structural aspects of non-covalent interactions is also at the heart of drug design where therapeutic molecules work by blocking or modifying the biological function of proteins, DNA or RNA.

Experimental approach to study biologically relevant non-covalent complexes includes different steps:

1) screening and identifying components of a complex,
2) measuring consequences of complex formation on secondary, tertiary, or quaternary structure.
3) mapping the interaction interface

During the last two decades, electrospray ionization (ESI) and matrix assisted laser desorption ionization (MALDI) mass spectrometry (MS) have become viable techniques for measuring the three aforementioned aspects of non-covalently bound macromolecular complexes.

Limited proteolysis coupled to MS has been shown to provide important structural information of solution-phase non-covalent interactions, albeit low resolution, by determining structural intermediates in protein folding studies [2-3] and mapping interfaces in protein-protein [4-5] and protein-DNA complexes [6]. Limited proteolysis relies on the ability of a protein to interact with the structural motif surrounding a protease's active site [7], i.e., a protease cannot cleave a protein if a cleavable site is protected by a protein's tertiary structure or by complex formation with another molecule. For example, Cohen et al. utilized limited proteolysis and MALDI MS to determine the interaction interface between the transcription factor Max and a Max-specific DNA sequence. Using peptide maps generated with MALDI MS, they observed a significant decrease in proteolysis rates and changes in proteolysis patterns in the Max-DNA complex relative to Max alone. The difference in peptide maps and digestion rates were used to infer the interfacial region of the complex and to suggest protein conformational changes.

In this Ph.D. work, we demonstrated the use of multiple approaches, time resolved limited proteolysis, MALDI MS, Surface Plasmon Resonance, to determine interacting region of the non-covalently bound STAT1-flavonoids complex.

1.1.1 Limited Proteolysis

The general principle behind this strategy is that solvent-exposed residues undergo chemical modification more quickly than non-exposed residues (Figure 1). When a target protein is digested in the presence and absence of a ligand, mass differences found by Mass Spectrometry (MS) analysis will help to determine the residues involved in the contacting sites. Typically, spatial resolution is achieved by proteolytically digesting the protein of interest in presence or absence of ligand and analyzing the resulting fragments by MS. Comparing the peptide maps can reveal areas in the protein of increased and decreased solvent exposure. Implicit in these data are details regarding protein-ligand interfaces and also regions which undergo conformational change in response to ligand.

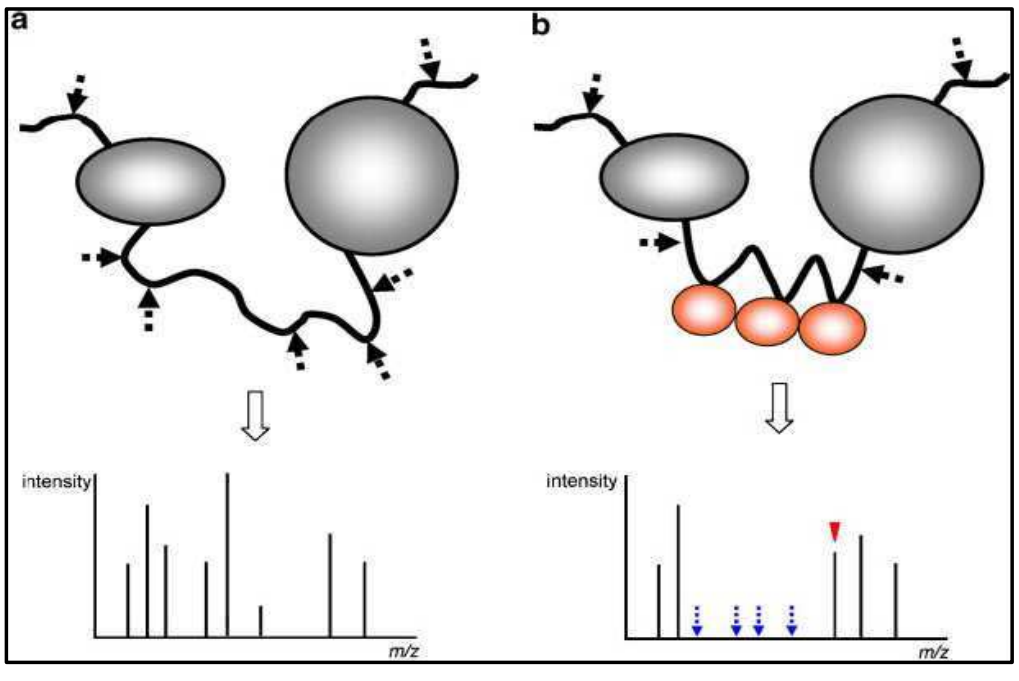

Figure 1: Illustration of limited proteolysis strategy: (a) before and (b) after ligand:protein interaction.

In this Ph.D. work, we chose as a readout step in combination with limited proteolysis, MALDI MS analysis. Intact protein and large proteolytic peptides can be recovered and directly analyzed by MALDI-MS, which allows for the determination of proteins that are resistant to proteolytic digestion by accurate measurement of molecular weights. Larger proteolytic peptides can be directly identified by the combination of measured mass, enzyme specificity and protein database searching.

1.2 Circular dichroism

Circular dichroism (CD) is the difference in absorption of left and right circularly polarized light, usually by a solution containing the molecules of interest. A signal is only measured for chiral molecules such as proteins. A CD spectrum provides information about the bonds and structures responsible for this chirality. When a small molecule (or ligand) binds to a protein, the protein can acquire an induced CD (ICD) spectrum through chiral perturbation to its structure or electron rearrangements. The intensity of the ICD spectrum is determined by the strength and geometry of its interaction with the ligand. Therefore, ICD can be used to probe the binding of ligands to proteins [8].

1.3 Surface Plasmon Resonance

Surface Plasmon Resonance (SPR) is used to monitor macromolecular interactions in real time. The BIAcore 3000 system (http://www.biacore.com/lifesciences/index.html) is an instrument that uses SPR technology for measuring the interactions of macromolecules with each other, and with small ligands. One of the ligands is immobilized on carboxymethylated dextran over a gold surface (Figure 2), while the second partner (analyte) is captured as it flows over the immobilized ligand surface. Most ligands can be directly immobilized onto the surface of the chip via amino groups, carbohydrate moieties, or sulfhydryl groups. Others are immobilized indirectly through the use of biotinylation of the ligand (such as biotinylated peptides or oligonucleotides), or through immobilized monoclonal antibodies (such as anti-GST). The bound analytes can be stripped from the immobilized ligand without affecting its activity to allow many cycles of binding and regeneration on the same immobilized surface. Interaction is detected via SPR, in real time, at high sensitivity, without the use of radioactivity.

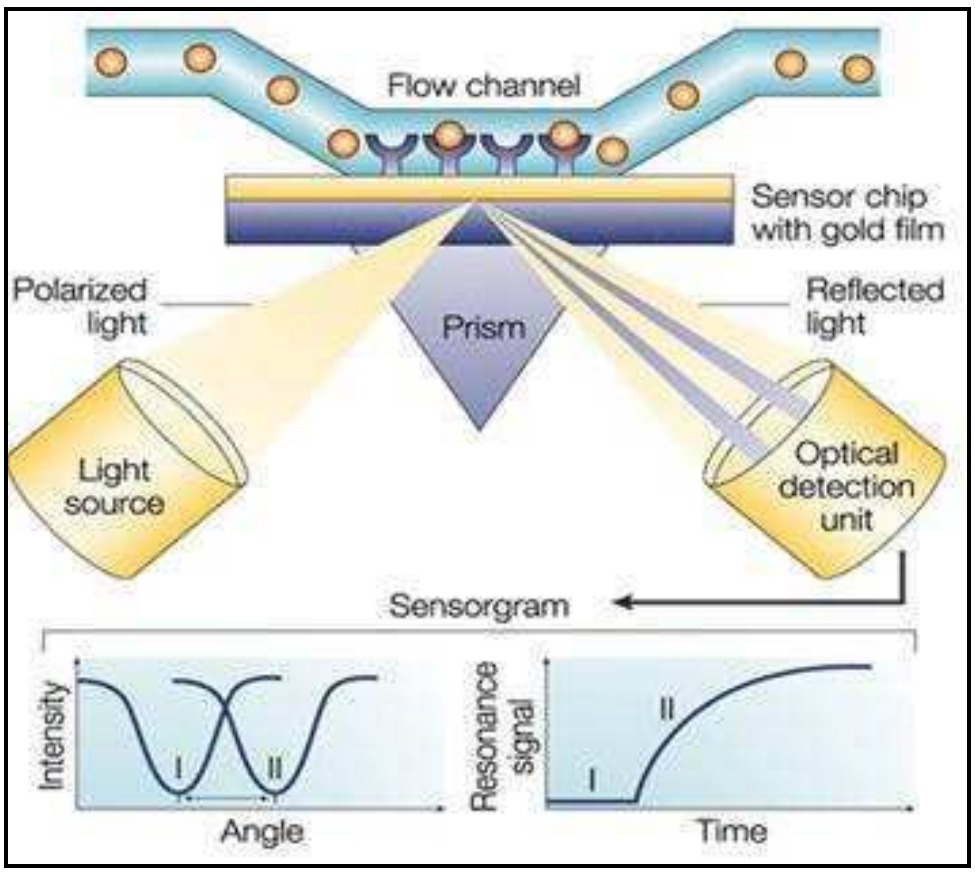

Figure 2: Illustration of Surface Plasmon Resonance technology.

1.4 STATs family

STAT1 is a member of the Signal Transducers and Activators of Transcription family. This family regulates many aspects of growth, survival and differentiation in cells. The transcription factors of this family are activated by Janus kinase (JAK) and deregulation of this pathway is frequently observed in primary tumours and leads to increased angiogenesis, enhanced survival of tumours and immunosuppression. Gene knockout studies have provided evidence that STAT proteins are involved in the development and function of the immune system and play a role in maintaining immune tolerance and tumour surveillance. There are seven mammalian STAT family members which have

been identified: STAT1, STAT2, STAT3, STAT4, STAT5 (STAT5A and STAT5B), and STAT6. STAT1 was discovered as target of interferon activation, but now it is known that all the STAT proteins can be activated after one or more cytokines interact with their cognate receptor [9]. These transcription factors are latent in the cytoplasm until they are activated by extracellular signaling proteins (mainly cytokines and growth factors, but also some peptides) that bind to specific cell-surface receptor. These extracellular-signaling proteins can activate various tyrosine kinases in the cell that phosphorylate STAT proteins. The activated STAT proteins accumulate in the nucleus to drive transcription. The duration and degree of gene activation are under strict regulation by a series of negatively acting proteins.

1.4.1 STATs structure and the JAK-STAT pathway

Mammalian STAT proteins contain three conserved domains: a DNA binding domain, an SH2 domain and a site of tyrosine phosphorylation (Figure 3) [10].

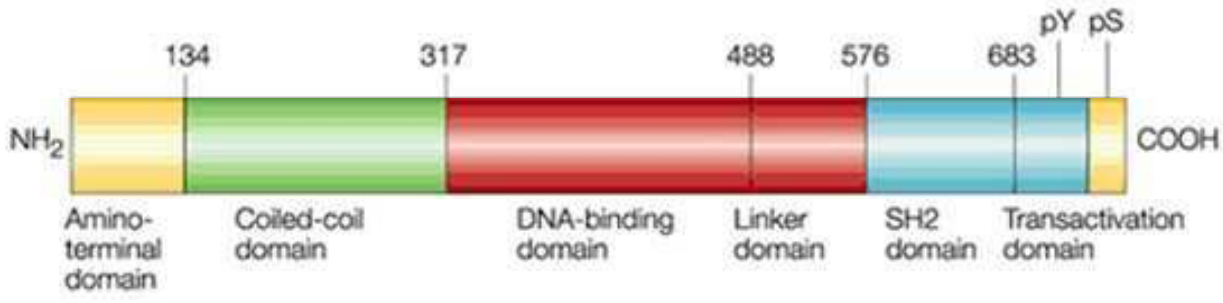

Figure 3: STATs domain.

In their carboxy-terminal regions, most mammalian STAT proteins contain a transcriptional activation domain. The amino-terminal proximal region interacts with other cellular proteins and very near to the amino terminus there is a weakly conserved region that directs the oligomerisation of STAT dimers. When a cytokine binds to its receptor, it induces conformational changes — most likely including oligomerisation or multimerisation — and this activates JAKs (Janus kinases) (Figure 4). JAKs are tyrosine kinases, one of which is constitutively associated with each receptor chain. The activated JAKs autophosphorylate, and/or transphosphorylate, and then phosphorylate the receptors. Classically the phosphorylated receptor tyrosine motifs act as docking sites for the SH2 domains of STATs, although recruitment of certain STATS at least can also occur independently of the SH2 domains and through the JAKs. The JAKs then tyrosine phosphorylate the STAT molecules and this triggers a re-shuffle; the STAT monomers dissociate from the receptor and dimerize with one another via reciprocal SH2 domain:phosphotyrosine interactions. The STAT homo- or heterodimers migrate to the nucleus via importin a/b and RanGDP complex and, with or without interaction with additional specificity modulating factors (e.g. p48 in the case of interferon-α), interact with transcriptional co-activators and the target DNA to activate transcription. For example, the active STAT dimer can bind to cytokine inducible promoter regions of genes containing gamma activated site (GAS) motif and activate transcription of these genes. The STAT protein can be dephosphorylated by nuclear phosphatases which leads to

inactivation of STAT and the transcription factor becomes transported out of the nucleus by exportin crm1/RanGTP.

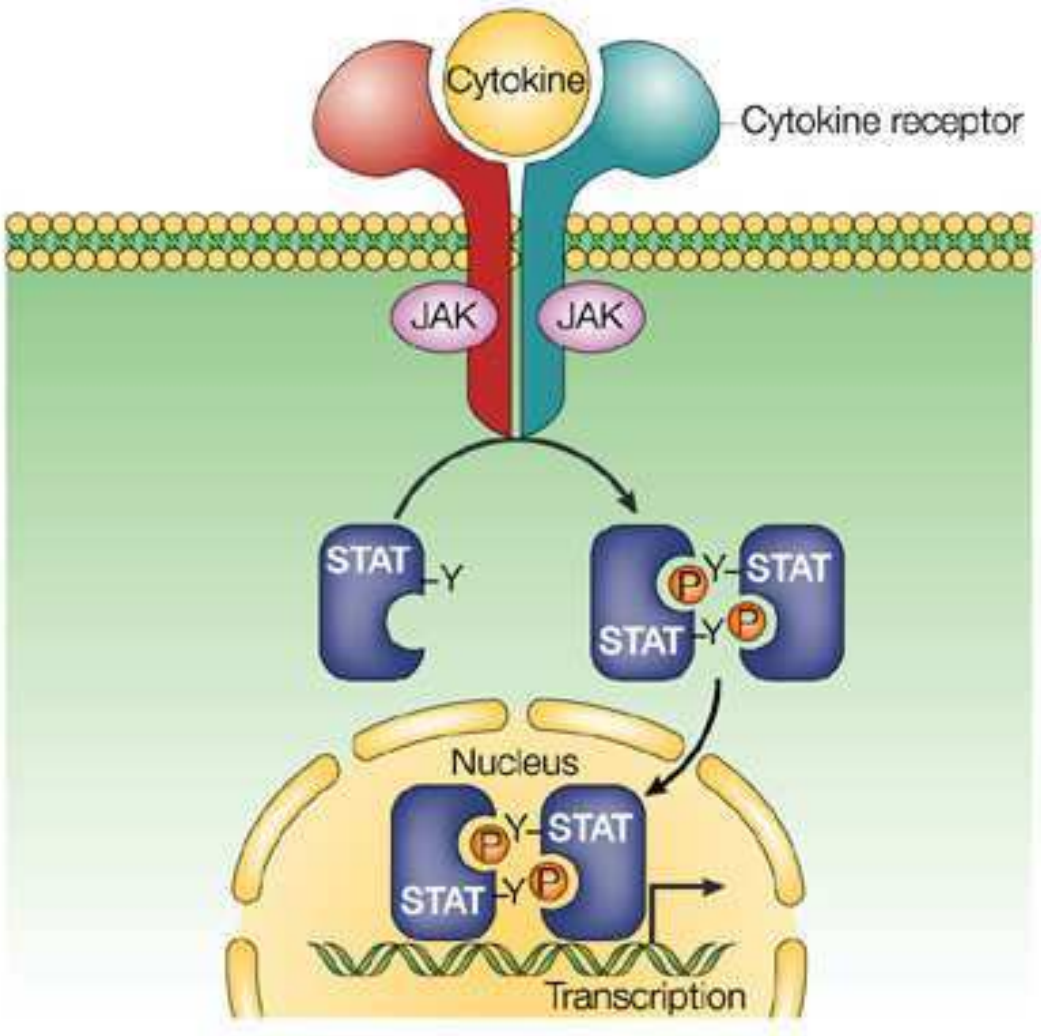

Figure 4: The JAK-STAT signaling pathway.

1.4.2 Biological functions of STATs

Transcription factors are crucial to biological outcomes in whole organisms. So, it is no surprise that STAT proteins are widely involved in many roles. One of them is in infection. Several STAT proteins in mammals have a crucial role in host defence. STAT1 and STAT2 are largely restricted to mediating the effects of IFNs; STAT4 and STAT6 mediate the effects of Il-12 and Il-4, respectively; and STAT3 mediates the effects of Il-6

and other gp130 ligands. Animals that lack either STAT1 or STAT2 are exquisitely sensitive to microbial infections [11-12-13], and subtle mutations of STAT1 in humans lead to decreased resistance to mycobacterial infection [14]. The absence of STAT6 blocks the differentiation of T cells, and the lack of STAT4 impairs IFN-γ production by T cells and development of natural killer cells during bacterial and viral infections [15].

Another known role is in growth control. Signaling pathways that originate at the cell surface and send active transcriptional proteins to the nucleus are frequently dysfunctional in cancer cells [16]. The STAT proteins are certainly no exception. Mice that lack STAT1 are much more susceptible to chemically induced primary tumours and to tumours that can be readily transplanted [17-18-19], and human cancer cells have often lost STAT responses to IFN, which normally imposes growth restraint [20].

Of great current interest is persistently active STAT3, which is known to occur in a wide variety of human tumours [21]. Furthermore, STAT3 can, by experimental mutation, be converted into an oncogene [22]. The persistently active protein is required because introduction of a dominant-negative form of STAT3 into head and neck cancer cells or into multiple myeloma cells causes apoptosis of recipient cancer cells [23]. Persistent activation of STAT3 in head and neck cancer is associated with mutations in the epidermal growth factor (EGF) receptor or mutations that result in the production of excess ligand or normal receptor [24].

1.4.3 STAT1: role in ischemia/reperfusion (I/R)-induced apoptosis in cardiac myocytes.

Loss of cardiomyocytes by programmed cell death (apoptosis) is an important mechanism in the development of cardiac failure during injury due to ischemia/reperfusion and myocardial infarction . Recent studies have indicated that apoptotic death occurs in cardiac cells exposed to a variety of damaging stimuli both *in vitro* and in the intact heart *in vivo*. Thus, cardiac cells exposed to a hypoxic/ischemic insult followed by reperfusion undergo apoptotic cell death *in vitro*. Similarly, apoptotic cell death is also observed in the intact heart following ischemia *in vivo*. Despite the convincing evidence that apoptosis occurs, the mechanism and signlling pathway that leads to hypoxic/ischemic stimuli resulting in apoptosis in cardiac cells is as yet unknown. However, as in other cell types, caspases have been implicated in apoptotic cell death in cardiomyocytes. Cytokines and growth factors are known to modulate growth, differentiation, and death in many cell types. For example, interferons (IFNs) have been shown to trigger cell cycle arrest and death in non-cardiac cells, whereas many interleukins stimulate growth and protect cells from apoptosis. These pro- and anti-apoptotic effects are mediated, at least in part, by signaling through a family of transcription factors called STATs. For example, a STAT-1-deficient cell line is resistant to tumor necrosis factor-a-induced apoptosis, and STAT-1 has been implicated in transcriptional activation of some caspases. There is little information on the role of STATs in mediating pro- and

anti-apoptotic signals in the heart. Only Stephanou et al. [25] reported that STATs are involved in apoptotic cell death induced by simulated ischemia/ reperfusion in primary cardiomyocytes *in vitro* and in the intact heart *ex vivo*. In particular, they showed that exposure of cardiac cells to simulated ischemia results in apoptosis and is accompanied by phosphorylation and increased expression and transcriptional activity of STAT-1. Furthermore, they observed that interferon-γ, which is known to induce STAT-1 activation, also induced apoptosis in cardiac cells. Both STAT-1 over-expression and interferon-γ treatment or exposure to ischemia activated the promoter of the pro-apoptotic caspase-1 gene in cardiomyocytes. Finally, ischemia/reperfusion also induced STAT-1 activation and caspase-1 processing in ventricular myocytes in the intact heart *ex vivo*. All these data suggested that STAT-1 plays a critical role in the regulation of ischemia/reperfusion-induced apoptosis in cardiac cells, acting at least in part via a caspase-1 activation-dependent pathway.

1.4.4 Dowregulation of STAT1 by flavonoids

Scarabelli et al. [26] showed that some specific flavonoids (Myricetin, Delphinidin, Epigallocatechin-3-gallate) (Figure 5) provide an efficient protection of the heart from ischemia/reperfusion-induced injury. Since these flavonoids are the main antioxidant components of green tea leaves, the consumption of antioxidant compounds could be able to mediate cardioprotection and enhance cardiac function during I/R injury. However, Scarabelli et al. found that the cardioprotection

showed by some flavonoids is not due to the different cellular redox state, but to the inhibition of STAT1 activation.

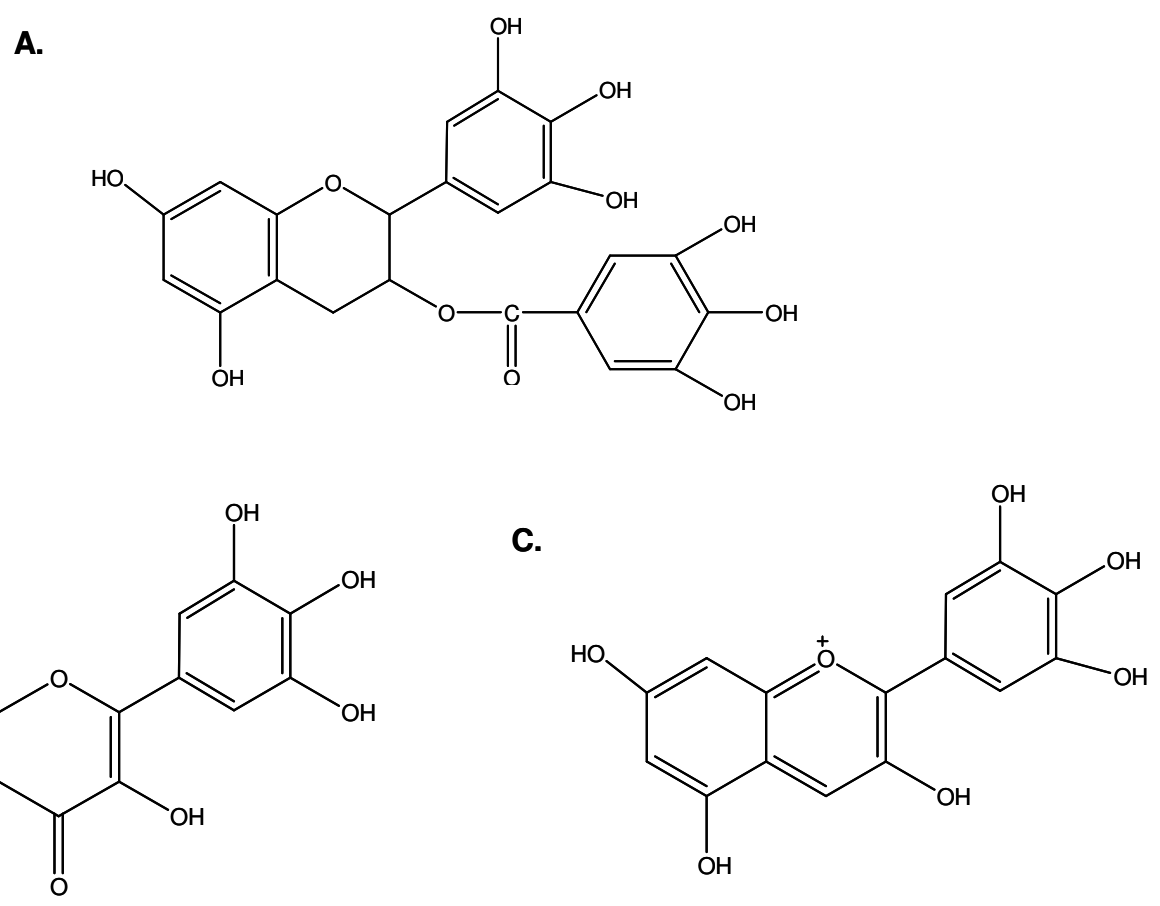

Figure 5: Chemical structure of natural molecules under investigation: (a) Epigallocatechin-3-gallate (EGCG), (b) Myricetin and (c) Delphinidin.

Since they screened several flavonoids, they found that only some flavonoids with a particular structural feature (three hydroxyl groups in the B ring and one in the 3 position of the C ring) were more efficient. Moreover, according to their data by computer modeling they predicted that anti-STAT1 flavonoids directly interact with STAT1 with high affinity at critical sites near the SH2 domain where there are tyrosine residue 701 (TYR701) and serine residue 727 (SER727). Since I/R rapidly induces phosphorylation of TYR701 and SER727, the mechanism leading to the efficient, specific inhibition of STAT1

activation could occur through the inhibition of phosphorylation of the previous sites.

1.5 Mapping of interaction between STAT1 and flavonoids

Obtaining detailed structural information about binding sites and protein conformational changes is critical to the development of therapeutic agents as well as development of chemical sensors based on molecular recognition principles. In this Ph.D. work, by the use of limited proteolysis combined with MALDI TOF MS and Surface Plasmon Resonance we determined binding site(s) between STAT1 and flavonoids.

As reported by Scarabelli et al., EGCG, Myricetin and Delphinidin protect the hearth from ischemia/reperfusion-induced injury through STAT1 inhibition. They proved that these molecules bind to the protein and probably inhibit its dimerization and activation. Identifying the molecular mechanism requires an understanding of protein structure and protein-ligand binding sites. Herein, we implement limited proteolysis of the non-covalently bound STAT1-flavonoid complex, using MALDI TOF MS and Surface Plasmon Resonance analysis, to determine flavonoid binding site(s). In addition to binding site determination, these methods also suggest the ability to address protein dynamics by determining conformational changes induced by ligand binding.

RESULTS AND DISCUSSION

-CHAPTER 2-

Identification of the binding region between STAT1 and flavonoids

2.1 Conformational Changes By Circular Dichroism

In order to explore the nature of interaction between STAT1 and some selected flavonoids (Myricetin, Delphinidin, EGCG), we investigated the secondary conformation of the protein in presence of these natural molecules by circular dichroism (CD). Therefore, we measured in far-UV (190-260 nm) a solution of STAT1 and STAT1:flavonoid complex in physiological conditions and at room temperature.

A drug effect is a function of time and dose. Measured effects are frequently recorded as maxima at time of peak effect or under steady-state conditions, so first we followed the interaction over the time. After mixed the protein and ligand solutions, we acquired CD spectra at different time points (every 10 minutes up to 60 minutes). Since we did not find any difference (data not showed) between STAT1 and STAT1:complex over the time, we performed a dose-response experiment at steady state conditions. Thus, we measured the secondary structure of STAT1 in presence of increased concentrations of the ligands (0, 4, 9, 17 μM). In parallel, before mixing the solutions, each component, protein or ligand, was also singly measured and the contribution of the each spectrum was evaluated during the data elaboration. Moreover, each condition was tested also on another protein, bovine serum albumin (BSA), which should not interact with the tested molecules and therefore represent a negative control.

Once the CD spectra have been acquired, they have been elaborated by Jasco software and the resulting files then

analyzed by CONTIN online software to have an evaluation of the protein secondary structure.

The CD data (Figure 6-7-8) showed how the secondary structure of STAT1 was affected by each natural compound. Indeed, without ligand the secondary structure of STAT1 is characterized exclusively of alpha-helix. The adding of the natural compound, singly, produced an intense modification of the secondary structure which lost the standard alpha-helix conformation.

Myricetin [υM]	STAT			
	fα	fβ	f*turn*	f*random*
0	1	0	0	0
4	1	0	0	0
9	0.393	0.133	0.201	0.273
17	0.221	0.263	0.213	0.303

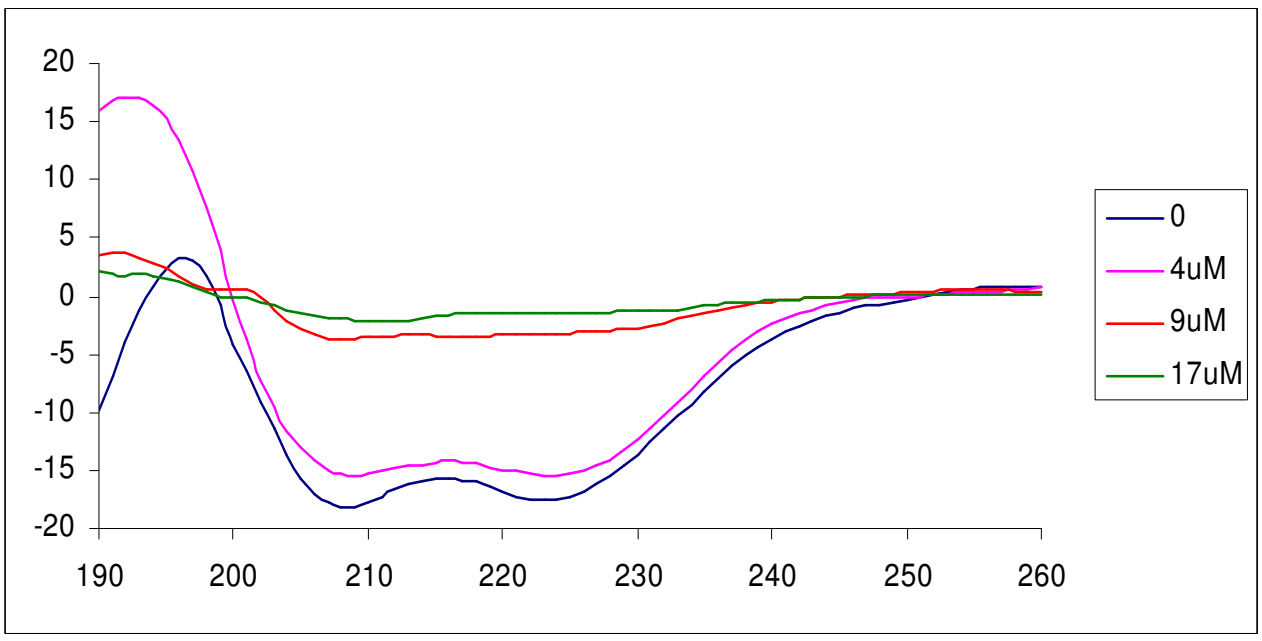

Figure 6: CD spectra and estimated secondary structure of STAT1 in presence of 0, 4, 9, 17 μM of Myricetin.

Delphinidin[υM]	STAT			
	fα	fβ	f*turn*	f*random*
0	1	0	0	0
4	0.736	0.033	0.203	0.028
9	0.343	0.135	0.267	0.255
17	0.103	0.385	0.209	0.303

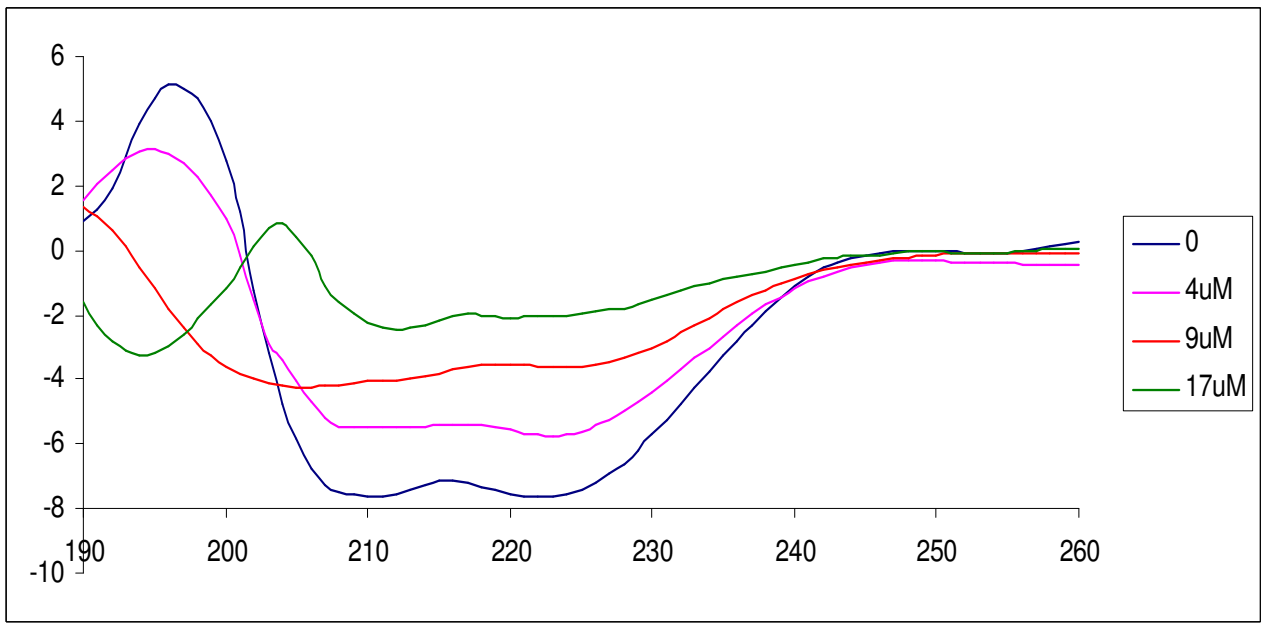

Figure 7: CD spectra and estimated secondary structure of STAT1 in presence of 0, 4, 9, 17 µM of Delphinidin.

EGCG [υM]	STAT			
	fα	fβ	f*turn*	f*random*
0	1	0	0	0
4	0.549	0.033	0.185	0.233
9	0.321	0.126	0.230	0.323
17	0.123	0.101	0.260	0.515

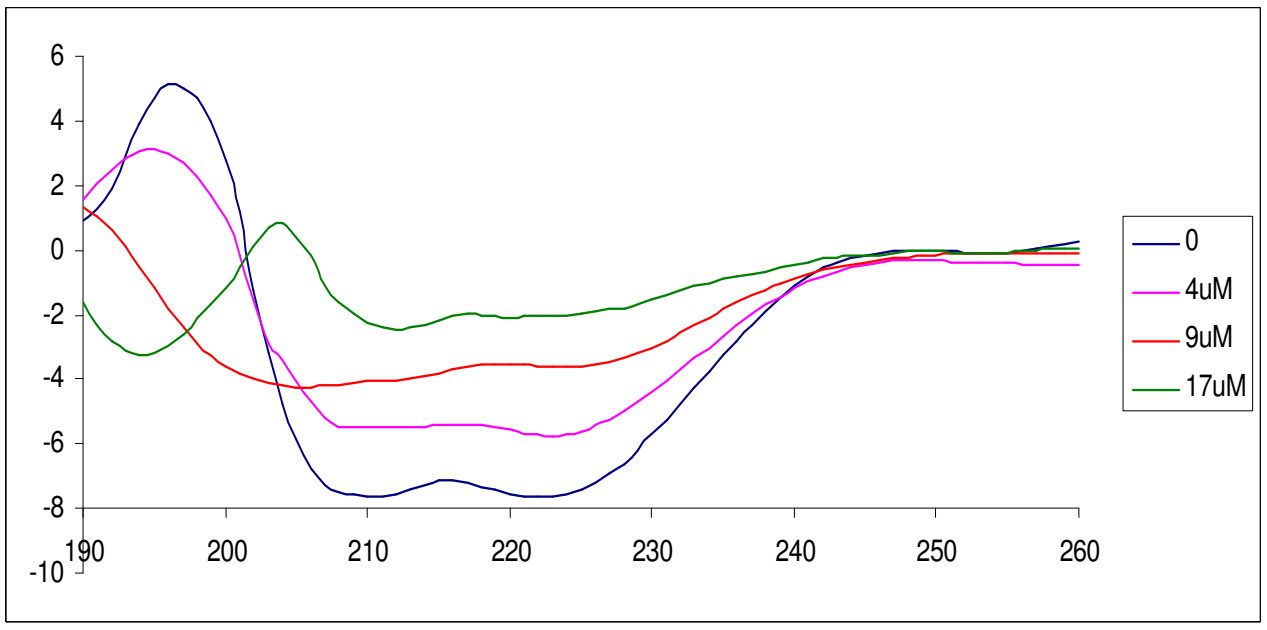

Figure 8: CD spectra and estimated secondary structure of STAT1 in presence of 0, 4, 9, 17 µM of Epigallocatechin-3-gallate (EGCG).

2.2 Mapping Site by Proteolysis Limited

The strategy adopted for the limited proteolysis of STAT1-ligand complexes can be considered in three parts: optimization of proteolysis, characterization of the fragments, identification of the binding domains.

2.2.1 Optimization of proteolysis

The protein-molecule complex has been digested with various proteases to establish which conditions are optimal for generating a protease resistant domain. We routinely modified two parameters (enzyme/substrate ratio and duration of digestion) when determining the best conditions for limited proteolysis. To determine the appropriate enzyme/substrate ratio for a particular protease, STAT1 solutions have been digested at several enzyme/substrate ratios (from 1:50 to 1:300), removing samples at regular time intervals for MALDI-MS analysis. The best ratio enzyme/substrate is when the enzyme is sufficiently diluted so that it digests only the most accessible regions, leaving the domains intact. We used two different enzyme: Trypsin, a protease which cleaves peptide bonds following a positively charged amino acid (lysine or arginine), and endoproteinase AspN (flavastacin) which selectively cleaves peptide bonds N-terminal to aspartic acid residues. For each of them we chose the best ratio enzyme/substrate and the best time points, which corresponded respectively to 1:500 and 1:300 from 0 up to 30 minutes.

The limited proteolysis experiments require molar excess ligand, to be certain that as many binding sites as possible are occupied (i.e., no excess ligand-free protein in solution) without forcing non-specific interactions to occur. Initially, molar ratios were varied from 1:1 to 1:50 protein: ligand. At a 1:1 molar ratio there was no quantitative difference in the proteolytic fragment ion abundances, as measured by MALDI MS, observed from STAT1 relative to the STAT1-ligand complex. This was likely

due to a large amount of unbound STAT1 in the protein-ligand solution. Conversely, at a 1:50 protein:molecule ratio there was a significant change in the spectrum quality suggesting that when present in great excess, molecules interacted with the crystallization of MALDI matrix. The best results were observed at a 1:10 STAT1: flavonoid molar ratio, and we chose this molar ratio to develop the limited proteolysis experiments.

2.2.2 Characterization of the fragments (Trypsin)

The first experiments have been performed with Trypsin on a solutions of STAT1.

MALDI MS analysis of the time resolved limited proteolysis experiments (every 5 min for 30 min) are represented in Figures 9 which shows MALDI mass spectra of the peptide map generated by a Trypsin digest from 0 to 30 min of STAT1. These mass spectra are typical of the ten spectra obtained for each respective digest time. Quenching the tryptic digest with acid and addition of MALDI matrix is likely to dissociate any specific non-covalent interactions remaining in solution after digestion.

MALDI MS usually creates singly charged ions, but multiply charged ions ($[M+nH]^{n+}$) can also be created, as a function of the matrix, the laser intensity and/or the voltage used. In agreement with the theory, before to adding the protease (time= 0 min), we observed two principal signals relative respectively to double- $[M+2H]^{2+}$ and triple-charged $[M+3H]^{3+}$ of a full-length STAT1 solution. We zoomed the spectrum in the range

m/z 30-75K to cut off the signal of mono-charged STAT1 because of its intensity. After 5 minutes of enzymatic digestion, we did not see more the double- and triple-charged signals of the intact protein but we saw new signals around 30 kDa and 51 kDa. In the next two time intervals (15 and 30 minutes), the scenario is quite the same as before, the only significant difference is the disappearance of the signal at 51 kDa and the appearance of another signal around 50 kDa.

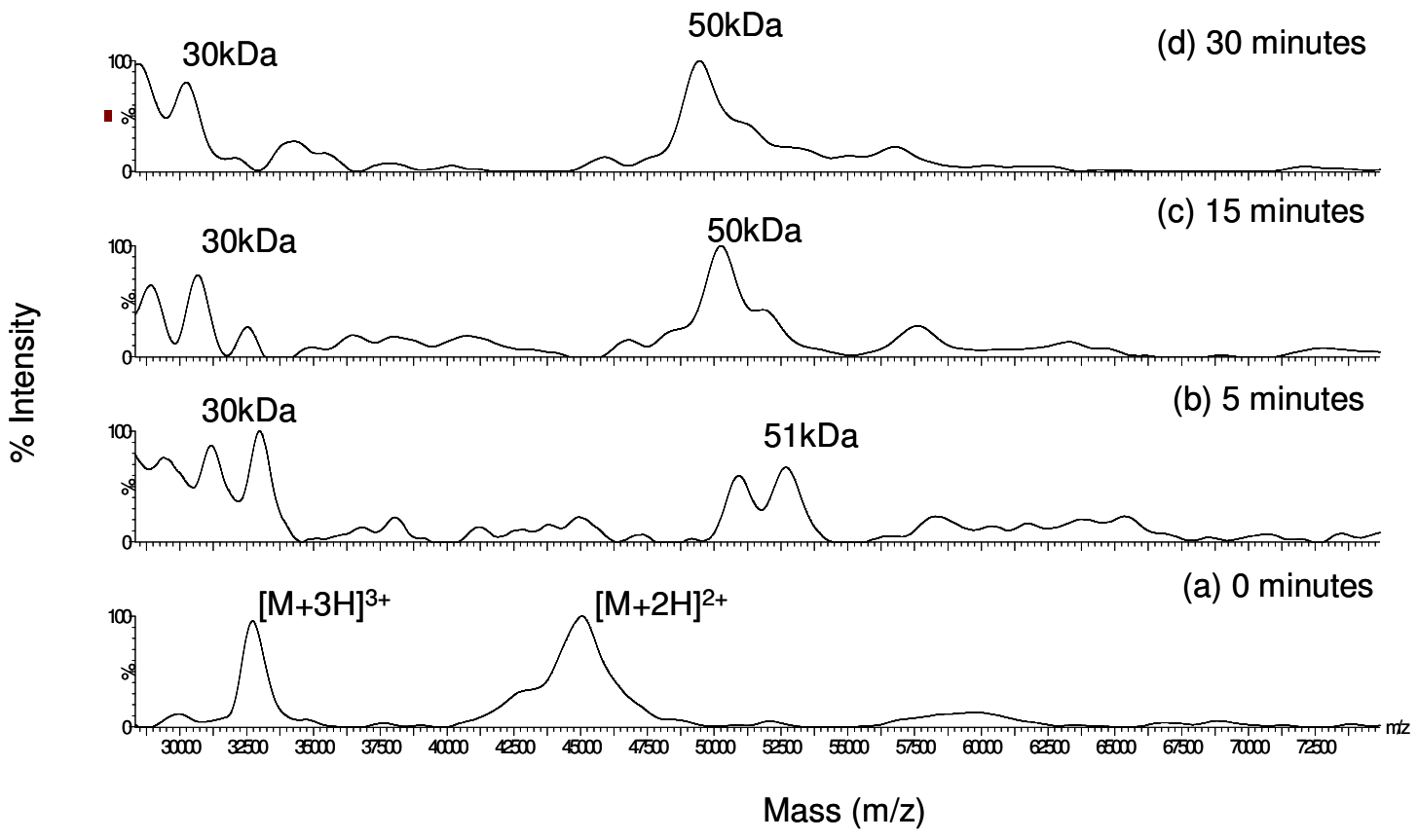

Figure 9: MALDI-TOF mass spectra of a (a) 0 min, (b) 5 min, (c) 5 min and (d) 30 min tryptic digest of a solution containing STAT1.

We repeated the enzymatic digestion more than 3 times, we collected the samples at each time point and we analyzed the fractions after 5 and 30 minutes of digestion by SDS-PAGE (Figure 10).

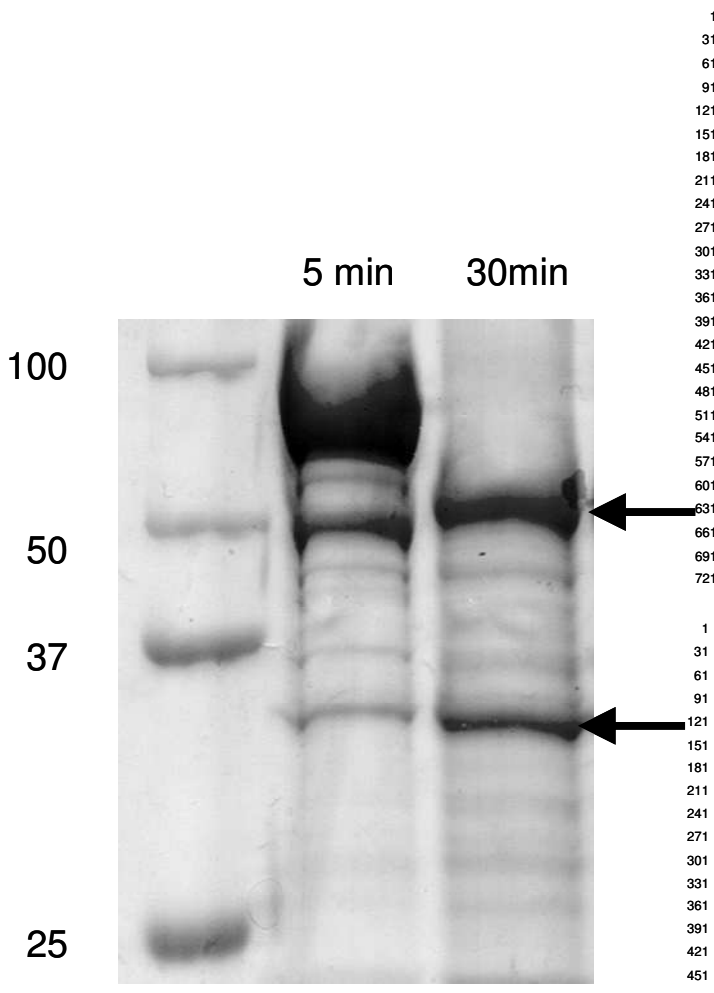

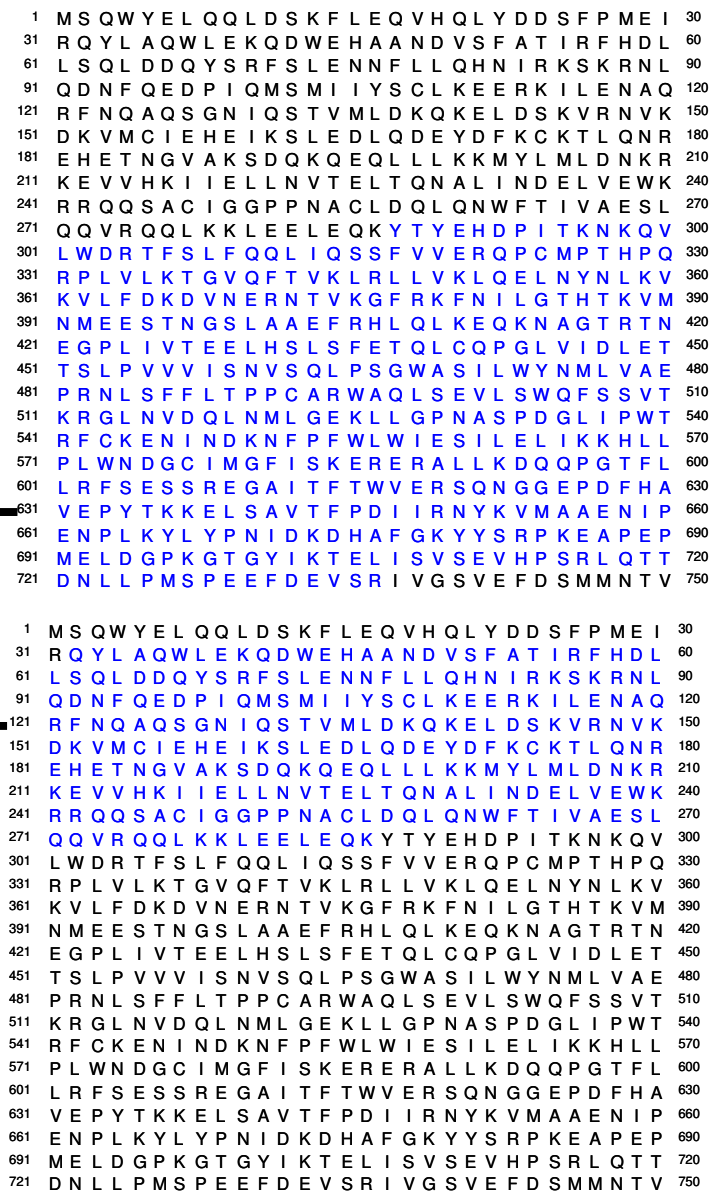

Figure 10: Coomassie gel of STAT1 fractions respectively at 5 and 30 minutes of proteolytic digestion with Trypsin.

After 5 minutes of digestion the major band was still that relative to undigested STAT1. The fraction collected after 30 minutes of digestion was characterized by two main 50kDa and 30kDa bands and the upper band relative to STAT1 was completely disappeared. We confirmed the results obtained by MALDI MS analysis. Moreover we cut from the gel the two major peptide fragments which have been identified by Mass Spectrometry. At this point we were able to create a digestion map reported in Figure 11. According to our data, the two major signals observed by MALDI-MS and SDS-PAGE were due to a

cleavage at Lysine 286 which produced two fragments respectively of 30280 kDa (a.a. 31-286) and 51674 kDa (a.a. 287-736). The last fragment (at 51 kDa) was further cleaved at Lysine 297 generating another fragment of 50425 kDa (a.a. 297-736) (Figure 11).

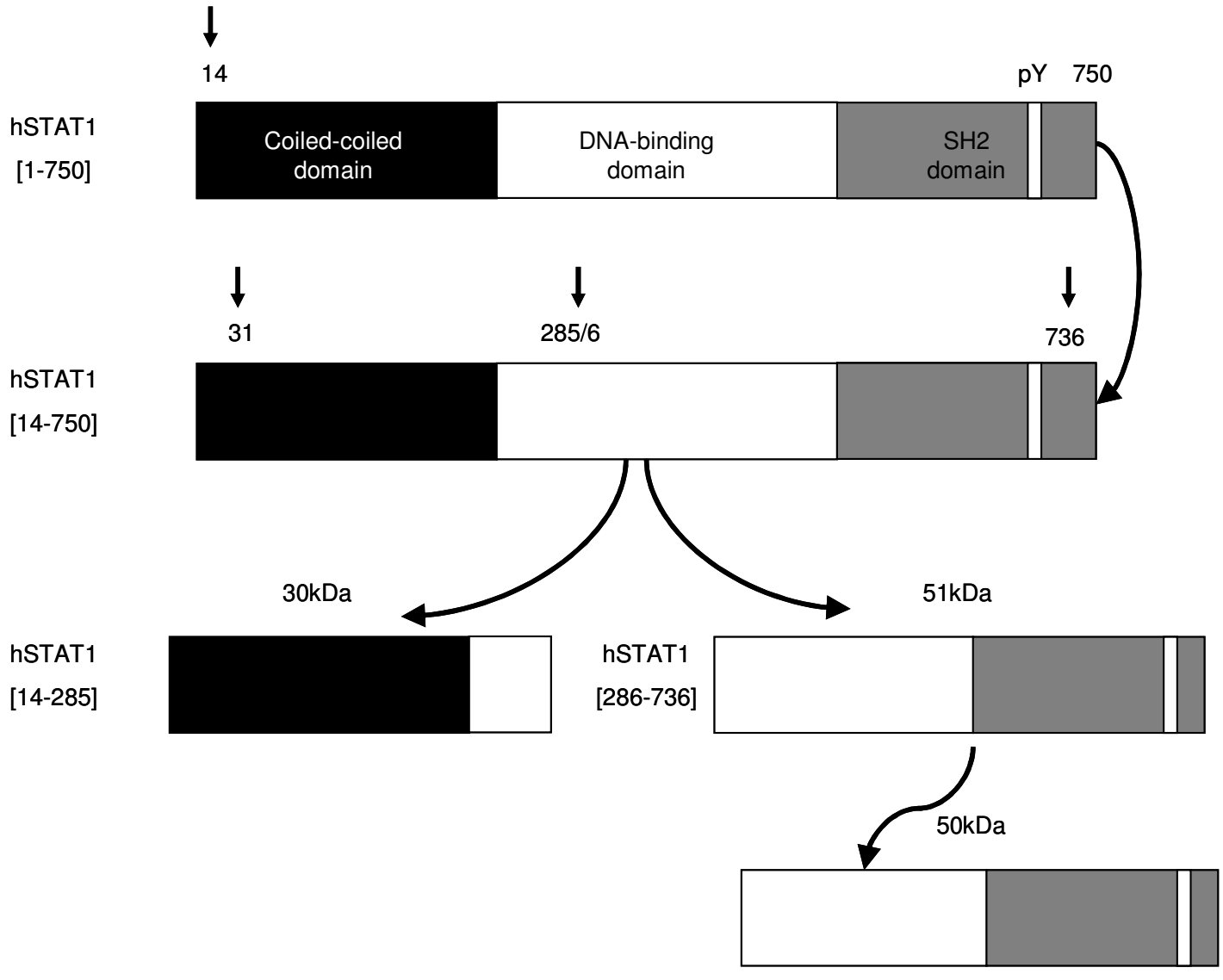

Figure 11: Representation of the digestion steps relative to STAT1-limited proteolysis by Trypsin.

2.2.3 Identification of the binding domains(Trypsin).

Once identified the domains produced by limited proteolysis of STAT1, we performed the limited proteolysis experiment on

solutions containing 1:10 molar ratio of STAT1:ligand and analyzed the proteolytic fragments by MALDI MS. We routinely used each of the three molecules (EGCG, Myricetin, Delphinidin). The peptide pattern of STAT1 and the STAT1:ligand complex in the mass spectra (data not shown) were qualitatively similar, we did not found any different signal. However, careful inspection of the MALDI mass spectra revealed significant differences in the rate of proteolysis at several signals. For example, we reported in Figure 12 the intensity of two signals at m/z 51675 [a.a. 287-736] and m/z 50426 [a.a. 297-736] generated by digestion at indicated time intervals of STAT1 (Figure 12B) and STAT1: ligand complex (Figure 12A).

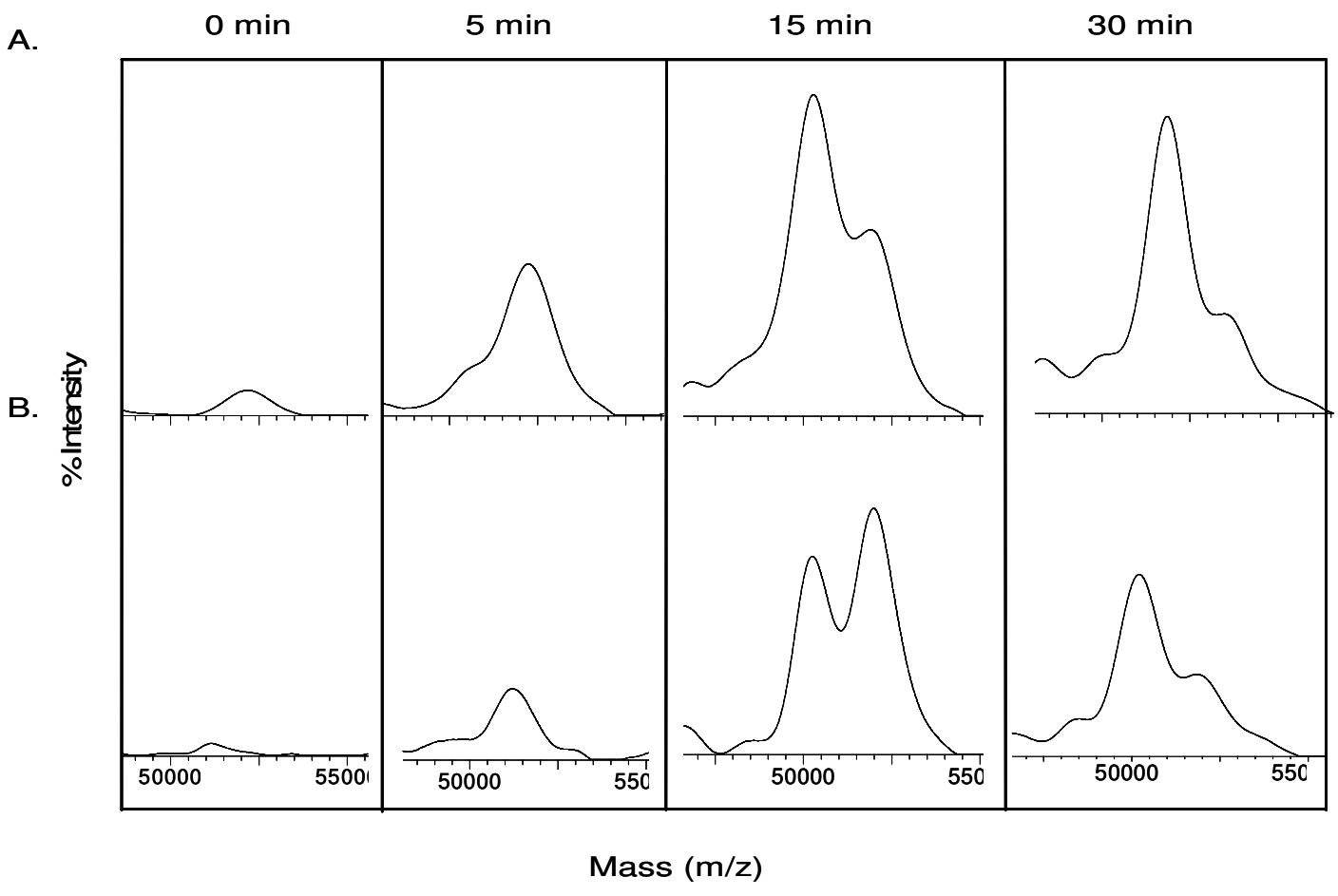

Figure 12: Mass spectra of the limited proteolysis of STAT1 in presence (A) and in absence (B) of ligands: we zoomed the mass

spectra to follow the digestion trend of two signals at m/z 51675 and 50426.

According to our data, in the same experimental conditions STAT1, when in complex with one of the three flavonoids, was more abundantly and quickly digested. Indeed, as illustrated in the Figure 12A, when STAT1 is associated with the natural compounds after 5 minutes of digestion the signal at m/z 51675 was already produced, whereas without ligands the same signal was still low (Figure 12B). After 15 minutes of tryptic incubation, in the STAT1: flavonoid samples the main signal corresponded to the new fragment at m/z 50426, differently from what observed from digestion of STAT1 without ligand.
Figure 13 shows the statistical representation of the percent relative ion abundance versus proteolysis time for the proteolytic fragment at m/z 51675 [amino acids (a.a.) 287-736] and at m/z 30281 (a.a. 31-286). The results herein reported are representative of one of the three tested natural compounds, but we observed the same phenomenon for each of them.

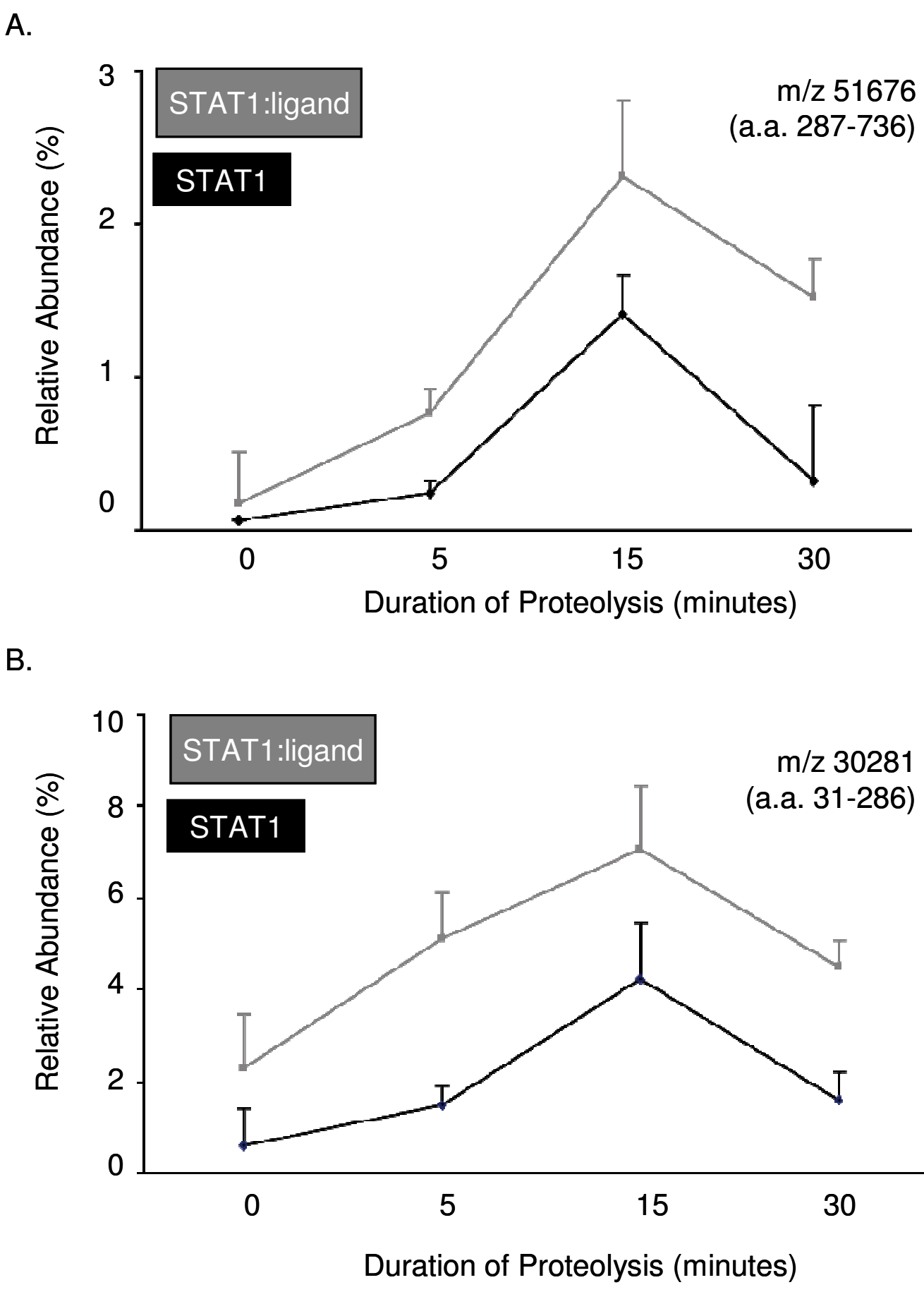

Figure 13: Comparison of percent relative ion abundance versus digest time for the fragments signals at m/z 51676 (A) and at m/z 30281 (B) observed in the STAT1 (black line) and the STAT1-ligand complex (grey) tryptic digests. The means ± SD of 3 independent experiments are shown.

From 0 to 30 min both fragments were higher in abundance in STAT1-ligand complex compared to STAT1 without ligand. The fact that the rates of proteolysis of these two fragments was augmented in the complex for the first 30 min suggests that upon binding, flavonoids induced a conformational change that altered the tertiary structures enough to increase the rate of proteolysis at a given site. Therefore the natural compounds favor the access of the protease to one or both termini of these proteolytic fragments.

2.2.4 Characterization of the fragments (Asp-N).

To get more information about the binding sites between STAT1 and our flavonoids, we assessed the effect of another enzyme. Therefore, we performed further experiments using Endoproteinase Asp-N, a protease which selectively cleaves peptide bonds N-terminal to aspartic acid residues (D). After optimized the experimental conditions (ratio enzyme:substrate and time intervals) for Asp-N, multiple experiments were done to characterize the fragments produced by STAT1 digestion. As before, we checked the limited proteolysis products through SDS-PAGE (Figure 14) and MALDI MS analysis (data not shown) and we illustrated the digestion map in the Figure 15.

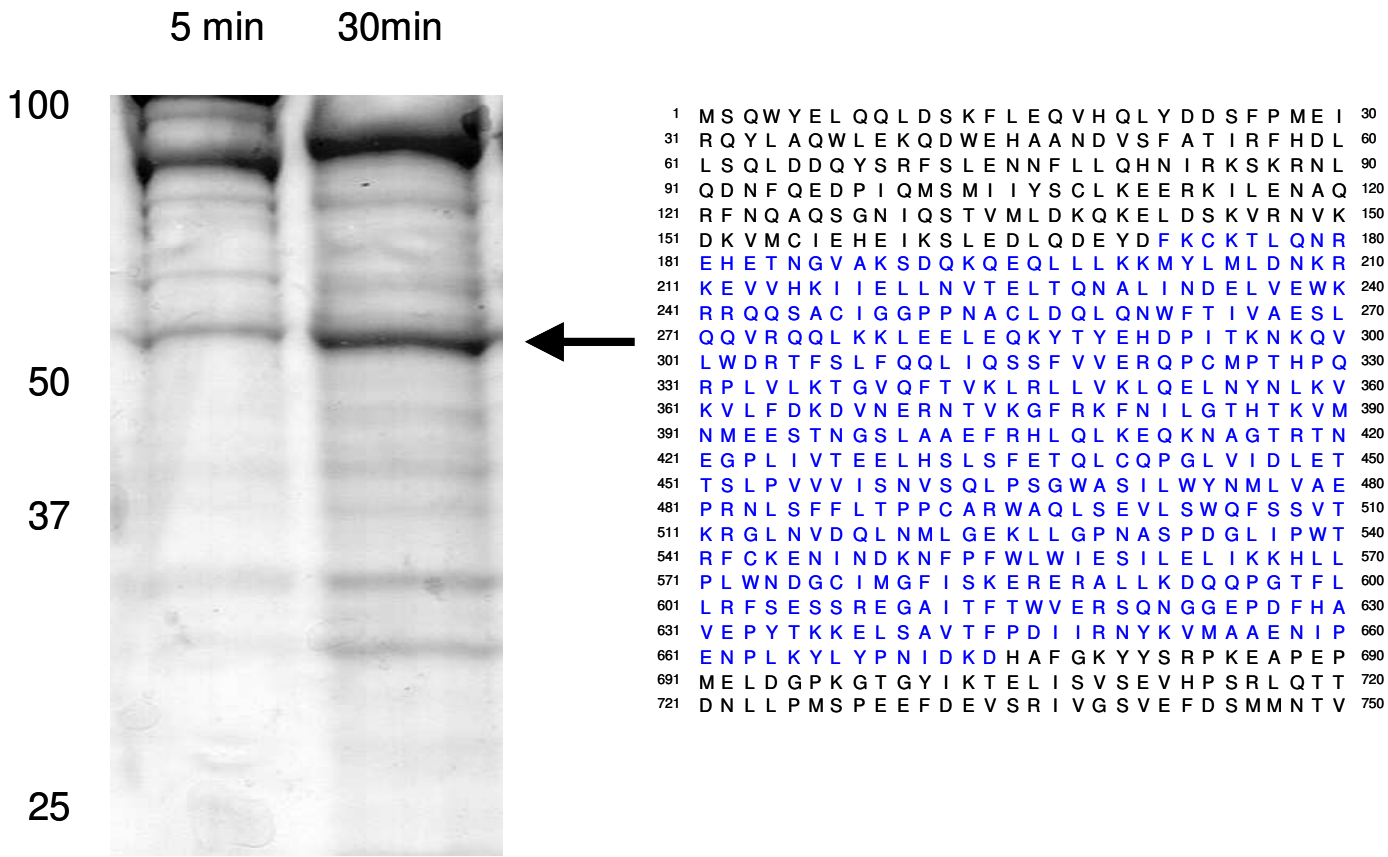

Figure 14: Coomassie SDS-PAGE of STAT1-fractions respectively at 5 and 30 minutes of proteolytic digestion with Asp-N. The arrows indicate the bands excised and identified by Mass Spectrometry.

According to our data, limited digestion by Asp-N of STAT1 produced one major fragment around 60 kDa which was due to a cleavage at aspartic acid residues 171 and 673, generating a fragment of 58196 Da (Figure 15).

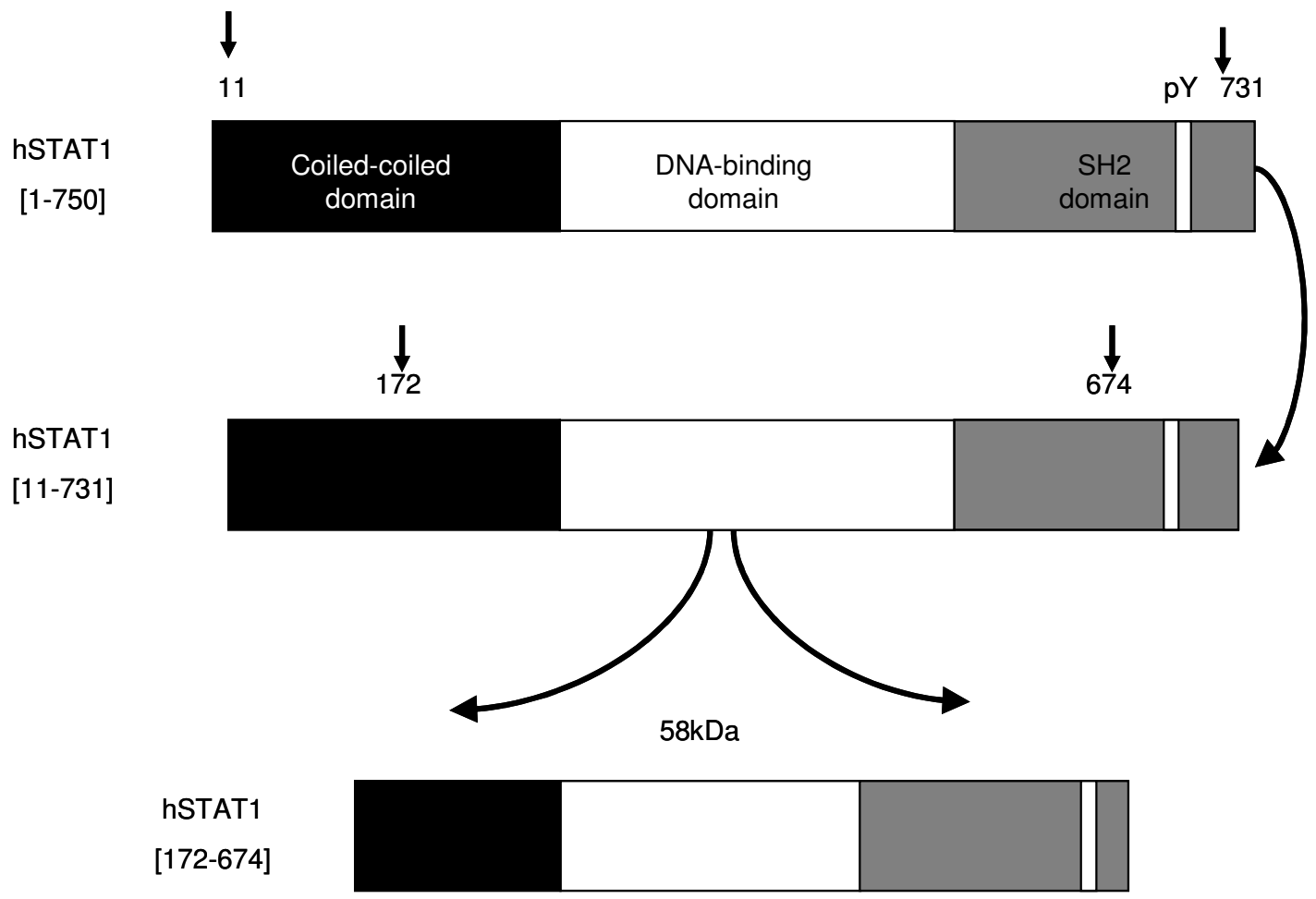

Figure 15: Representation of the digestion products from STAT1-limited proteolysis by Asp-N.

2.2.5 Identification of the binding domains (Asp-N).

When we performed the limited proteolysis of STAT1:ligands complex with Asp-N, MALDI mass spectra were poorly defined (data not shown) and apparently we did not caught any difference between the digestion of STAT1 and STAT1:flavonoid complex. Then, we collected samples from three experiments after 5 and 30 minutes of digestion and we analyzed them by SDS-PAGE (Figure 16).

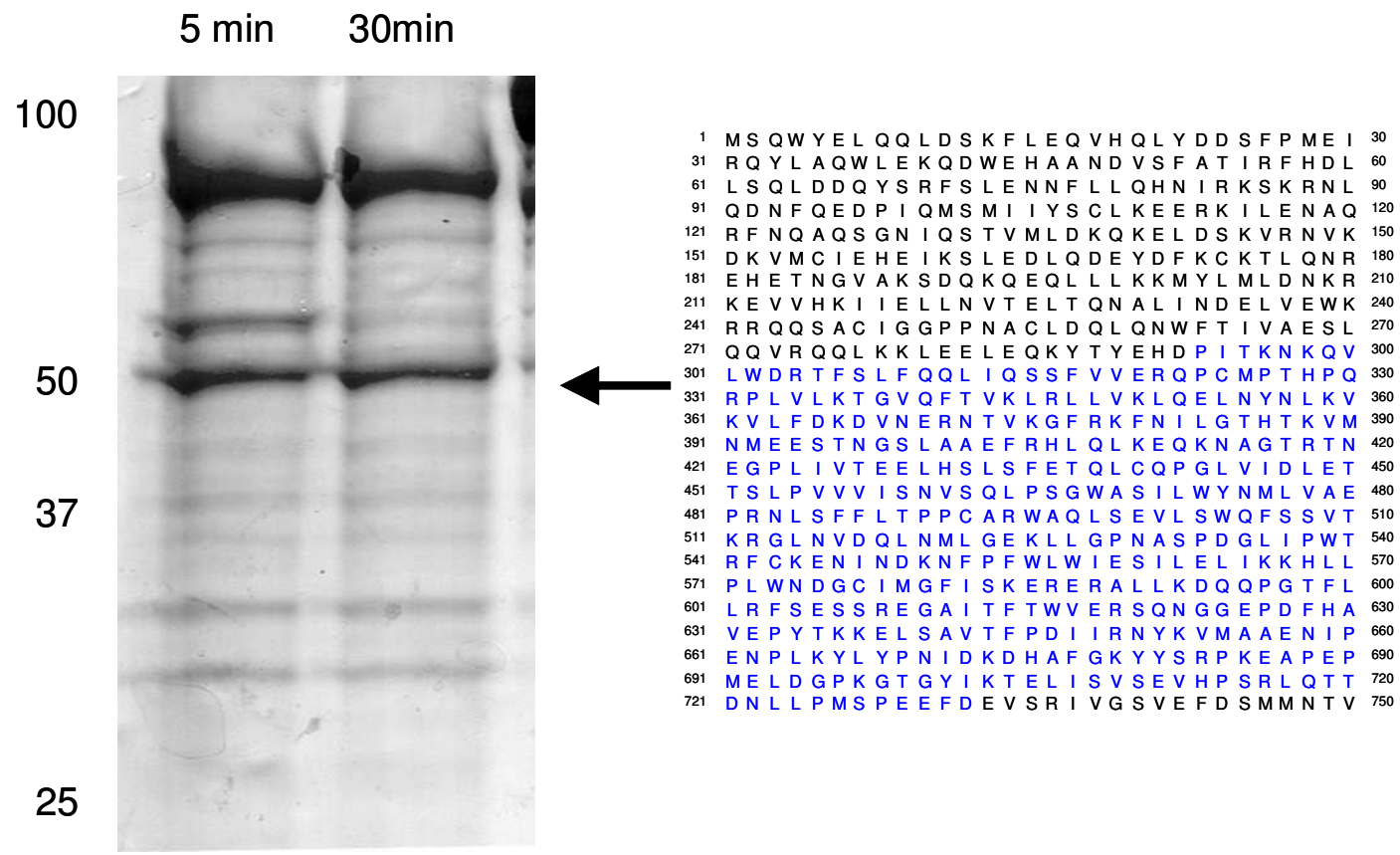

Figure 16: Coomassie SDS-PAGE of STAT1:ligand complex fractions respectively at 5 and 30 minutes of proteolytic digestion with Asp-N. The arrows indicate the bands excised and identified by Mass Spectrometry.

At 5 minutes of digestion we still saw the band around 60 kDa, which corresponded to the same fragment observed in the previous experiment (58196 Da; a.a. 172-674) (Figure 14-15). In addition Asp-N produced another band whose molecular weight was about 50 kDa. After 30 minutes of digestion this band (indicated by the arrows in the Figure 16) has been cut and identified by Mass Spectrometry. The MASCOT database search confirmed that the Asp-N digestion of STAT1:flavonoid complex produced a totally different fragment which was identified as 50393 Da (a.a. 293-732) (Figure 17).

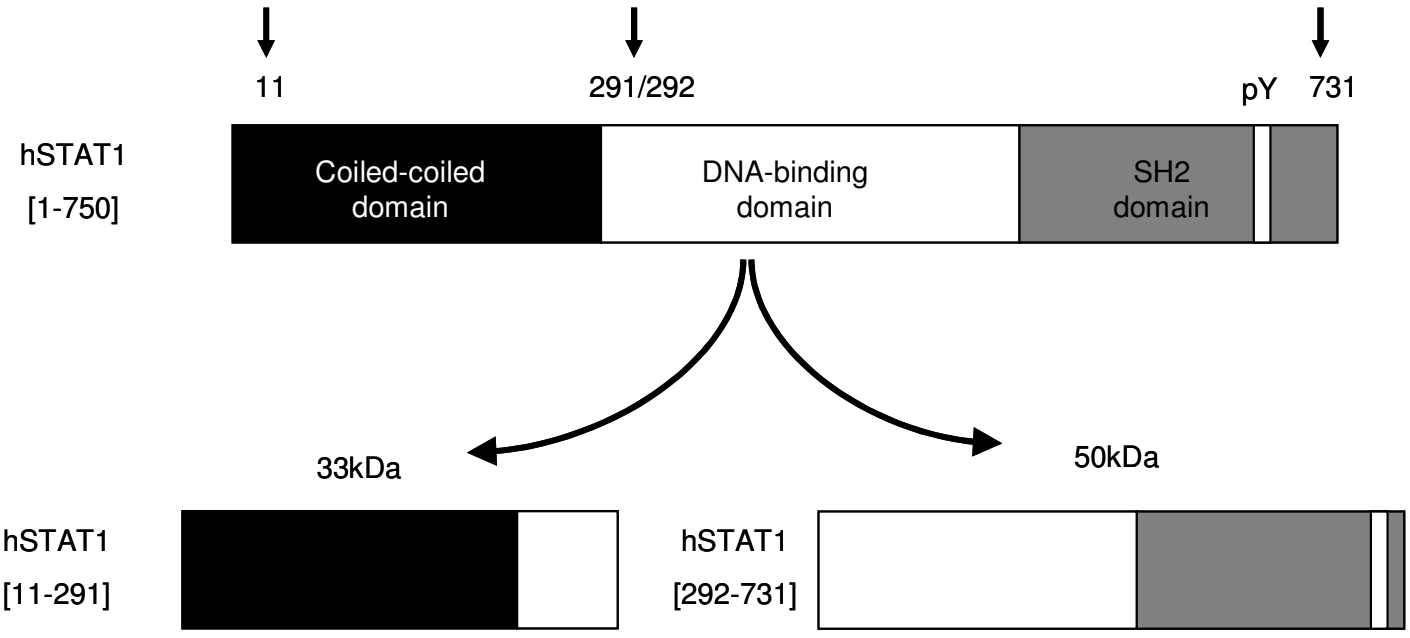

Figure 17: Representation of the digestion steps relative to STAT: ligand-limited proteolysis by Asp-N.

Finally, the data show that the tested flavonoids (EGCG, Myricetin and Delphinidin) protect the access of the protease to one or both termini of the proteolytic fragment 58196 Da (a.a. 172-674), favoring the cleavage of STAT1 in two new fragments: 33553 Da (a.a. 12-292) and 50393 Da (a.a. 293-732) (Figure 16-17). Therefore, taken together, data from Trypsin and Asp-N digestion led us to hypothesize that the binding sites of the flavonoids could be near to a.a. 172 (N-terminal) or 674 (C-terminal) of STAT1.

2.3 Flavonoid-interaction of N-and C- terminal domains by Surface Plasmon Resonance.

In order to distinguish between the two potential binding sites, we thought to investigate the flavonoid-binding ability of N- and

C-terminal domains of STAT1 by Surface Plasmon Resonance (SPR). N- and C-terminal truncation mutants of STAT1 produced by deletion mutagenesis can be therefore used to localize the ligand-binding sites.

In collaboration with the University of Padua, we tried to express and purify the recombinant N- and C-terminal truncation mutants of STAT1, but because of technical issues we were not able to get them. However, a truncated form of our protein (called *short* STAT1, *s*STAT1, Figure 18) lacking the first 134 a.a. has been expressed and used for the next experiments.

Therefore, we used an alternative way to obtain the N- and C-terminal domains of STAT1. By limited proteolysis with Trypsin we evaluated if the protein could be split in two main proteolytic fragments corresponding to the N- and C- terminal domains.

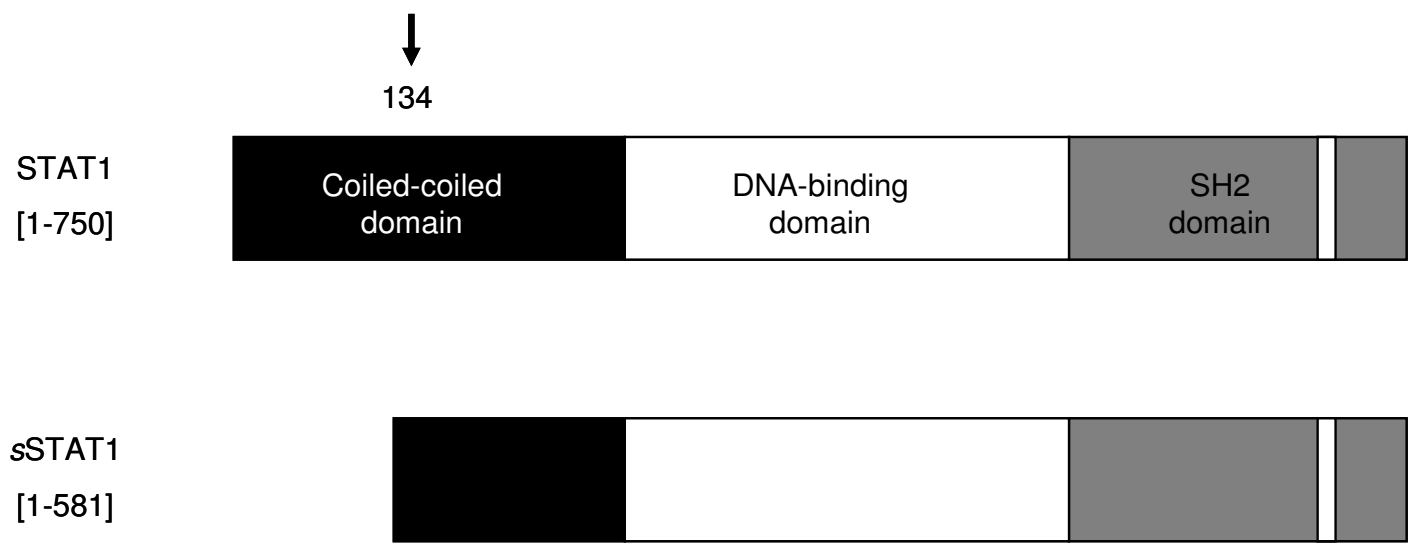

Figure 18: Representation of the sequences respectively of full length STAT1 and truncated mutant of STAT1 (short STAT1, sSTAT1).

Therefore, we digested *s*STAT1 with Trypsin (1:500 enzyme:substrate) and after 0, 5, 15 and 30 minutes of digestion we collected the samples which have been analyzed by MALDI MS and SDS-PAGE (Figure 19-20).

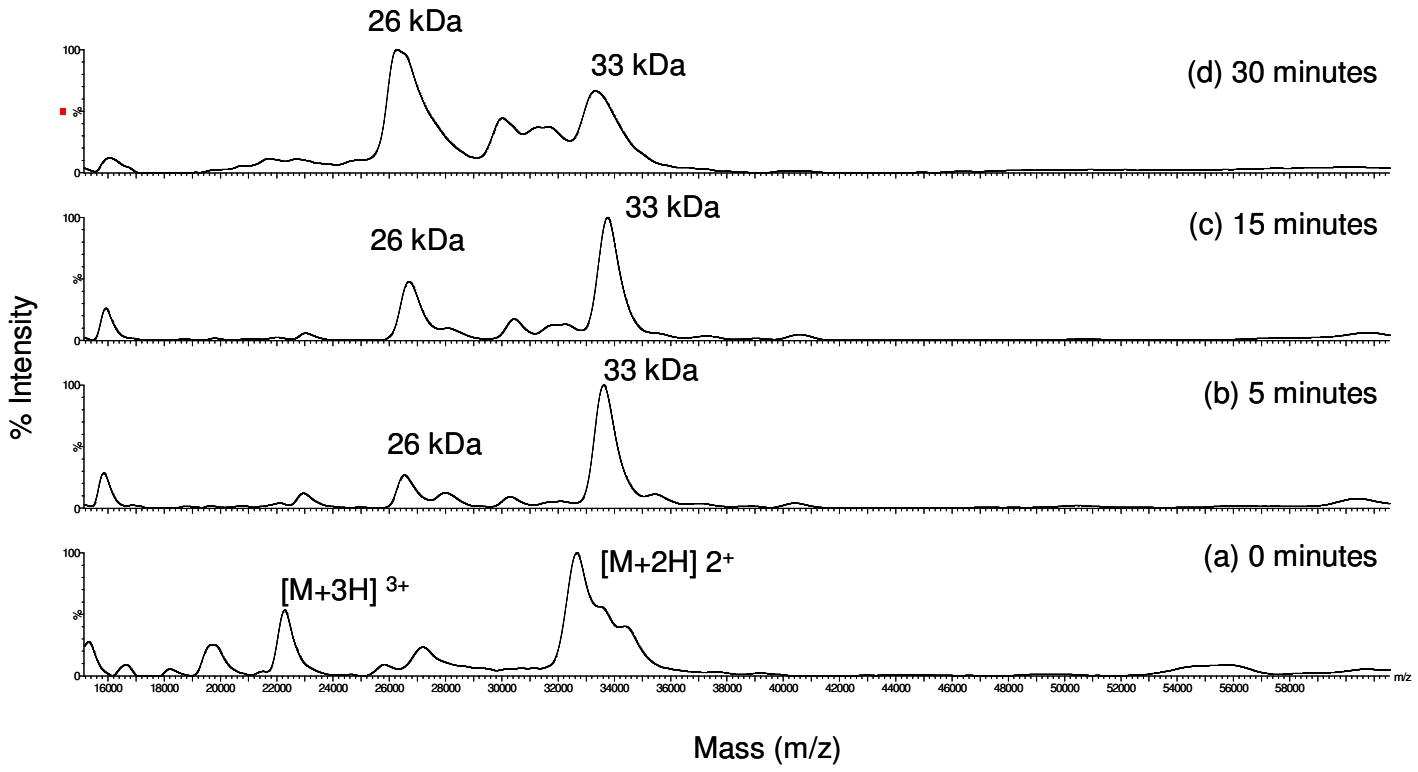

Figure 19: MALDI-TOF mass spectra of a (a) 0 min, (b) 5 min, (c) 5 min and (d) 30 min tryptic digest of a solution containing sSTAT1.

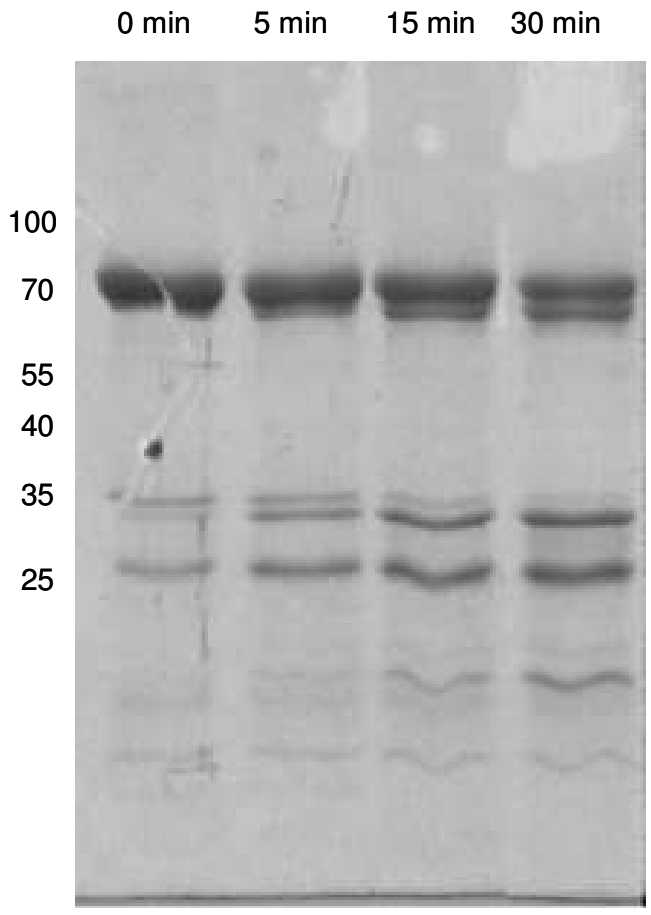

Figure 20: Coomassie SDS-PAGE of sSTAT1 solutions after 0, 5, 15 and 30 minutes of tryptic digestion.

According to MALDI MS spectra and Coomassie SDS-PAGE, the enzymatic digestion produced two main 26-kDa and 33-kDa fragments, which have been identified by Mass Spectrometry, respectively as C-terminal [a.a. 352-581 (26387 Da)] and N-terminal domains [1-287 (33750 Da)] (Figure 21).

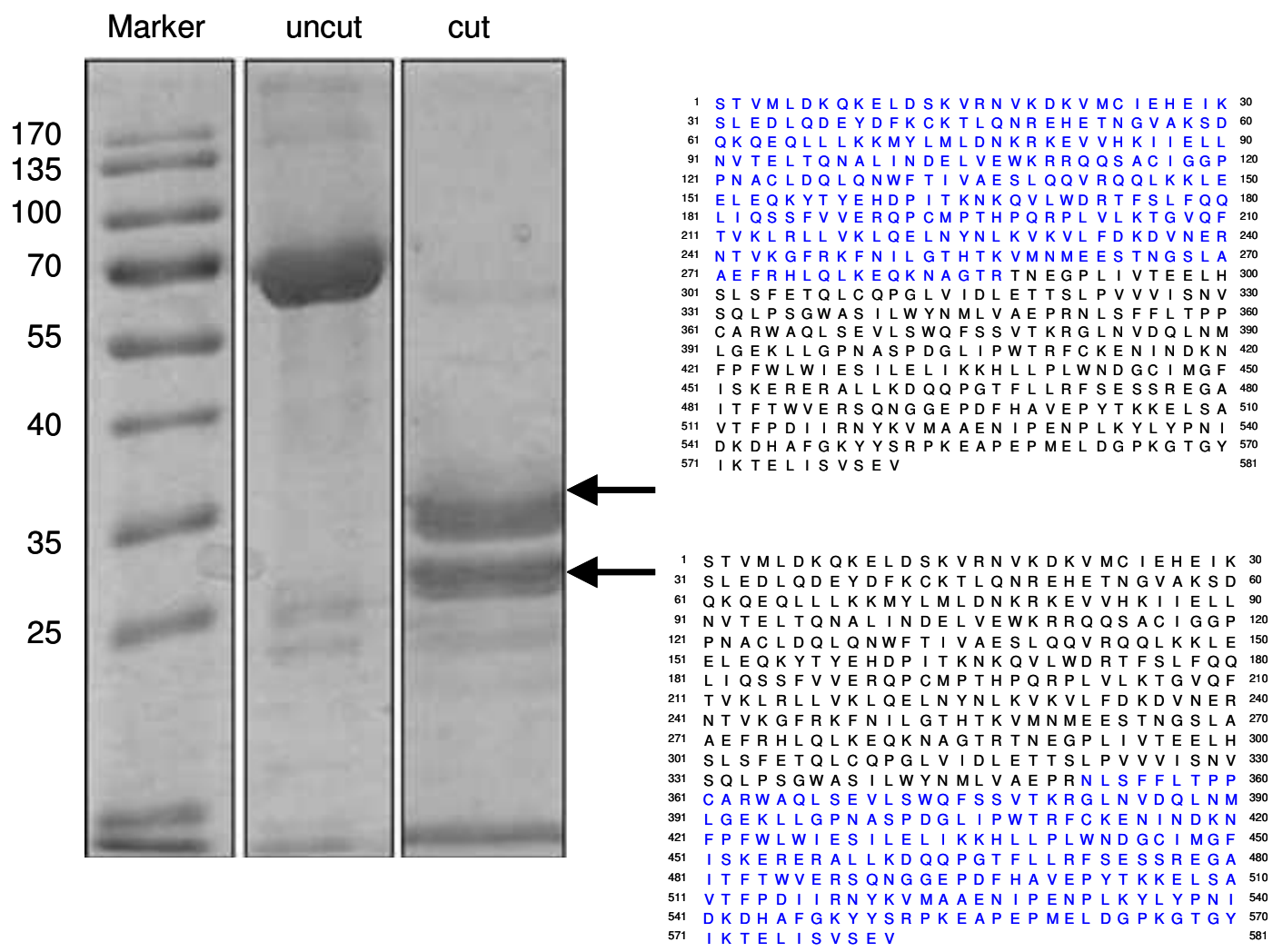

Figure 21: Coomassie SDS-PAGE of sSTAT1 solutions before and after 60 minutes of digestion. The arrows indicate the bands excised from the gel and identified by Mass Spectrometry.

To get enough material for the interaction analysis by SPR, we digested a huge amount of *s*STAT1 with Trypsin (1:500) for 60 minutes and we purified the two main fragments by RP-HPLC (Figure 22). As reported from the chromatogram, the red line corresponding to the digested solution, produced mainly two RP-HPLC peaks (indicated as #1 and #3) which have been collected and analyzed by SDS-PAGE (Figure 23), whereas the blue line represented the undigested solution of *s*STAT1 which is characterized only by one major RP-HPLC peak.

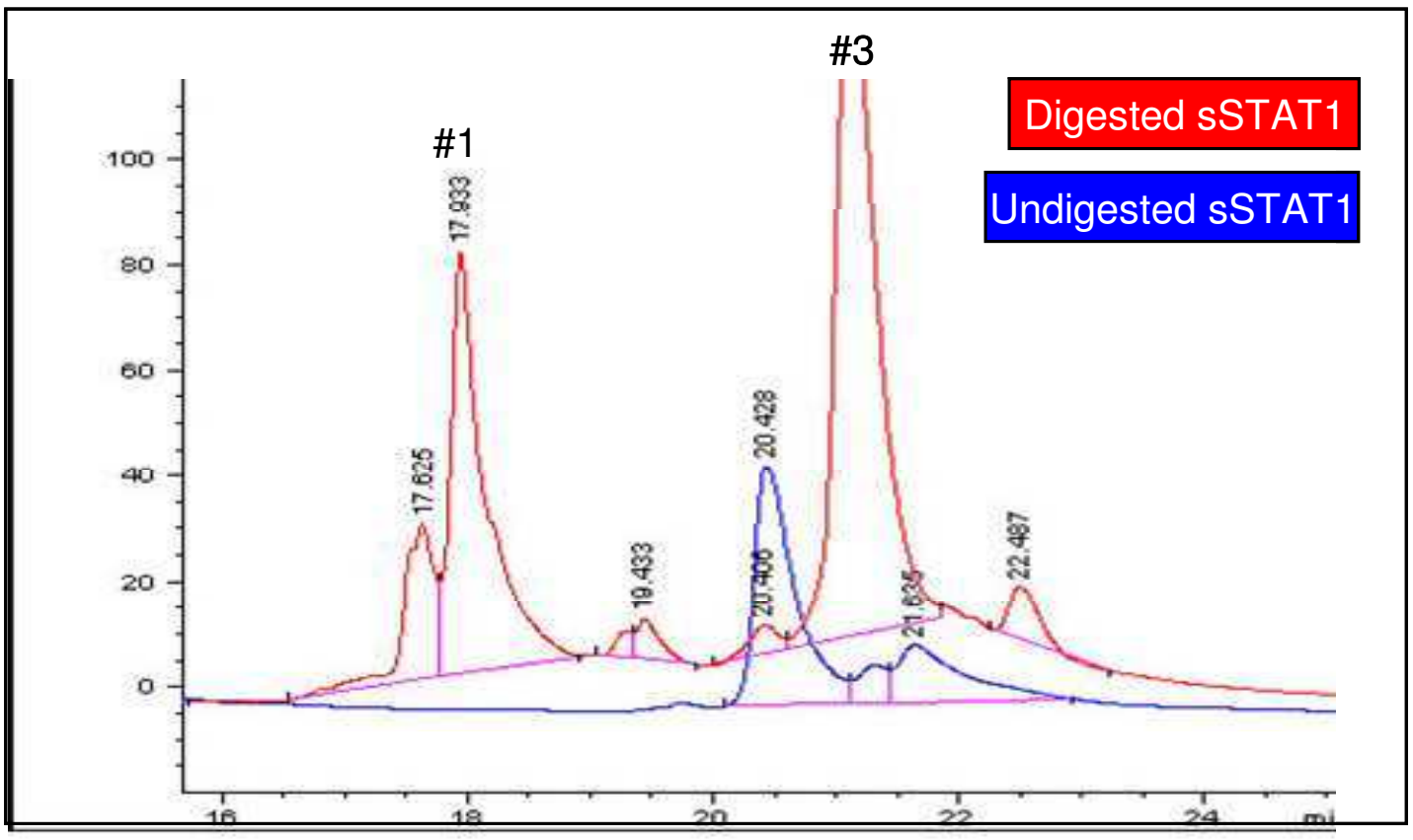

Figure 22: Chromatographic profile of undigested (blue line) and digested (red) of sSTAT1 after 60 minutes of tryptic digestion.

As illustrated in the Figure 23, aliquots of undigested and digested *s*STAT1 have been loaded onto the gel and have been compared with the purified fractions collected from HPLC. Each of the two HPLC purified fractions (#1 and #3) produced in the gel one main band corresponding exactly and respectively to the N- and C- terminal domains of *s*STAT1.

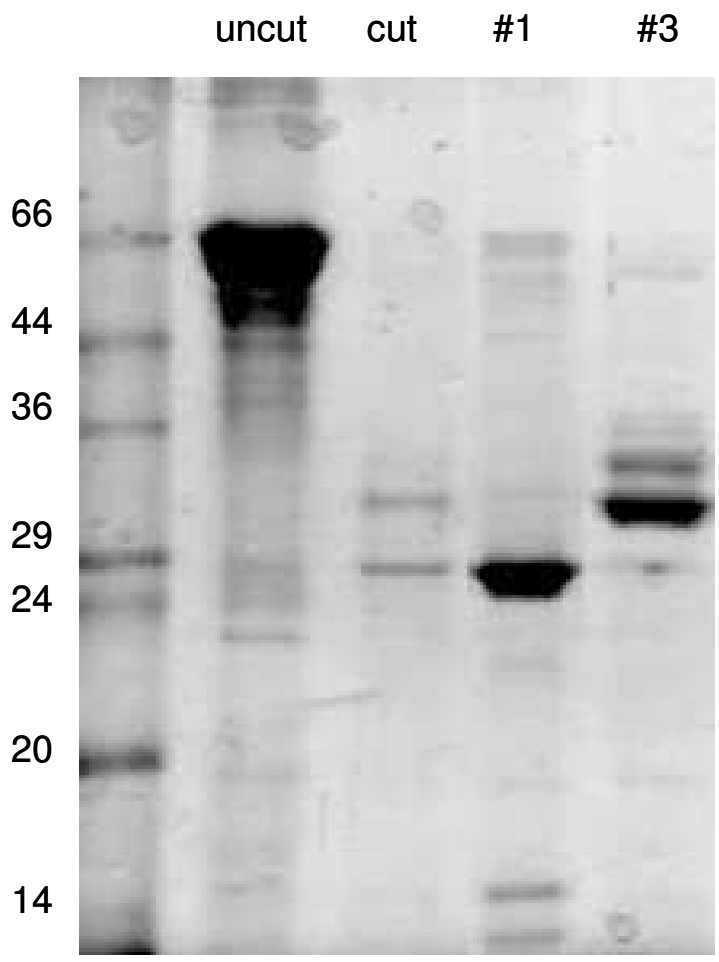

Figure 23: Coomassie SDS-PAGE of sSTAT1 undigested, digested and HPLC fractions solutions.

Moreover, to confirm their identity we excised the major bands from the #1 and #3 lanes and identified them by Mass Spectrometry.

Once we assigned the identification, we used the N- and C-terminal domains of sSTAT1 to evaluate the affinity and the binding specificity of our flavonoids by SPR.

Thus, we immobilized on a CM5 sensor chip the following solutions:

- undigested *s*STAT1.
- undigested and HPLC-purified *s*STAT1.
- HPLC-purified N- and C-terminal domains of *s*STAT1.

Flavonoid solutions (EGCG, Myricetin and Delphinidin) have been injected over at concentrations ranging from 0.5 to 10 µM.

In Figure 24 we reported the SPR sensograms relative to the interaction between EGCG and *s*STAT1.

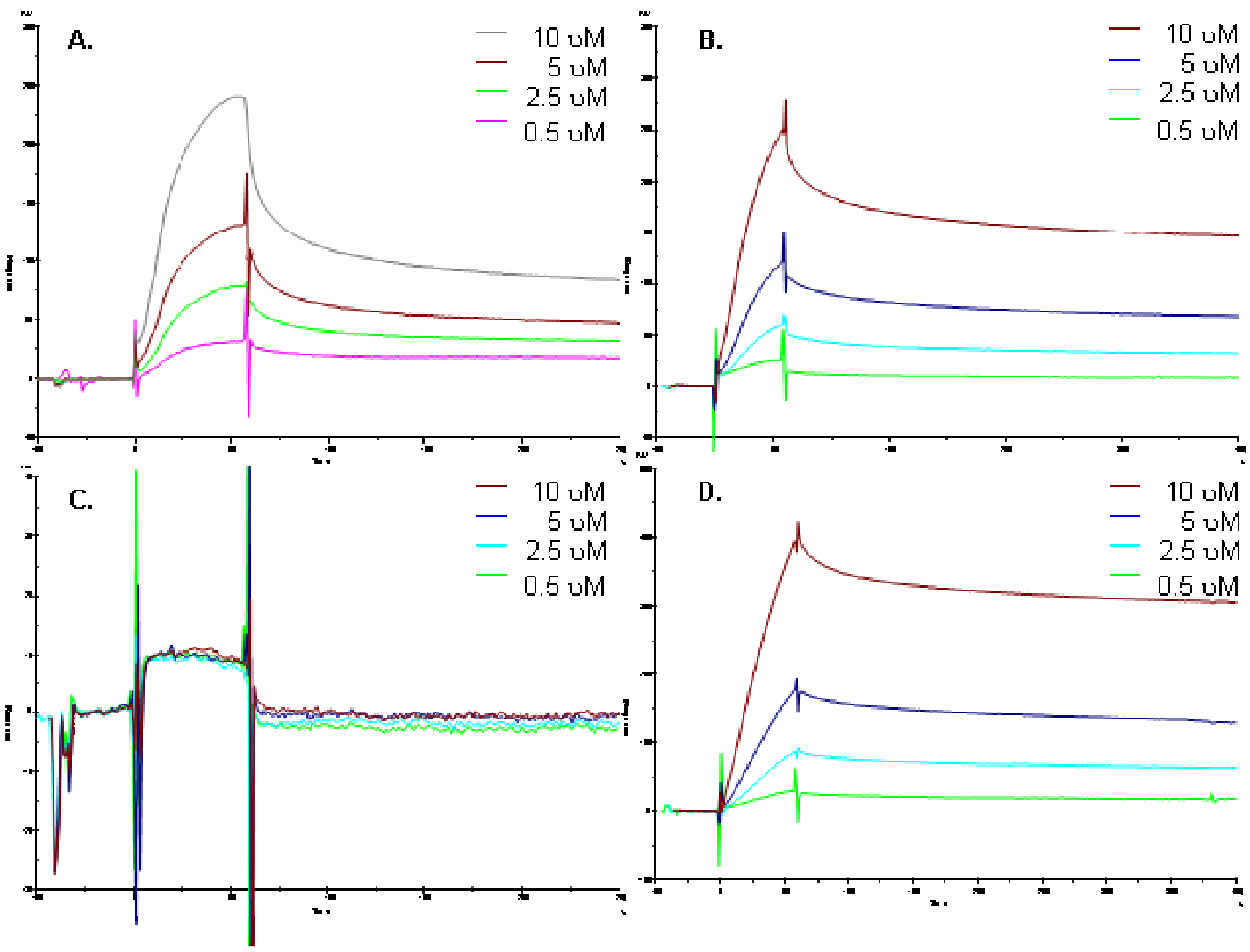

Figure 24: Sensograms obtained from the binding of EGCG at indicated different concentrations to (a) undigested sSTAT1; (b) undigested and HPLC-purified sSTAT1; (c) and (d) N- and C terminal domains of sSTATs, purified by HPLC.

As expected, undigested *s*STAT1, before and after HPLC purification, interacted with EGCG with an affinity comparable to that reported by Scarabelli et al. (Figure 24A and 24B). The increase of response units (RU) in the association phase and the slope of the dissociation phase of the complex are clearly dependent on the ligand concentration. Surprisingly, only C-terminal domain of *s*STAT1 was able to interact with EGCG

(Figure 24D), whereas the N-terminal fragment produced a typical curve shape (Figure 24C) corresponding to an absence of binding.

Therefore the flavonoid-interacting region is restricted to the C-terminal domain where we found one of the potential binding sites by Limited Proteolysis experiments.

Taken together, Limited Proteolysis and SPR data demonstrate that the flavonoids (EGCG, Myricetin and Delphinidin) binding sites of sSTAT1 are adjacent to Tyrosine residue 701 which is the phosphorylation site. This proves that the flavonoid protection of the hearth observed by Scarabelli et al. is due to the inhibition of STAT1 phosphorylation and therefore its activation.

CONCLUSIONS

-CHAPTER 3-

3.1 Conclusions

The limited proteolysis experiments followed by MALDI MS analysis of the resulting peptide maps, demonstrated herein, have been done to characterizing binding sites and protein conformation changes in protein-small molecule non-covalent complexes with μM dissociation constants. Determining small molecule binding sites is critical to investigators for designing drugs to inhibit protein function or designing molecules for molecular recognition applications.

In this Ph.D. work, we combined limited proteolysis and Surface Plasmon Resonance (SPR) analysis to identify the binding region of STAT1 with specific flavonoids (Epigallocatechin-3-gallate, Myricetin and Delphinidin). Knowing the interacting sites is an significant step to understand the molecular mechanism of antiSTAT1 flavoinds and it could help for the development of phytochemical-derived compounds capable of selectively inhibiting STAT1 activation in the prevention and/or treatment of inflammatory diseases in which STAT1 plays a critical role.

Therefore, we first assessed the conformational structure of STAT1 in flavonoid:complex by circular dichroism. Then, combining several bio-chemical approaches (Limited proteolysis/Mass Spectrometry/ Surface plasmon resonance) we tried to identify the interacting domain. Taken together, the limited proteolysis and SPR results suggest that the binding sites of STAT1 are likely close to the Tyrosine residue 701. Thus, we supposed that the flavonoids binding these sites could disturb

the phosphorylation of TYR701 and the following dimerization and activation of STAT1.

EXPERIMENTAL SECTION

-CHAPTER 4-

4.1 Materials

All employed solvents and reagents were HPLC grade and were purchased from Baker and Fluka, respectively. Myricetin, Delphinidin, EGCG and Quercetin were purchased from Sigma–Aldrich and human recombinant STAT1 was purchased from Enzo Life Sciences. For all experiments high purity water, obtained from a Milli-Q system (Millipore, Bedford, MA), was used.

4.2 Circular dichroism spectroscopy

Circular dichroism measurements were performed using a Jasco J- 810 spectrometer equipped with a cell holder thermostatically controlled by a circulating water bath. Measurements were recorded at
25 °C, with an 8 s time constant and 5 nm/min and averaged for ten acquisitions. The protein concentration was 0.2 μM and spectra were collected with rectangular quartz cells of 1 cm path length. The spectra were the average of 10 accumulations from 190 to 260 nm, recorded with a band width of 1 nm, at a scanning speed of 50 nm/min.
Complex formation between STAT1 and ligands was analyzed in a 200 μM Tris buffer, at pH 7.5, incubating the protein with 20/40/80:1 molar excess of ligand for 10 min at room temperature. Spectra were recorded before and after the addition of the ligand and routinely subtracted by blanks, corrected for the background signal and for dilution effects. Each condition

was analyzed al least three times. Cotton effects are reported as molar ellipticity. Estimation of the secondary structure composition was carried out using the K2D algorithm by DICROWEB [27].

4.3 Limited Proteolysis experiments

Time resolved limited proteolysis of STAT1 and STAT1/ligands were performed using sequencing grade modified trypsin (Promega, Madison, WI) in a 300:1 protein:enzyme wt:wt ratio or using Endoproteinase Asp-N (Sigma–Aldrich) in a 150:1 protein:enzyme wt:wt ratio . STAT1 (4 μM) and a STAT1:ligand mixture (4:40 μM) in 10 mM ammonium acetate (pH 7.7) were digested simultaneously. A 1 μL aliquot of each digest was extracted after 5, 15, 30, 60 min of digestion. To quench trypsin/Asp N activity, each 1 μL aliquot was added to 0.5 μL of 0.1% TFA (pH 1.9).

4.4 MALDI MS analysis

All MALDI experiments were carried out using a Waters Micromass MALDI micro MX mass spectrometer with time-of-flight (TOF) analyzer (Waters Micromass, Milford, MA). All sample solutions were mixed in a 1:1 volume ratio with a matrix solution. For linear mode the matrix solution consisted of e 10mg/mL sinapinic acid in 4:6 AcN:0.1% TFA. . 0.8 μL of each sample matrix mixture was spotted on the target plate and allowed to dry under moderate vacuum for approximately 1

minute. The acceleration voltage was set to 20 kV for all experiments, and typically 50 single-shot mass spectra were summed to give a composite spectrum. All data were reprocessed using Waters MassLynx software. The mass scale was calibrated externally using a mixture Cytochrome-C, Myoglobin and Albumin.

4.5 Assignment of protease cleavage sites

The positions of the protease cleavage sites in the STAT1 amino acid sequence were identified by considering the molecular masses of the polypeptide fragments detected by MALDI-MS and the specificity of the proteases used. The search of the corresponding fragments in the amino acid sequence of STAT1 was carried out using the program PAWS (http://bioinformatics.genomicsolutions.com/Paws.html). The molecular masses of all peptides measured matched the theoretical ones, obtained from the STAT1 amino acid sequence, within an accuracy of 0.15% or better.

4.6 Surface Plasmon Resonance analysis

Interaction analysis were performed using Biacore 3000 equipped with research-grade CM5 sensor chip (GE Healthcare, UK). Amine coupling reagents (EDC, NHS, ethanolamine HCl) were purchased from GE Healthcare, UK and used as described in Biacore User Manual to immobilize STAT1 and its derivates

in 1X PBS pH 7.4 at 30 mg/ml. Four different concentrations of ligands were prepared from 50 to 10000 nM diluted in 1X PBS at 2% methanol and each was injected in triplicate at flow rate of 10, 20 and 30 ml/min using the KINJECT command. The dissociation of enzyme/small molecule was monitored for 300 s and between sample injections, the sensor chip was efficiently regenerated by NH2OH injection cycle. Data collected on SPR biosensor were processed by BiaEvaluation Program from GE Healthcare, UK through 1:1 Langmuir drift baseline algorithm. The effect of 2% of MeOH has been taken into account during the data processing.

4.7 SDS-PAGE electrophoresis

Different solutions of STAT1 (before and after chromatographic separations) were separated in 12% SDS-PAGE (handmade). Proteins were then stained overnight using Coomassie colloidal blue. The molecular weight of the proteins was estimated using protein molecular weight standards.

4.8 High-Performance Liquid Chromatography (HPLC)

Finally, aliquots of the undigested and digested sSTAT1 solutions (20µg of protein) have been purified by reverse-phase HPLC on a Vydac C4 column (5µm, 2.1mm ID x 250mm L) using a Waters HPLC instrument and an elution system consisting of 0.1% TFA (solvent A) and 95% acetonitrile (ACN)

in 0.07% TFA (solvent B). Protein separation was achieved by means of a linear gradient from 25 to 75% solvent B over 30 min. Elution was monitored at 220 nm. Multiple main fractions have been manually collected, dried in a Speed-Vac centrifuge (Savant) and stored at -20°C.

4.9 In-gel tryptic digestion and RP-LC-MS/MS analysis

Each gel spot was destained in 25 mM ammonium hydrogencarbonate, 50 mM ammonium hydrogencarbonate/acetonitrile 1:1 and covered with acetonitrile until gel pieces shrunk. Gel spots were washed in 25 mM ammonium hydrogencarbonate, 50 mM ammonium hydrogen carbonate/acetonitrile 1:1 and covered with acetonitrile until gel pieces shrunk. Residual acetonitrile was removed and the gel pieces dried by centrifugation under vacuum by SPD SpeedVac. In-gel digestion was performed by adding 12.5 ng/ml of bovine trypsin (Promega Madison, WI, USA) in 25 mM ammonium hydrogen carbonate at 37°C overnight under stirring. The resulting peptides were extracted and analysed by LC/MS/MS: peptide separation was performed on a capillary BEH C18 column (0.075 mm x 100 mm, 1.7 mm Waters) using aqueous 0.1% formic acid (A) and CH3CN containing 0.1% formic acid (B) as mobile phases. Peptides were eluted by means of a linear gradient from 5% to 50% of B in 45 min and a 300 nL/min flow rate. Capillary ion source voltage was set at 2.5 kV, cone voltage at 35 V, and extractor voltage at 3 V. Peptide fragmentation was achieved using argon as collision gas and a

collision cell energy of 25 eV. Mass spectra were acquired in a m/z range from 500 to 1800, and MS/MS spectra in a 25e2000 range. Mass and MS/MS spectra calibration was performed using a mixture of angiotensin and insulin as external standard and [Glu]-Fibrinopeptide B human as lock mass standard. Selected spots were subjected to identification by Mascot search of MS/MS data from the peptide digest with databases (NCBI, MSDB and SWISS-PROT). MS/MS data that did not match in the Mascot search, were subjected to de novo sequencing by using Mascot Distiller software (version 2.3.2, Matrix Science, London, UK).

Bibliography

[1] Borch, J.; Jørgensen, T. J. D.; Roepstorff, P. Mass Spectrometric Analysis of Protein Interactions. Curr. Opin. Chem. Biol. 2005, 9, 509 –516.

[2] Seielstad, D. A.; Carlson, K. E.; Kushner, P. J.; Greene, G. L.; Katzenellenbogen, J. A. Analysis of the Structural Core of the Human Estrogen-Receptor Ligand-Binding Domain by Selective Proteolysis Mass Spectrometric Analysis. Biochemistry 1995, 34, 12605–12615.

[3] Leite, J. F.; Amoscato, A. A.; Cascio, M. Coupled Proteolytic and Mass Spectrometry Studies Indicate a Novel Topology for the Glycine Receptor. J. Biol. Chem. 2000, 275, 13683–13689.

[4] Gervasoni, P.; Staudenmann, W.; James, P.; Pluckthun, A. Identification of the Binding Surface on β-Lactamase for Groel by Limited Proteolysis and MALDI Mass Spectrometry. Biochemistry 1998, 37, 11660 –11669.

[5] Spolaore, B.; Bermejo, R.; Zambonin, M.; Fontana, A. Protein Interactions Leading to Conformational Changes Monitored by Limited Proteolysis: Apo Form and Fragments of Horse Cytochrome c. Biochemistry 2001, 40, 9460 –9468.

[6] Cohen, S. L.; Ferredamare, A. R.; Burley, S. K.; Chait, B. T. Probing the Solution Structure of the DNA-Binding Protein Max by a Combination of Proteolysis and Mass Spectrometry. Protein Sci. 1995, 4, 1088 –1099.

[7] Schechter, I.; Berger, A. On the Size of the Active Site in Proteases. Biochem. Biophys. Res. Commun. 1967, 27, 157–162.

[8] Rodger A, Marrington R, Roper D, Windsor S. Circular dichroism spectroscopy for the study of protein-ligand interactions. Methods Mol Biol. 2005;305:343-64.

[9] Levy DE, Darnell JE Jr., Stats: transcriptional control and biological impact. Nat Rev Mol Cell Biol. 2002 Sep;3(9):651-62.

[10] Williams JG., STAT signalling in cell proliferation and in development. Curr Opin Genet Dev. 2000 Oct;10(5):503-7.

[11] Durbin, J. E., Hackenmiller, R., Simon, M. C. & Levy, D. E. Targeted disruption of the mouse Stat1 gene results in compromised innate immunity to viral disease. Cell 84, 443–450 (1996).

[12] Meraz, M. A. et al. Targeted disruption of the Stat1 gene in mice reveals unexpected physiologic specificity in the JAK–STAT signaling pathway. Cell 84, 431–442 (1996).

[13] Park, C., Li, S., Cha, E. & Schindler, C. Immune response in Stat2 knockout mice. Immunity 13, 795–804 (2000).

[14] Dupuis, S. et al. Impairment of mycobacterial but not viral immunity by a germline human STAT1 mutation. Science 293, 300–303 (2001).

[15] Ostrand-Rosenberg S, Sinha P, Clements V, Dissanayake SI, Miller S, Davis C, Danna E. Signal transducer and activator of transcription 6 (Stat6) and CD1: inhibitors of immunosurveillance against primary tumors and metastatic disease. Cancer Immunol Immunother. 2004 Feb;53(2):86-91. Epub 2003 Oct 30.

[16] Blume-Jensen, P. & Hunter, T. Oncogenic kinase signalling. Nature 411, 355–365 (2001).

[17] Kaplan, D. H. et al. Demonstration of an interferon - dependent tumor surveillance system in immunocompetent mice. Proc. Natl Acad. Sci. USA 95, 7556–7561 (1998).

[18] Lee, C. K., Smith, E., Gimeno, R., Gertner, R. & Levy, D. E. STAT1 affects lymphocyte survival and proliferation partially independent of its role downstream of IFN-. J. Immunol. 164, 1286–1292 (2000).

[19] Lee, C. K. et al. Distinct requirements for IFNs and STAT1 in NK cell function. J. Immunol. 165, 3571–3577 (2000).

[20] Shankaran, V. et al. IFN and lymphocytes prevent primary tumour development and shape tumour immunogenicity. Nature 410, 1107–1111 (2001).

[21] Bowman, T. & Jove, R. STAT Proteins and cancer. Cancer Control 6, 615–619 (1999).

[22] Bromberg, J. F. et al. Stat3 as an oncogene. Cell 98, 295–303 (1999).

[23] Bowman, T., Garcia, R., Turkson, J. & Jove, R. STATs in oncogenesis. Oncogene 19, 2474–2488 (2000).

[24] Song, J. I. & Grandis, J. R. STAT signaling in head and neck cancer. Oncogene 19, 2489–2495 (2000).

[25] Stephanou A, Brar BK, Scarabelli TM, Jonassen AK, Yellon DM, Marber MS, Knight RA, Latchman DS. Ischemia-induced STAT-1 expression and activation play a critical role in cardiomyocyte apoptosis. J Biol Chem. 2000 Apr 7;275(14):10002-8.

[26] Scarabelli TM, Mariotto S, Abdel-Azeim S, Shoji K, Darra E, Stephanou A, Chen-Scarabelli C, Marechal JD, Knight R, Ciampa A, Saravolatz L, de Prati AC, Yuan Z, Cavalieri E, Menegazzi M, Latchman D, Pizza C, Perahia D, Suzuki H. Targeting STAT1 by myricetin and delphinidin provides efficient protection of the heart from ischemia/reperfusion-

induced injury. FEBS Lett. 2009 Feb 4;583(3):531-41. Epub 2008 Dec 29.

[27] Whitmore L., Fallace B.A. (2004) DICHROWEB, an online server for protein secondary structure analysis from circular dichroism spectroscopic data. Nucleic Acids Res;32:668–673.

ROLE OF PDIA6-BIP COMPLEX IN THE REGULATION OF THE UNFOLDED PROTEIN RESPONSE

INTRODUCTION

-CHAPTER 5-

Endoplasmic reticulum stress and unfolded protein response

5.1 Endoplasmic reticulum

The endoplasmic reticulum (ER) is an organelle of cells in eukaryotic organisms that forms an interconnected network of tubules, vesicles, and cisternae (Figure 25). Its membrane typically constitutes more than half of the total membrane of an average animal cell [28]. The tubules and sacs are all thought to interconnect, so that the ER membrane forms a continuous sheet enclosing a single internal space. This highly convoluted space is called the ER lumen or the ER cisternal space, and it often occupies more than 10% of the total cell volume. The ER membrane separates the ER lumen from the cytosol, and it mediates the selective transfer of molecules between these two compartments.

Figure 25: picture of the endoplasmic reticulum.

There are two types of ER: rough, which is coated with ribosomes, and smooth, which isn't.

Rough endoplasmic reticula (RER) have several functions:

- Lysosomal enzymes with a mannose-6-phosphate marker added in the cis-Golgi network.
- Secreted proteins, either secreted constitutively with no tag or secreted in a regulatory manner involving clathrin and paired basic amino acids in the signal peptide.
- Integral membrane proteins that stay embedded in the membrane as vesicles exit and bind to new membranes. Rab proteins are key in targeting the membrane; SNAP and SNARE proteins are key in the fusion event.
- Initial glycosylation as assembly continues. This is N-linked (O-linking occurs in the golgi).
    - N-linked glycosylation: If the protein is properly folded, glycosyltransferase recognizes the AA sequence NXS or NXT (with the S/T residue phosphorylated) and adds a 14-sugar backbone (2-N-acetylglucosamine, 9-branching mannose, and 3-glucose at the end) to the side-chain nitrogen of Asn.

The smooth endoplasmic reticulum (SER) is involved in several metabolic processes, including synthesis of lipids and steroids, metabolism of carbohydrates, regulation of calcium concentration, drug detoxification, attachment of receptors on cell membrane proteins, and steroid metabolism.

5.1.2 Folding function of the ER and UPR machinery.

A common feature of any protein is its requirement for a specific three-dimensional structure to fulfil its biological function. The ER is a major site of protein synthesis with many nascent polypeptides being co-translationally translocated into and across its membrane. These polypeptides pass through the translocation sites of the ER membrane as partially unfolded polypeptide chains. It should therefore be no surprise that the inside, or lumen, of the ER functions as a specialised folding environment and that it contains a number of molecular chaperones and folding factors [29]. This ensures that as newly synthesised polypeptides enter the ER lumen, the nascent chains begin to fold rapidly into their native structures.

One of the ER chaperone proteins is binding immunoglobulin protein (BiP), also known as 78 kDa glucose-regulated protein (GRP-78) or heat shock 70 kDa protein 5 (HSPA5). Like other chaperones, BiP recognizes incorrectly folded proteins, as well as protein subunits that have not yet assembled into their final oligomeric complexes. To do so, it binds to exposed amino acid sequences that would normally be buried in the interior of correctly folded or assembled polypeptide chains. An example of a BiP-binding site is a stretch of alternating hydrophobic and hydrophilic amino acids that would normally be buried in a β sheet. The bound BiP both prevents the protein from aggregating and helps to keep it in the ER (and thus out of the Golgi apparatus and later parts of the secretory pathway). Like the hsp70 family of proteins, which bind unfolded proteins in

the cytosol and facilitate their import into mitochondria and chloroplasts, BiP hydrolyzes ATP to provide the energy for its roles in protein folding and posttranslational import into the ER. Despite all the help from chaperones, many protein molecules (more than 80% for some proteins) translocated into the ER fail to achieve their properly folded or oligomeric state. Folding failures are then retrotranslocated to the cytosol, where they are submitted to ubiquitination and proteasomal degradation, a process referred to as ER-associated degradation (ERAD).

Cells carefully monitor the amount of misfolded proteins they contain in various compartments. If ER function is perturbed by various pathological conditions, the entry of newly synthesized proteins may exceed the folding and modification capacity, resulting in accumulation of unfolded proteins and ER stress. This accumulation leads to an activation of signaling events known as the Unfolded Protein Response (UPR) which should rebalance folding capacity and folding demand within the ER (Figure 26).

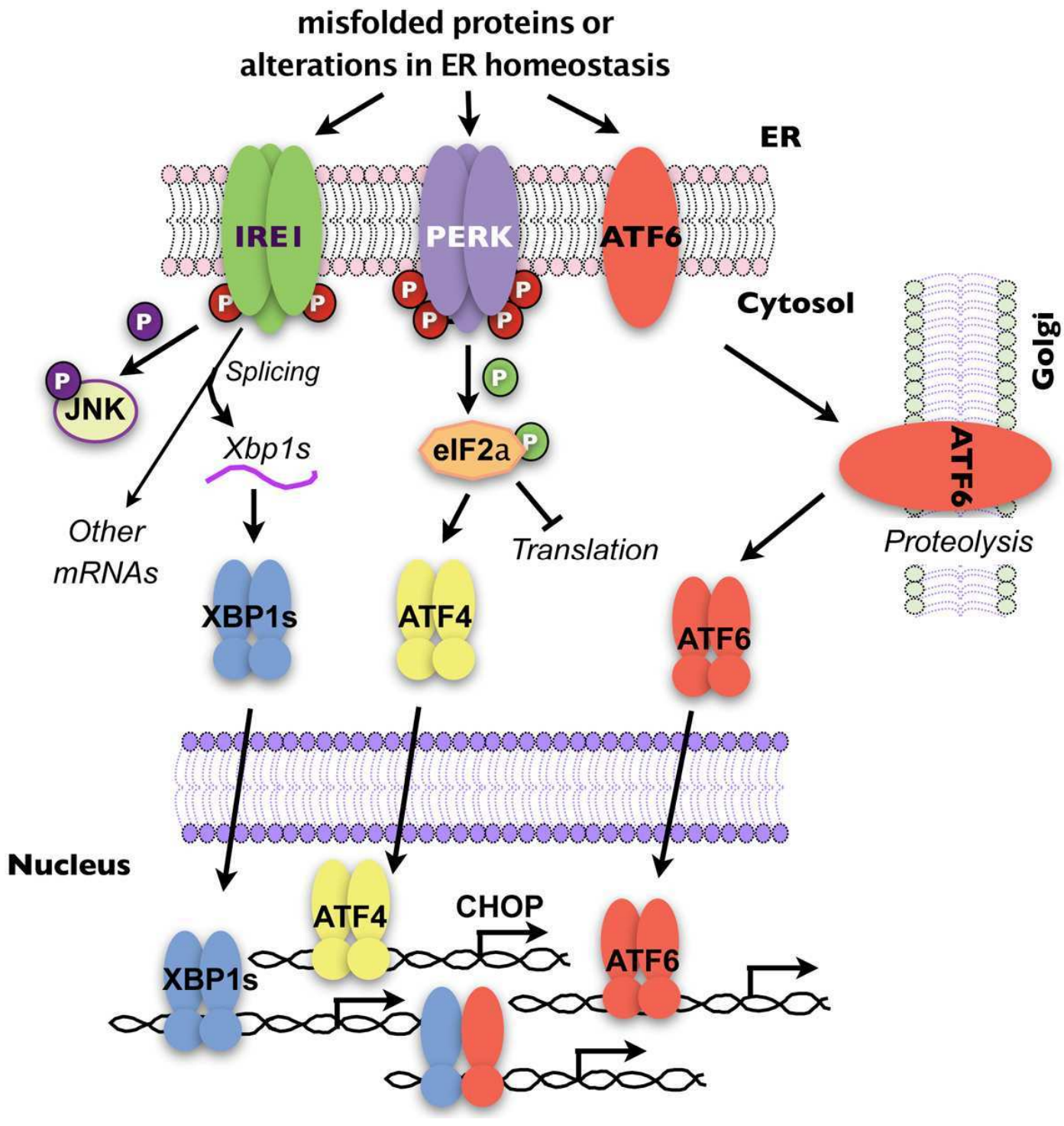

Figure 26: Illustration of the Unfolded Protein Response machinery.

On a cellular level, the adaptive phase of the UPR triggers three kinds of protective cellular responses: (i) up-regulation of ER chaperones such as BiP/GRP78 to assist in the refolding of proteins [30]; (ii) attenuation of protein translation which is mediated by the serine–threonine kinase PERK which phosphorylates the initiation factor—eIF2a thereby reducing translation [31]; and (iii) degradation of misfolded proteins by

the proteasome by a process called ER associated degradation (ERAD) [32]. These three responses are protective measures to limit protein load and alleviate ER stress. When adaptation fails, ER-initiated pathways signal alarm by activating NF-kB, a transcription factor that induces expression of genes encoding mediators of host defense [33]. Excessive and/prolonged stress leads to a maladaptive response and apoptosis [34].

Such homeostatic control is achieved through the action of signal transduction pathways that have sensors facing the ER lumen and effectors that convey the message to other compartments of the cell. Three different classes of ER stress transducers have been identified. Each class defines a distinct arm of the UPR that is mediated by inositol-requiring protein-1 (IRE1), activating transcription factor-6 (ATF6) or protein kinase RNA (PKR)-like ER kinase (PERK). In each case, an integral membrane protein senses the protein folding status in the ER lumen and transmits this information across the ER membrane to the cytosol [35].

The first stress transducer identified has been IRE1, which is a type 1 ER-resident transmembrane protein with a novel lumenal domain and a cytoplasmic portion that contains a protein kinase domain. In response to unfolded proteins, IRE1 oligomerizes in the plane of the membrane, allowing for trans-autophosphorylation of juxtaposed kinase domains. Trans-autophosphorylation of the kinase domain of IRE1 activates its unusual effector function, which causes the precise endonucleolytic cleavage of the only known substrate: an mRNA that encodes a transcription factor named Hac1 (homologous to ATF/CREB1) in yeast [36-37] or XBP1 (X-box

binding protein-1) in metazoans [38-39]. IRE1 is therefore a bifunctional enzyme, possessing both a protein kinase and a site-specific endoribonuclease that is regulated by its intrinsic kinase module. The IRE1-dependent splicing event causes, in yeast and in metazoans, the activation of UPR.

A search for additional proteins that bind UPR-activated promoter elements led to the identification of ATF6, a founding member of a novel class of metazoan-specific ER stress transducers. ATF6 is e synthesized as inactive precursor, tethered to the ER membrane by a transmembrane segment and have a stress-sensing portion that projects into the ER lumen. Under conditions of ER stress, ATF6 is transported from the ER to the Golgi apparatus, where it is cleaved by Golgi-resident proteases, first by S1P (site 1 protease) and then in an intramembrane region by S2P (site 2 protease) to release the cytosolic DNA-binding portion, ATF6f ('f' for fragment). From there, ATF6f moves to the nucleus to activate gene expression [40]. ATF6 probably activates a subset of UPR target genes, although these remain to be characterized.

The third ER stress transducer, PERK, superficially resembles IRE1. Both are ER-localized type I transmembrane proteins with lumenal stress-sensing domains that are phylogenetically related, similar in structure and function. The cytoplasmic portion of PERK also contains a protein kinase domain, which undergoes activating trans-autophosphorylation by oligomerization in ER-stressed cells; however, unlike IRE1, for which the only substrate is itself, PERK phosphorylates the α-subunit of eukaryotic translation initiation factor-2 (eIF2α) at Ser51. This phosphorylation inhibits the guanine nucleotide

exchange factor eIF2B, a pentameric complex that recycles eIF2 to its active GTP-bound form. Lower levels of active eIF2 result in lower levels of translation initiation, globally reducing the load of newly synthesized proteins, many of which are destined to enter the already stressed ER lumen [41]. In addition to decreasing global protein synthesis to reduce the ER load, PERK-mediated eIF2α phosphorylation also contributes to transcriptional activation in the UPR. Several other signaling pathways unrelated to ER stress also converge on eIF2α phosphorylation and activate a common set of target genes. Because of this integrative feature, signaling downstream of phosphorylated eIF2α was termed the integrated stress response (ISR) [42]. There is little doubt that cells must tightly regulate the level of phosphorylated eIF2α to survive. PERK activation by ER stress is rapidly reversible and, within minutes of restoring ER homeostasis, activated PERK is dephosphorylated. The regulatory mechanisms and the phosphatase(s) involved remain unknown, but it has been established that phosphorylated eIF2α is also subject to negative regulation.

The three arms of the UPR can communicate with each other or activate independently in ER-stressed cells. It is still not clear the contribution from single transducer. The only thing known is that the UPR protects cells against normal and unusual levels of ER stress by enhancing the capacity of the secretory apparatus and by reducing ER load.

Even if the understanding of the aspects of gene activation in the UPR is rudimentary, it is time to begin to consider the implications of manipulating signaling in the UPR. For example,

drugs targeting PERK and IRE1 selectively could be found and evaluated their effects on cells.

The mechanism by which the three sensors activate remains disputed. One model proposes that transducers activity is mainly regulated by the ER-resident chaperone BiP. In this model, BiP inhibits sensors activity by binding to them in the absence of stress. During stress, BiP is titrated away by unfolded proteins, leaving the sensor free to oligomerize and activate [43]. An alternative model of sensor regulation postulates that unfolded proteins bind to the lumenal domain of the sensor, triggering it self-association and activation of its cytoplasmic effector domains. Recently a hybrid, two-step model for UPR regulation has been proposed in which both BiP and unfolded proteins regulate the sensors: initial dissociation of BiP from the sensor drives its oligomerization, while subsequent binding to unfolded proteins leads to its activation [44].

5.2 BiP-GRP94

BiP has been already showed above as an ER molecular chaperone which drives the folding of proteins for secretory pathways. Another ER chaperone protein which also plays critical roles in folding and/or assembly of secreted and membrane proteins is Heat shock protein 90kDa beta member 1 (HSP90B1), known also as endoplasmin, GP96, GRP94 and ERp99. As reported by Melnick et al. [45], GRP94 and BiP are two ER proteins which can cooperate in the maturation step of secreted proteins. Indeed, once synthesized light and heavy

chains come into the ER and associate sequentially to two ER stress proteins: BiP and GRP94. They first bind to BiP presumably through promiscuously exposed hydrophobic sequences after their translocation into the ER and then they bind to GRP94 with an interaction biochemically, kinetically and structurally distinct from BiP.

It is also true that some clients do not require both of these chaperones: many proteins associate with BiP but not GRP94, and at least one, Insulin-like growth factor (IGF), interacts with GRP94 and apparently not with BiP [46]. The cooperation with BiP is not an inherent property of the action cycle of GRP94.

As reported by Eletto et al. [47] GRP94 is transcriptionally co-regulated with other chaperones to increase the efficiency of folding and reduce the chance of misfolded proteins leaving the ER. Moreover Hendershot et al. found a functional and physical network in the ER, where BiP and GRP94 are the most abundant components [48].

As seen so far, depletion of one chaperone would affect reciprocally either the activity or expression of each other. Indeed, Link et al. [49] reported that when GRP94 is silenced by RNAi, they observed an induction of BiP expression and an involvement of the IRE1/XBP1 branch of the UPR.

The co-regulation of GPR94 and BiP has been also confirmed and explored by Eletto et al. [*manuscript in submission*]. When the expression of GRP94 or BiP was silenced by RNAi introduced by lentiviral infection (shRNA), they observed over-expression of BiP or GRP94, alternatively. Moreover, they also noted the induction of another KDEL-containing protein with an apparent molecular mass of 50KDa (p50) (Figure 27). p50 was

characterized later by Eletto et al. as PDIA6 (Figure 28). The induction of BiP and p50 was observed in several cell lines, from different species or tissue types (embryonic cells 10T1/2 and myoblasts precursors C2C12 in Figure 3; 293T, NIH 3T3 and HeLa cells data not shown).

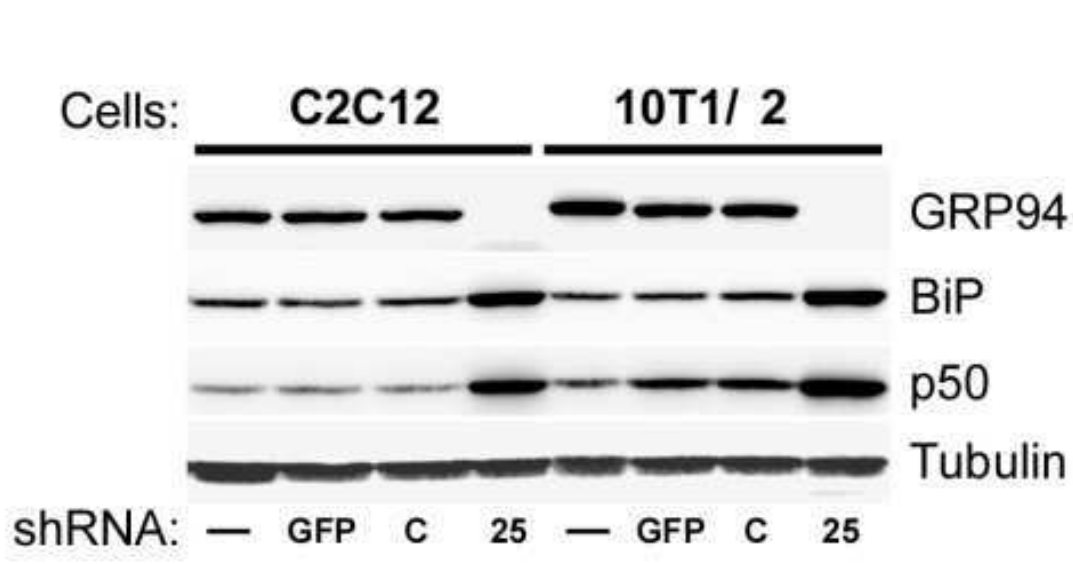

Figure 27: GRP94 silencing in C2C12 and 10 T1/2 triggers the expression of BiP and another KDEL-cointaining protein (p50).

5.3 PDIs: PDIA6

Native disulphide bond formation is a complex process. Disulphide bonds must not only be formed (oxidation), but also incorrect bonds must be broken (reduction) or rearranged (isomerisation). In the last decade there have been significant advances in understanding of these processes which are thought to be catalysed only by members of the protein disulphide isomerase (PDI) family.

The enzyme PDIs are multi-domain, multi-functional members of the thioredoxin superfamily [50]. PDI family includes 17 members, with a wide range of domain architectures and active-site chemistries. Each member can catalyse thiol-disulphide oxidation, reduction and isomerization, the last of which occurs directly through intramolecular disulphide rearrangement or through cycles of reduction and oxidation [51]. PDIs comprise at least two thioredoxin-like catalytic domains, a and a', which are separated by two non-catalytic domains, b and b'. The catalytic domains contain a characteristic CXXC active-site motif, with the two amino acids that lie between the cysteine residues having a major role in determining the redox potential of the enzyme and hence its function as a thioldisulphide reductase, oxidase or isomerase. To perform disulphide exchange reactions, the individual active sites must be maintained in either the oxidised disulphide form to allow disulphide formation, or the reduced dithiol form for isomerisation or reduction of disulphide bonds.

The members of the PDI family of oxidoreductases are not minor components of the ER; indeed several are highly abundant and ubiquitously expressed, so it is likely that they have important functions. For example, PDI is capable of both the formation and isomerisation of disulphide bonds within proteins, while ERp57 even if is highly homologous to PDI and shares the same arrangement of thioredoxin-like domains, catalyses only the reduction of non-native disulphides. In addition, PDI is involved in the regulation of protein function [52] and polypeptide binding [53].

It is highly likely that each oxidoreductase has a defined role to play in protein maturation, which might be specific to cell or tissue type, or to specific stages of development.
PDIA6 as the other members of the family catalyzes formation, reduction, and isomerization of disulfide bonds in proteins and is thought to play a role in folding of disulfide-bonded proteins. Jessop et al [54] found that PDIA6 forms a non-covalent complex BiP and shows specificity towards BiP client proteins.
PDIA6 is a 440-amino acid protein with a molecular mass of 48.1 kD. It has a putative N-terminal signal sequence, followed by two thioredoxin like domains and a C-terminal ER retention signal. Mutation analysis revealed that the first thioredoxin-like motif of P5 was more important than the second for isomerase activity, and that the first cysteine in each motif was necessary for isomerase activity [55]. Thioredoxin motif mutants of P5 lacking isomerase activity retained chaperone activity with citrate synthase as substrate, indicating that, like PDI, the isomerase and chaperone activities of P5 are likely independent.
PDIA6 is an abundant and ubiquitously expressed member of the protein disulfide isomerase (PDI) family. This superfamily comprises more than 13 members and only for few of those a specific function has been revealed. It has long been assumed that most PDIs are functionally redundant, we hypothesized that PDIA6 could have distinct functions from other PDIs members. Our hypothesis was supported by what reported by Jessop et al. who showed that mammalian PDIs have distinct clients, using a trap mutant of each of five PDIs, which forms mixed disulfides that cannot be released [54]. Importantly, his lab failed to

observe any requirement for PDIA6 in the biosynthesis of these proteins, while PDIA1 and ERp57 were required.
Thus, we tried to investigate its chaperone activity monitoring the specificity of the two thioredoxin-like domains by proteomic analysis. Then, after we found BiP as its major interacting-protein, we examined the biological meaning of this complex. Since BiP is the master regulator of the UPR, we hypothesized a role of PDIA6-BiP complex in the UPR and by PDIA6 knockdown approach we asked whether PDIA6 could be involved in the regulation of the UPR machinery.

RESULTS AND DISCUSSION

-CHAPTER 6-

PDIA6: a new physiological ER stress down-regulator

6.1 PDIA6: Mutagenesis And Proteomic Analysis

Kikuchi et al. [55] proved that the first thioredoxin-like domain in PDIA6 was more important than the second domain for isomerase activity because the CS12 mutant (50% activity), in which the N-terminal CXXC motif was destroyed by replacing both cysteine residues with serine, had a lower isomerase activity than the CS34 mutant (75% activity), in which the C-terminal CXXC motif (the second active site) was destroyed in the same manner. Moreover, they showed that PDIA6 had substrate specificity with respect to chaperone activity because it had rhodanese and citrate synthase as substrates, but not with D-glyceraldehyde-3-phosphate dehydrogenase which is a PDIA1 substrate.

Since the two thioredoxin-like domains are not equal for enzymatic kinetics, we hypothesized that the client protein may interact preferentially with one motif than the other. To this aim, we analyzed how the binding of PDIA6 to potential substrates is dependent on the formation of mixed disulfides.

To identify proteins interacting with each active motif, we performed a proteomic analysis of co-purified proteins by immuno-isolation of PDIA6.

The experimental strategy is illustrated in the Scheme 1. In the first phase, human cell line, HEK-293T (Human Embryonic Kidney 293T), are transiently transfected with PDIA6-tag expressing plasmids. After two days of transfection (II phase), once the protein of interest should be efficiently expressed, PDIA6-tag proteins are purified from cell lysates through beads conjugated with anti-tag antibody. In the III phase, proteins co-

purified with PDIA6 are eluted from the beads and analyzed by SDS-PAGE. PDIA6-bound protein fractions are detected by coomassie and/or silver staining and identified by Mass Spectrometry.

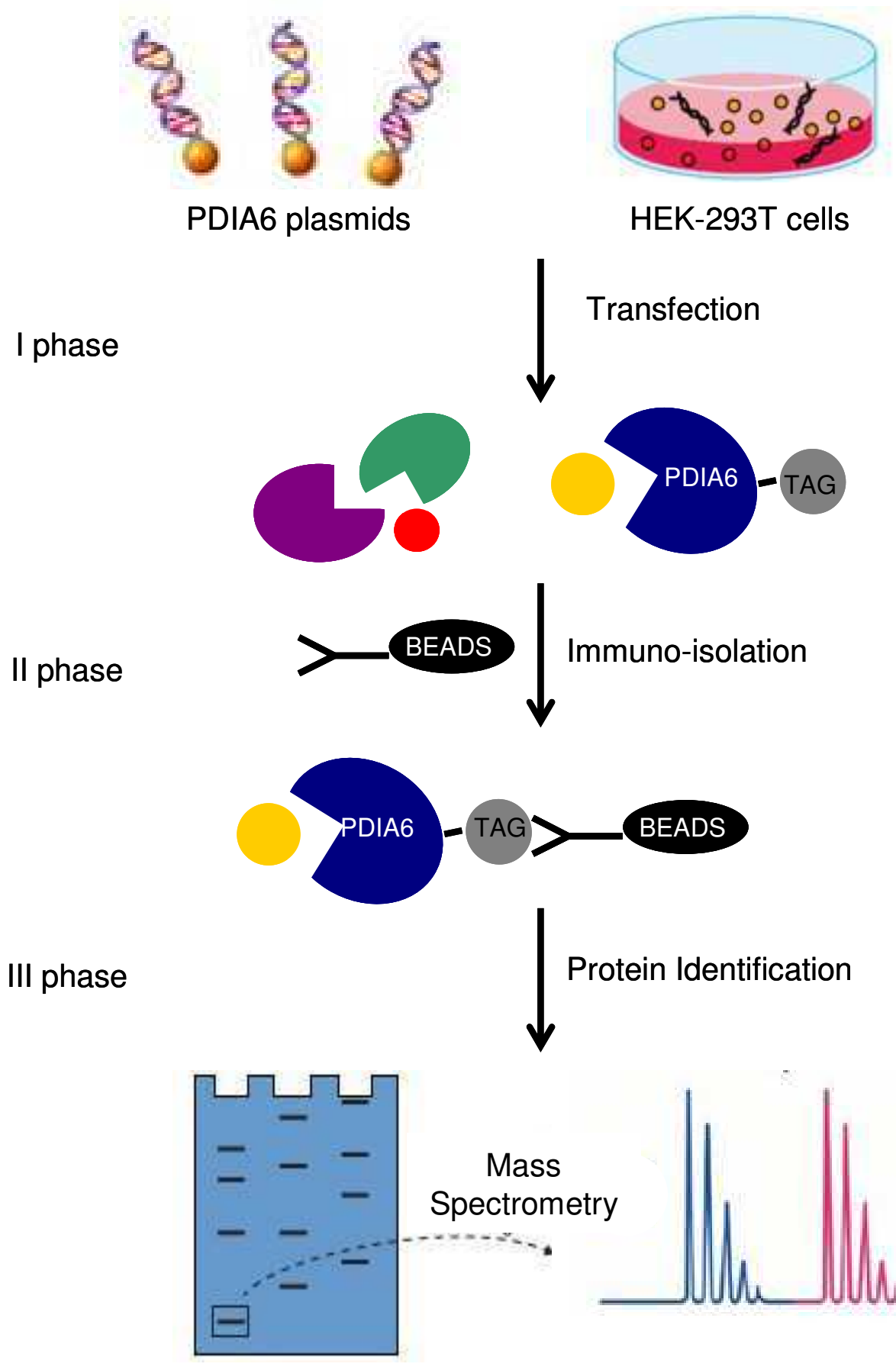

Scheme 1: Workflow of the experimental strategy for the proteomic analysis of PDIA6 interacting-proteins.

To answer the experimental question, we used multiple PDIA6 mutants which were missing the resolving cysteine of its N- and C-terminal active sites. Thus, we introduced a mutation on the second cysteine residue of each active site by replacing cysteine residue with alanine (CxxA). According to Kikuchi, such mutants cannot resolve mixed disulfides utilizing the first cysteine and work therefore as "trapping" mutants, binding substrates without releasing them (Scheme 2). Kikuchi showed, indeed, that the first cysteine in each PDIA6 motif is necessary for isomerase activity, and the second cysteine makes a lesser contribution. Replacing the second does not affect the binding ability of PDIA6, but makes it unable to release the client protein.

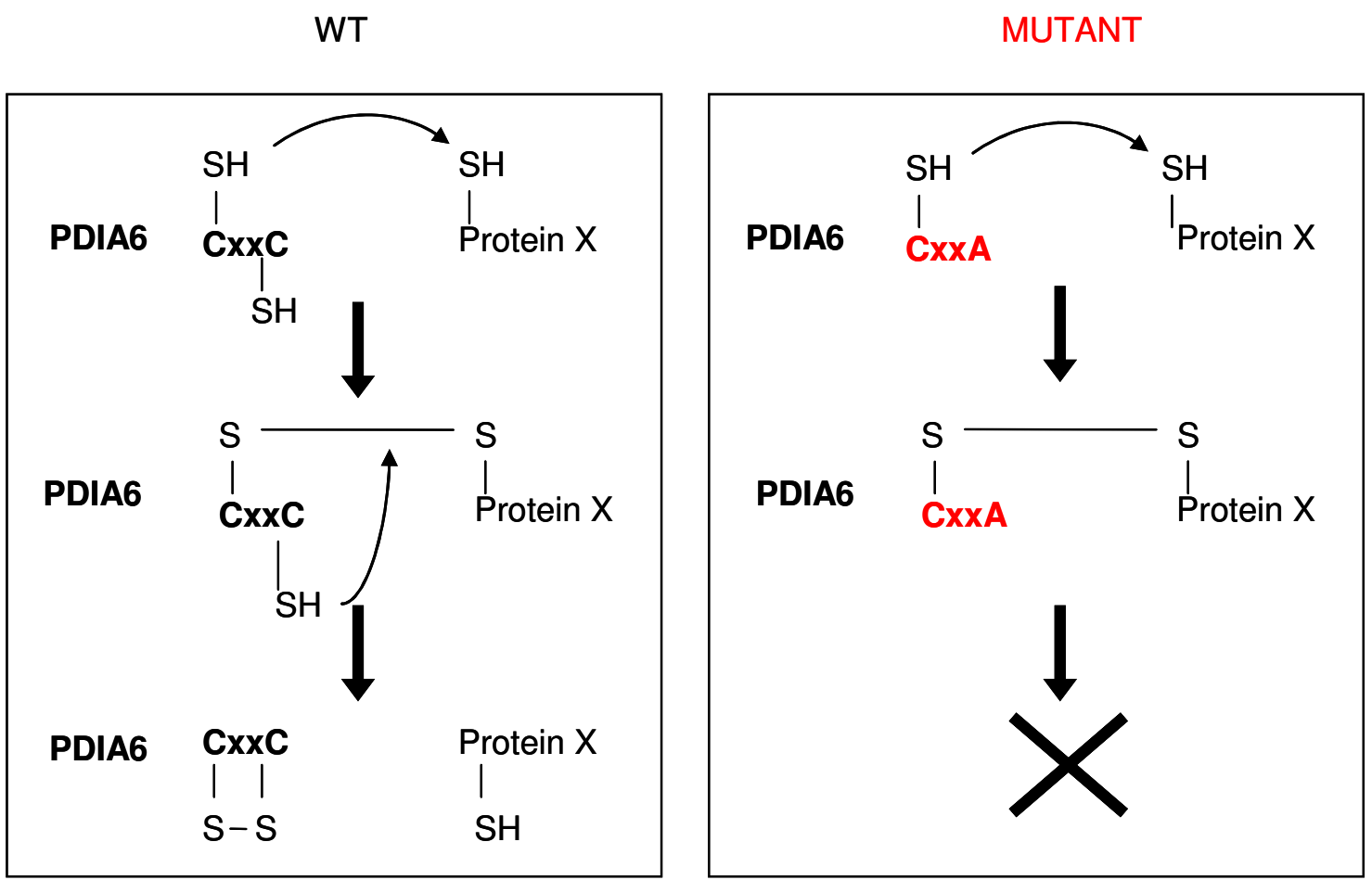

Scheme 2: Representation of the mechanism of action of wild-type (WT) versus a PDIA6"trapping" mutant.

Each of the two thioredoxin-like domains was mutated on the second cysteine residue, singly and in combination, as descripted in Figure 28.

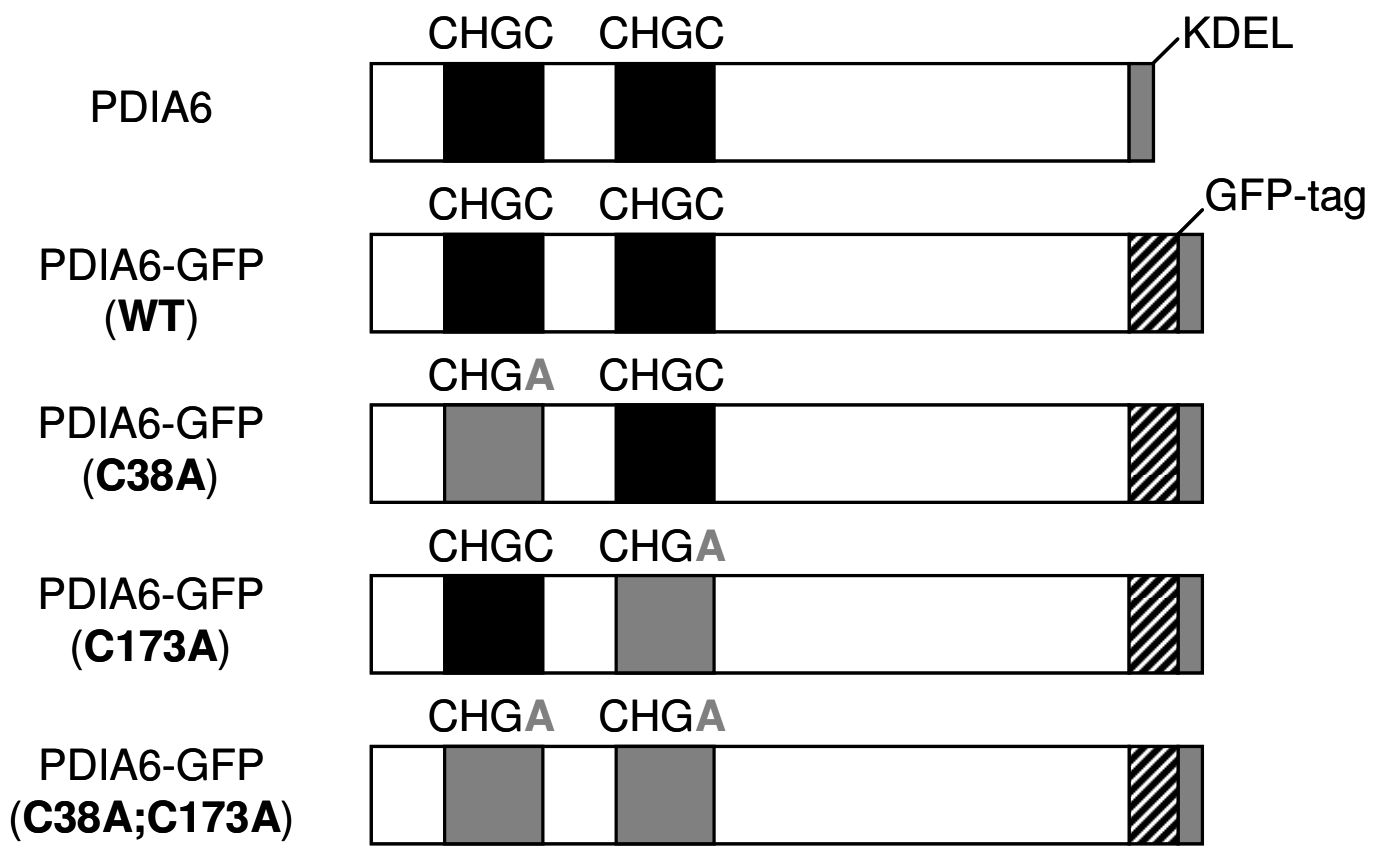

Figure 28: Schematic representation of the GFP-tagged PDIA6 mutants compared with endogenous PDIA6.

The mutants and wild-type were fused to green fluorescent protein and were transiently transfected into HEK-293T cells with high efficiency. Before performing the immunoisolation experiment, we proved that GFP-tag did not alter the sub-cellular localization of PDIA6 proteins. Thus, we transfected endoplasmic reticulum-localized GFP (ER-GFP) and wild-type

PDIA6-GFP into HEK-293T cells and we verified by fluorescence microscopy at 40x magnification if PDIA6-GFP was expressed in the ER correctly as well as ER-GFP (Figure 29). The localization into ER was checked also for each PDIA6 mutant (data not showed). Comparison of the fluorescence images (Figure 29A and 29B) confirmed the right localization of PDIA6-GFP in the ER.

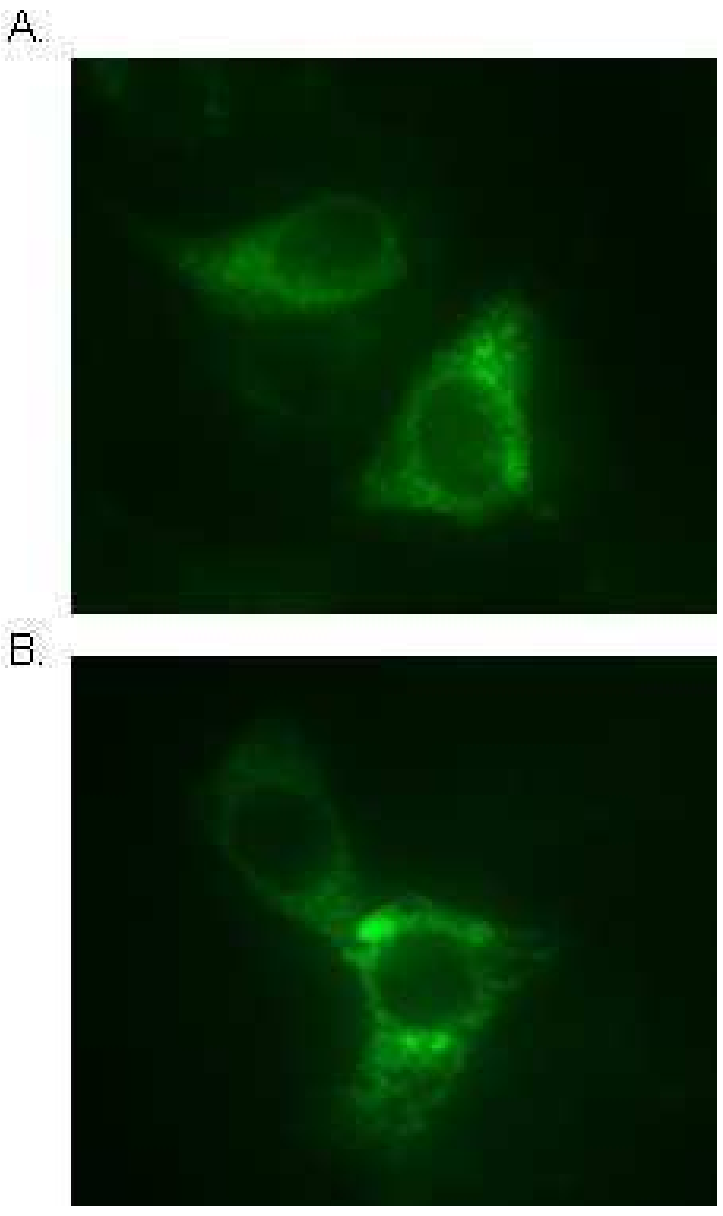

Figure 29: Microscopy analysis at 40x magnification of the HEK-293T cells expressing (A) ER-GFP; (B) PDIA6-GFP.

After 48 hours of transfection, PDIA6 was immuno-precipitated by anti-GFP conjugated beads, followed by SDS-PAGE.

Proteins interacting with PDIA6 were detected by coomassie and silver staining as non-PDIA6 bands in the gels (Figure 30A). The bands that differed in intensity between the wild-type (WT) and the mutant PDIA6 immunoprecipitates were excised from the SDS-PAGE containing the trapped complexes to be identified. After in-gel reduction, alkylation, and digestion with trypsin, the peptides eluted from the gel slices were analyzed by liquid chromatography (LC-MS/MS). Mass data collected during LC-MS/MS analysis were processed by Masslynx 4.1 and converted into a peak list file (called PKL) to be submitted to the search software MASCOT. Searches were conducted with a tolerance on mass measurments of 50 ppm in MS mode and 0.25 Da in MS/MS mode. The search described above allowed us to obtain a list of several proteins. Known cytosolic, nuclear, and mitochondrial proteins were removed from the list and the remaining proteins were sorted by their score number (Figure 30B). Multiple spots with a molecular weight between 75kDa and 40kDa have been identified as PDIA6. Each of these spots corresponded to faster-migrating species and we considered them as reduced or intrachain disulphide-bonded forms, as well as reported by Jessop et al. [54]. They assumed that the faster-migrating redox forms of PDIA6 are not a result of the mutations introduced because they have been seen also to a much lesser extent in the wild-type cell line.

A.

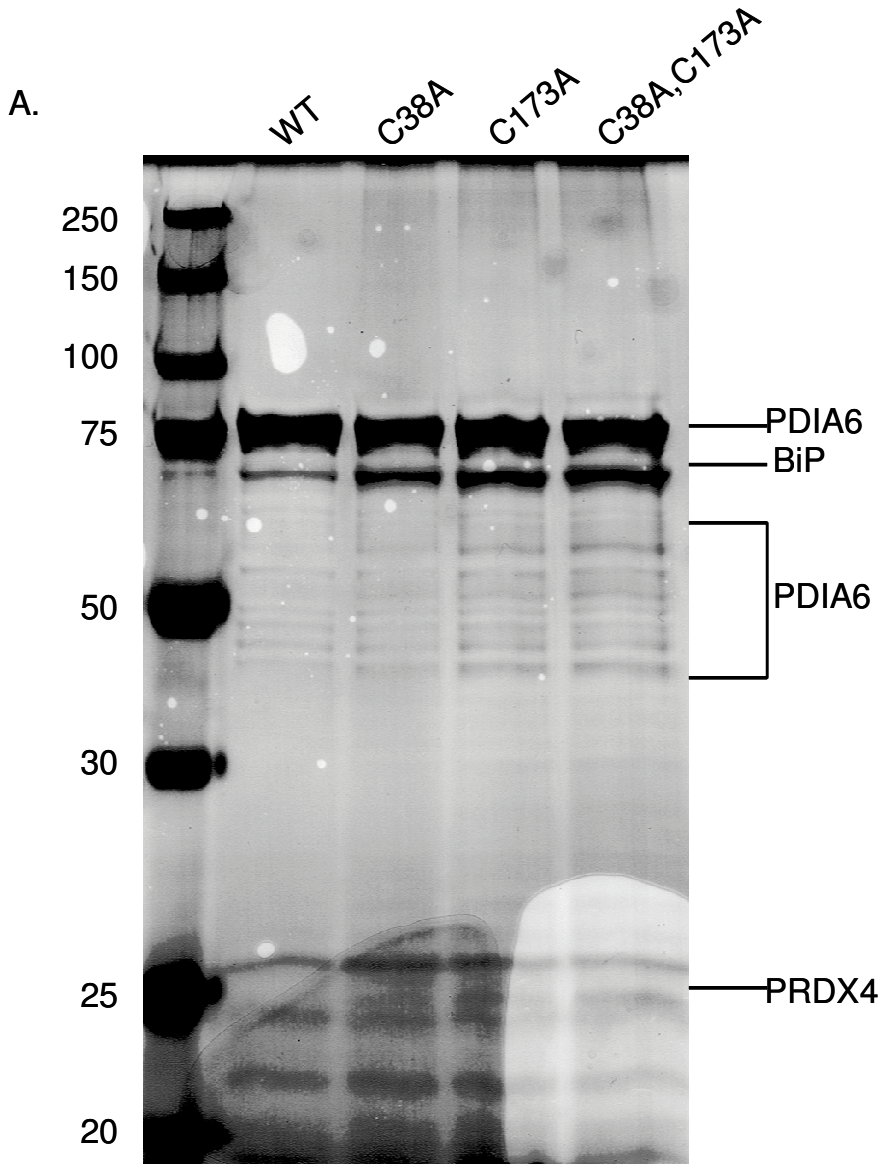

B.

ACCES. NUMB.	PROTEIN	SCORE
Q2KHP4	protein disulfide isomerase-related protein 5 [Homo sapiens] **(PDIA6)**	744
Q53GZ6	78 kDa glucose-regulated protein precursor [Homo sapiens] **(BiP)**	299
Q13162	peroxiredoxin-4 OS [Homo sapiens] **(PRDX4)**	150

Figure 30: PDIA6 active-site trapping mutants engage interacting proteins in mammalian cells. (A) Coomassie-silver stained reducing SDS-PAGE of proteins immunopurified in complex with GFP-tagged PDIA6 trapping mutants from transfected HEK-293T cells. (B) List of proteins identified by LC-MS/MS sequencing of tryptic peptides of endogenous proteins captured in a disulfide-linked complex by a GFP-tagged trapping mutant PDIA6 expressed in HEK-293T cells (shown in A).

The high scoring proteins discovered in complex with PDIA6 were ER-localized peroxiredoxin IV (PRDX4) and BiP. PRDX4 has been already found by Jessop et al. to bind PDIA6 [54], and moreover Zito et al. [56] proved that PRDX4 operates in a dependent pathway in parallel to ERO1 for the PDIA1 oxidation in the ER.

The most intense band from the immuno-precipated samples corresponded to BiP and the amount of PDIA6-interacting BiP seems to increase from WT to PDIA6 mutant proteins. This verified the data of Jessop et al. who reported that BiP is the major PDIA6-interacting protein and in addition provided evidence that this interaction was affected by the state of activity of the thioredoxin-like motifs in PDIA6.

We tried to confirm the previous data about the interaction between PDIA6 and BiP, running two experiments of reciprocal co-immunopurification (co-IP) (Figures 31-34). In the first co-IP we expressed double (C38A; C173A)-trapping mutant GFP-tagged or V5-tagged human PDIA6 proteins by transient transfection of HEK-293T cells. We wanted to prove that the interaction was not affected by any kind of tag protein fusion and that the amount of bound BiP was comparable between the two-tagged proteins. Protein complexes were immunopurified by anti-GFP or anti-V5 conjugated beads. The species were detected with anti-BiP antibody which showed endogenous protein and anti-PDIA6 antibody which revealed endogenous and exogenous PDIA6. Immunoblot showed that BiP associated to both tagged-double mutants PDIA6 $_{C38A,C173A}$ (Figure 31) and the amount of trapped BiP was equivalent in both co-IP.

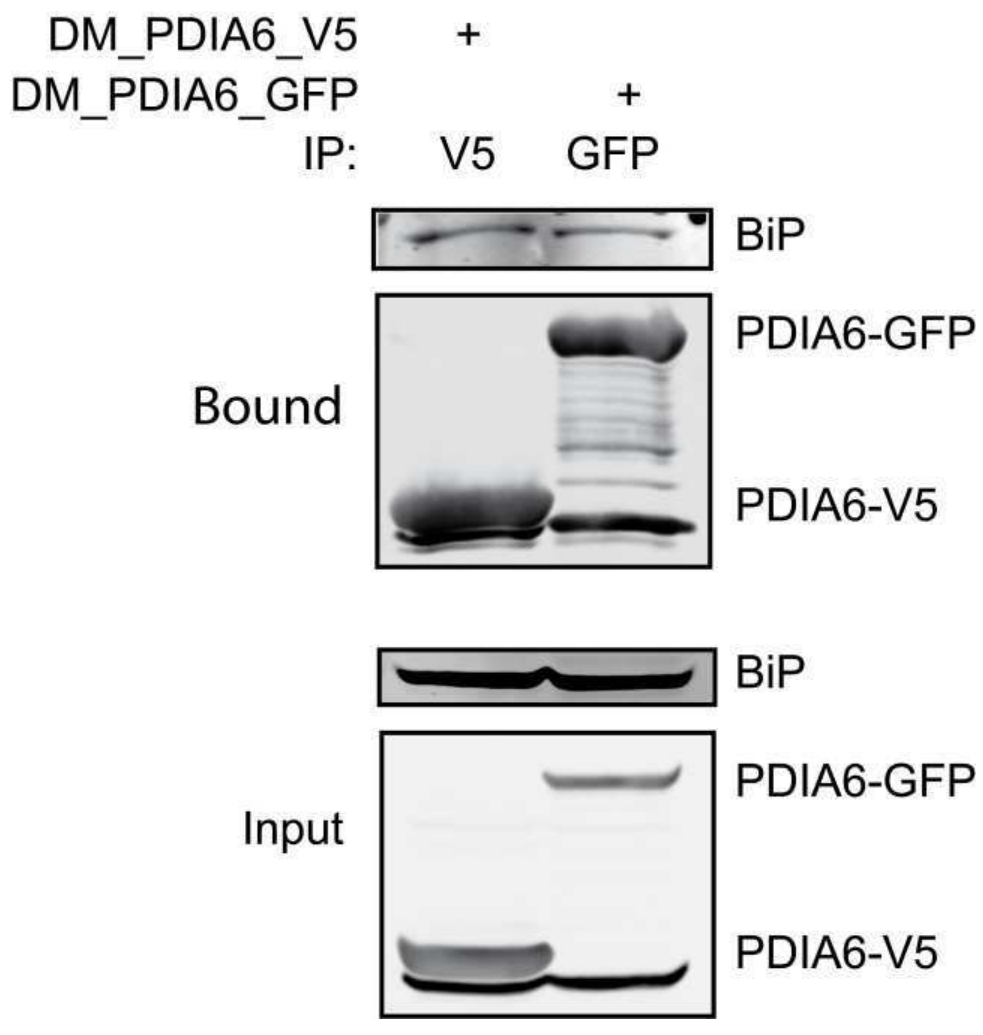

Figure 31: Immunoblots of GFP (right) or V5 (left)-tagged proteins PDIA6 $_{C38A,C173A}$ *(called DM as double mutant) immunopurified with the GFP or V5 antibody from lysates of HEK-293T cells.*

In the second experiment we performed a reciprocal co-IP: pull-down of BiP and co-purification of PDIA6. To have chance to see the interaction (because BiP is involved in many other interactions), we though to use a hamster BiP mutant with well-characterized point mutations in the ATP binding domain, called T19G [30] (Figure 32). BiP is characterized by two main domains: N-terminal ATPase domain and peptide-binding domain. The first binds ATP (Adenosine triphosphate) and hydrolyzes it to ADP (Adenosine diphosphate). The exchange of ATP drives conformational changes and substrate-binding

ability in the other domain. The replacement of the threonine with glycine affects the ability of BiP to hydrolyze ATP and makes the mutant able to bind permanently protein substrates. It has been proved by Hendershot et al. [57] that this kind of mutation increases the amount of co-purified proteins and helps to detect dynamic interactions between BiP and its peptide-substrates.

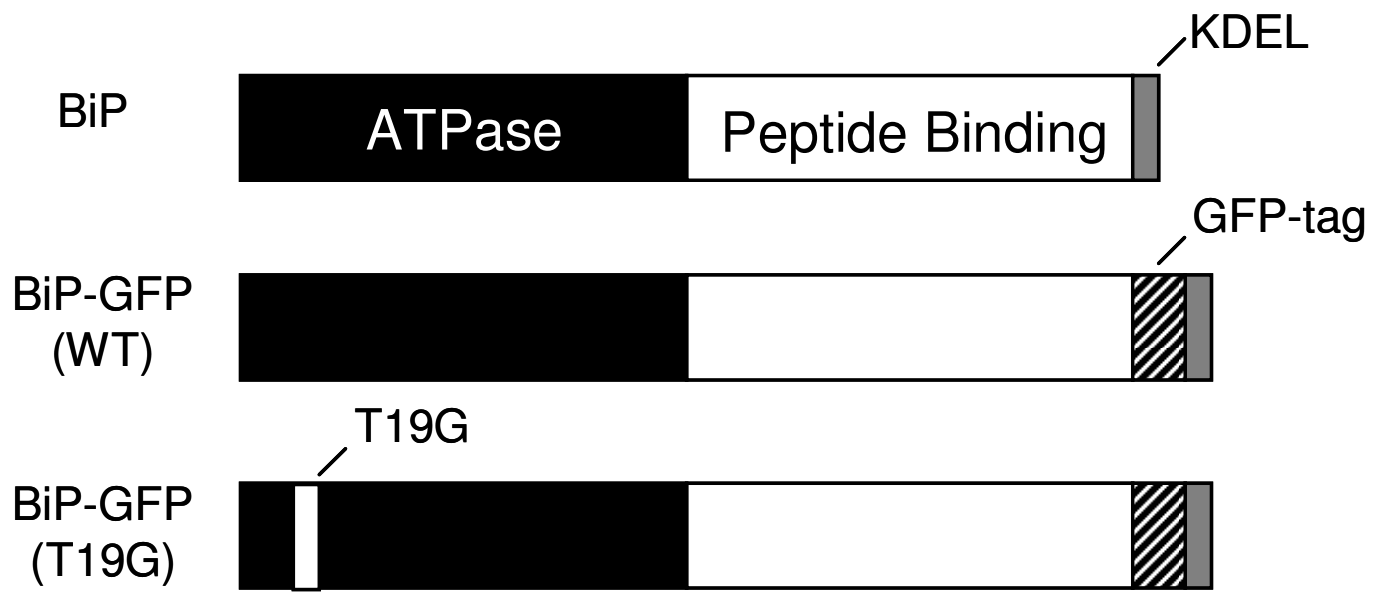

Figure 32: Schematic representation of the GFP-tagged wild-type and BiP mutants compared to endogenous BiP.

Before to perform the co-IP experiment, we verified that the wild-type and the BiP mutant were correctly expressed. So, we transfected plasmids expressing WT and T19G BiP-GFP into mouse fibroblasts, NIH-3T3 cells and by fluorescence microscopy we confirmed that both proteins were localized exactly in the ER (Figure 33).

A.

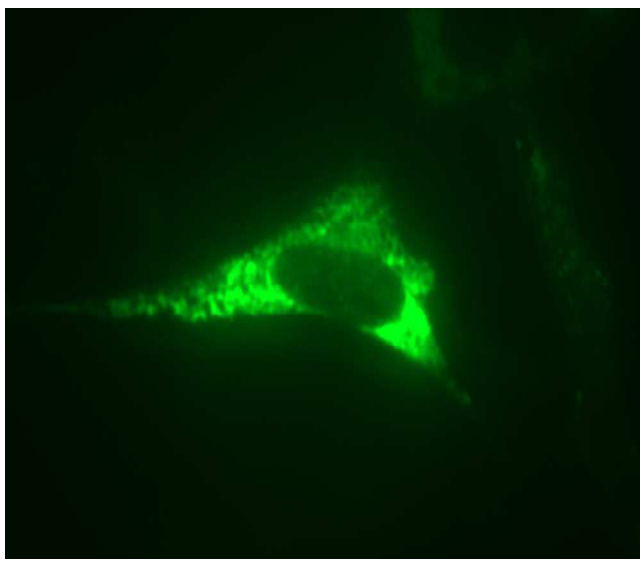

B.

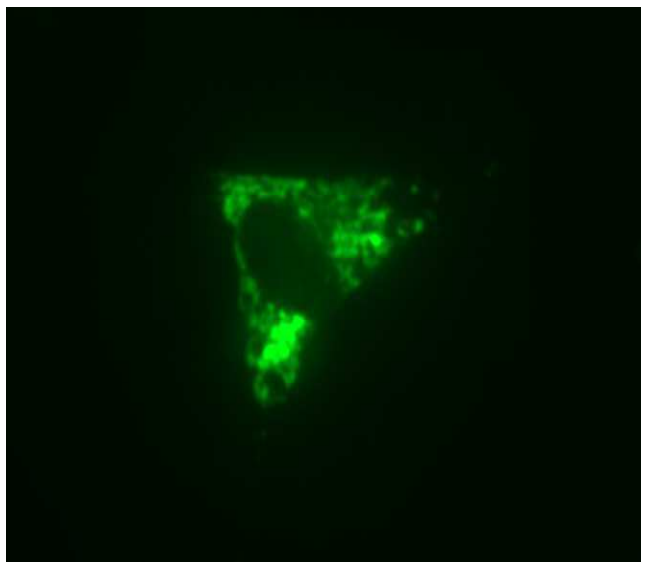

Figure 33: Microscopy analysis at 40x magnification of the 3T3 NIH cells expressing (A) WT BiP-GFP; (B) T19G BiP-GFP (A)

Hamster wild-type and T19G BiP mutant proteins were expressed in HEK-293T cells by transient transfection. We also transfected cells with canine wild-type GFP-tagged GRP94, another ER chaperone protein, strictly related to BiP, in order to prove the specificity of the interaction between BiP and PDIA6. Protein complexes were immunoisolated by anti-GFP conjugated beads and detected on reduced gel with anti PDIA6 and anti GFP antibodies. Immunoblot (Figure 34A) confirmed the interaction between BiP and PDIA6 and moreover showed that the T19G BiP mutant associated with more endogenous

PDIA6 than the wild-type. Bars in Figure 34B represent levels of expression of co-purified PDIA6 determined by densitometry of immunoblots (normalized on input) and show that T19G binds PDIA6 more than two-fold compared to wild-type. In addition the interaction seems to be specific because the amount of PDIA6 associated to GRP94 is undetectable.

A.

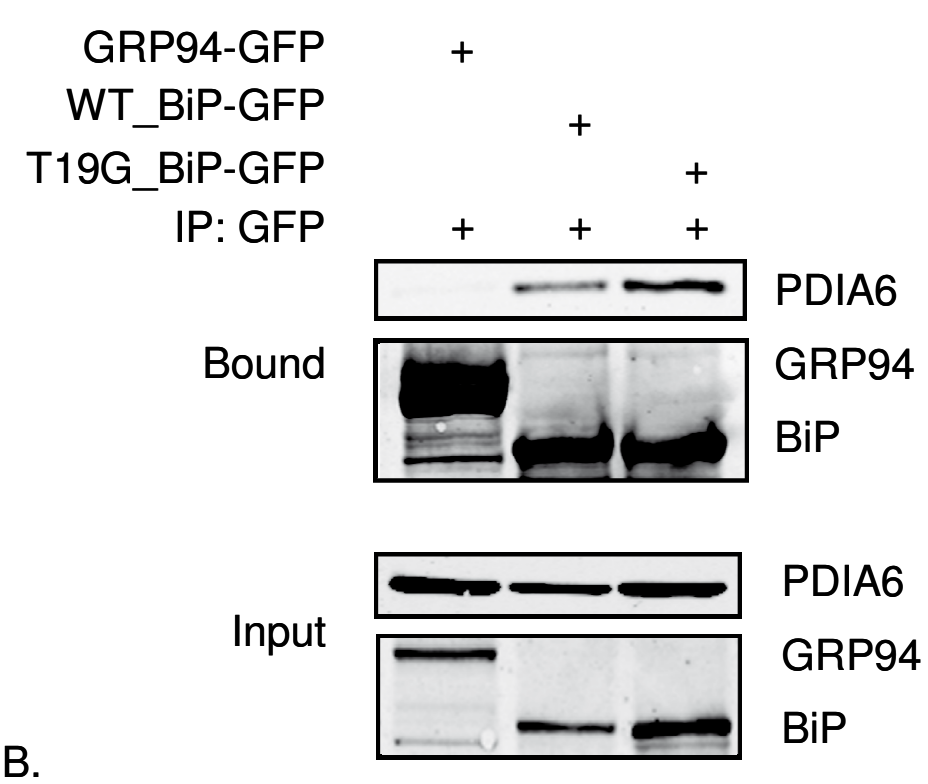

B.

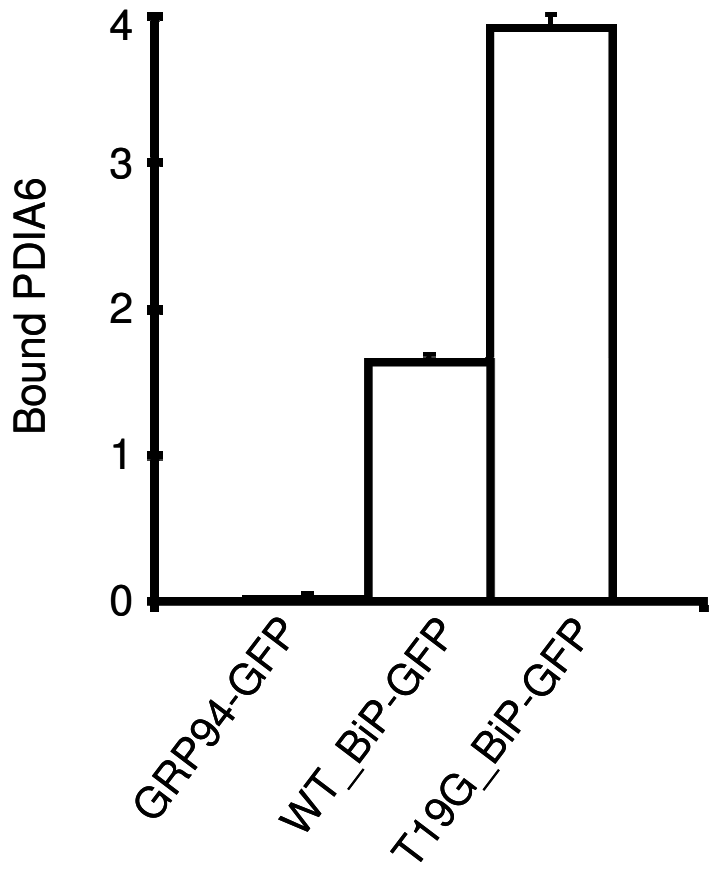

Figure 34: (A) Immunoblot of GFP tagged proteins BiP/GRP94 immunopurified with the GFP antibody from lysates of HEK293T cells ; (B) Bars representing levels of PDIA6 expression determined by densitometry of immunoblots. The means ± SD of 3 independent experiments are shown.

Our analysis, drawn through the mutual isolation of each partner, confirmed unequivocally the binding between PDIA6 and BiP.

6.2 PDIA6-BiP Complex And The UPR

What is the biological significance of the complex between PDIA6 and BiP?

As mentioned before, the folding of secretory proteins occurs in the ER and is performed by molecular chaperones like GRP94 and BiP. The proteins that fold incorrectly (called *misfolded* protein) are removed by a pathway of degradation called endoplasmic-reticulum-associated protein degradation (ERAD). Perturbations that alter ER homeostasis therefore disrupt folding and lead to the accumulation of unfolded proteins and protein aggregates, which are harmful to cell survival. ER stress which can be provoked by a variety of physiological conditions, including perturbations in calcium homeostasis, glucose/energy deprivation, redox changes, ischemia, hyperhomocystinemia, viral infections and mutations is alleviated by the ER stress response or the *unfolded protein response* (UPR) [58].

The UPR is initiated by 3 sensors (IRE1, PERK, ATF6) that reside in the ER membrane and connect the ER with the nucleus through well-defined signaling pathways [59]. Once activated, each of these kinases trans-phosphorylates itself and oligomerizes to activate the transduction signal.

BiP serves as a master UPR regulator and plays essential roles in activating IRE1, PERK, and ATF6 in response to ER stress [43]. Under non-stressed conditions, BiP binds to the luminal domains of IRE1, PERK, and ATF6 to maintain them within the ER. Upon accumulation of unfolded proteins, BiP is released from IRE1 and PERK to permit their spontaneous dimerization/oligomerization, trans-autophosphorylation, and subsequent activation. Thus, this BiP-regulated activation provides a direct mechanism for all three UPR transducers to sense the "stress" in the ER and an autoregulatory mechanism by which the UPR is shut off upon increased expression of BiP.

Given that the best PDIA6-interactin protein, BiP acts as a central regulator of the unfolded protein response (UPR), I asked the question whether PDIA6 itself could play role in the UPR?

To answer this question, we determined the consequences of depleting PDIA6 for the UPR machinery and monitored the expression of ER stress hallmarkers (BiP or GPR94) via Western blot analysis.

As proved by Eletto et al. (*manuscript in submission*), they silenced efficiently PDIA6 expression in NIH-3T3 cells through RNAi knockdown (KD) approach. They also observed that the depletion of PDIA6 did not affect the level of expression of GRP94 and BiP at steady state.

Therefore, we thought to examine cells sensitivity to exogenously added chemical stressors (tunicamycin, inhibitor of the of N-glycosylation, and thapsigargin: inhibitor of ER-calcium pump SERCA) and to measure the changes in BiP levels. Cells were exposed to a 4 hours treatment of 2.5 µM thapsigargin (TG) or to a 24 hours of 10 µg/mL tunicamycin (TM) and after treatment were analyzed by immunoblot with anti BiP and PDIA6 antibodies. (Figure 35). In response to chemical agents, BiP was upregulated in PDIA6 knockdown cells more than control cells (Figure 35A). We normalized on loading control (14.3.3) and quantified BiP expression from three different experiments. The values are reported in bar diagram (Figure 35B) where PDIA6 lacking cells (black bar) are more sensitive than control cells (white) to TM and TG exposition.

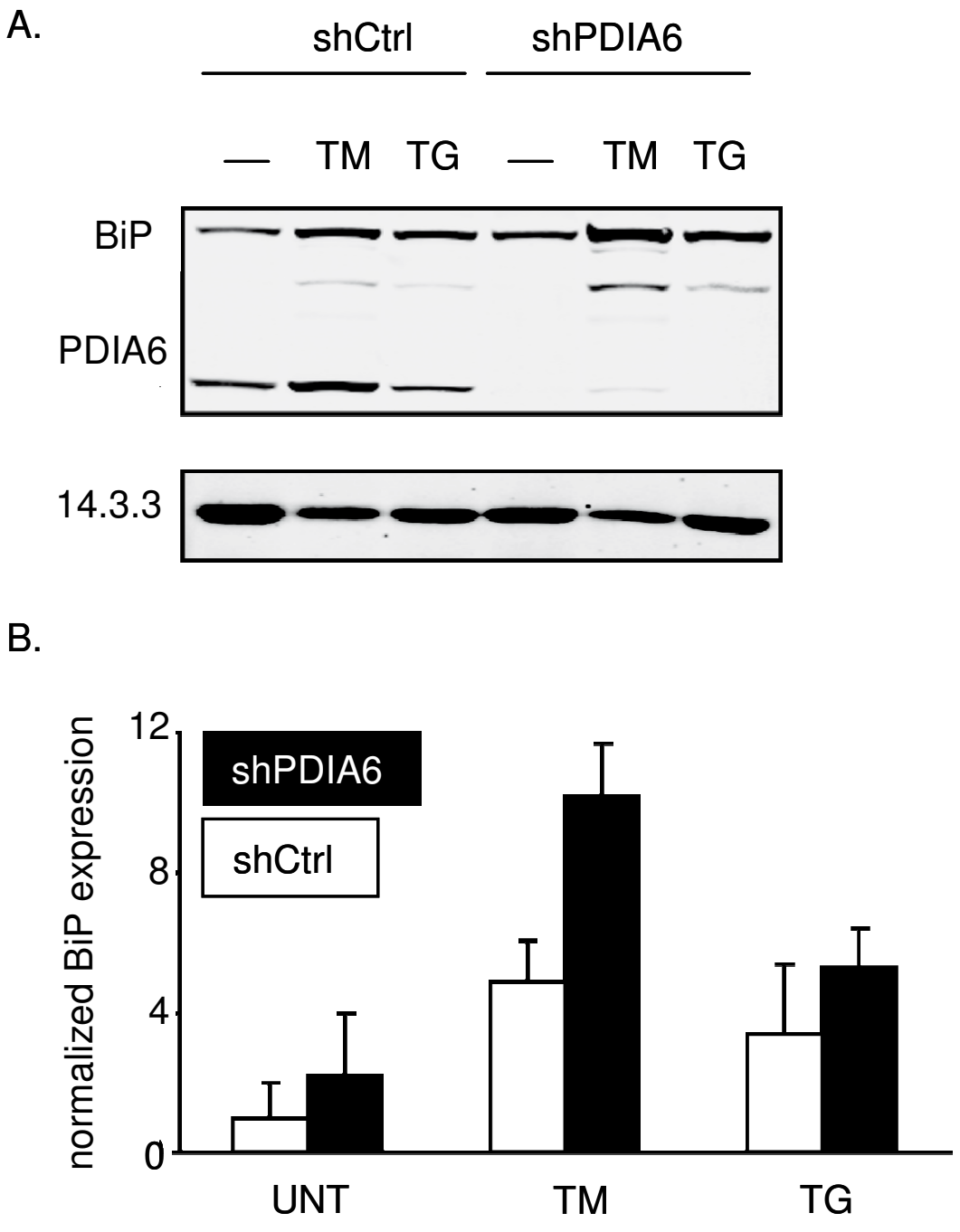

Figure 35: Silencing PDIA6 makes cells hypersensitive to ER chemical stressors: (A) Immunoblot of endogenous BIP, PDIA6, and 14.3.3 in control and PDIA6-knockdown (shPDIA6) cells after tunicamycin (TM) or thapsigargin (TG) treatment. (B) Bar diagram of normalized BiP expression determined by densitometry of immunoblots. The means ± SD of 3 independent experiments are shown.

Because BiP is involved in the activation of the UPR, its level may be monitored by the cell as an indicator of changes in the folding environment and ER processing capacity. So, the

overexpression of BiP in mammals is associated to the activation of the UPR and we therefore assumed that the hypersensitivity of PDIA6-deficient cells under ER stress is due to an hyperactivation of the UPR.

Thus, we investigated the hyper-response of PDIA6 KD cells to ER stress performing a dose response and a time course experiment upon TM exposition.

In the first experiment, dose response, NIH 3T3 cells, shCtrl and shPDIA6, were treated with increasing doses of TM (0, 2, 5, 10 µg/mL) for 24 h (Figure 36A). In the second, time course, we used 10 µg/mL of TM to treat the cells for 0, 2, 6, 24 h (Figure 37A). After the treatment the cell lysates were analyzed by immunoblot and BiP levels were normalized on loading controls levels and reported respectively in the Figure 36B and 37B.

A.

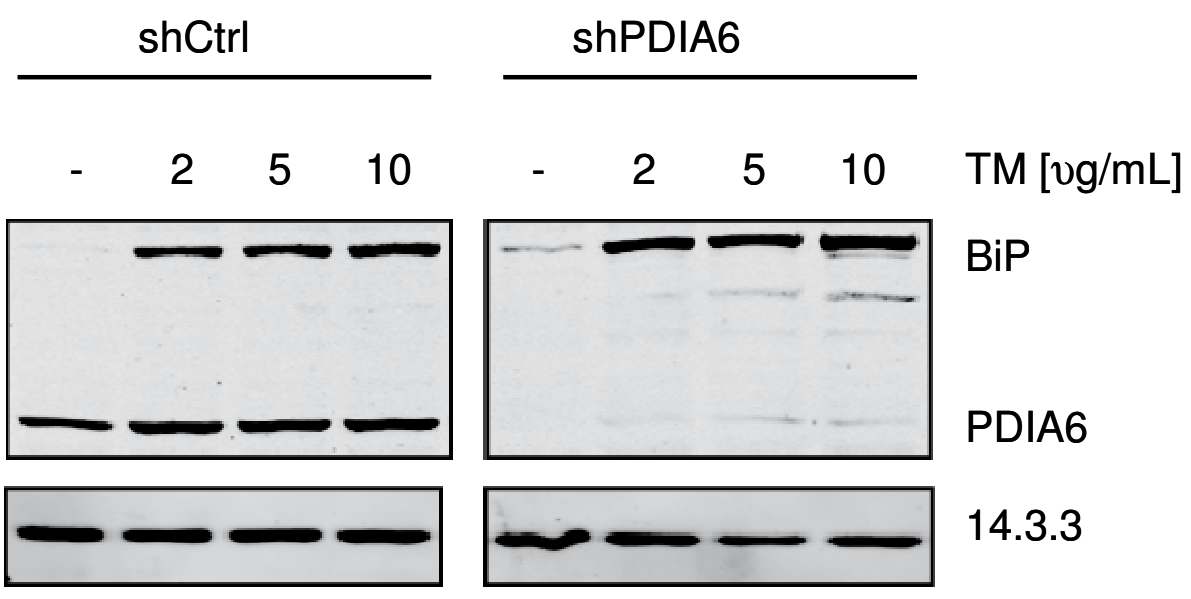

B.

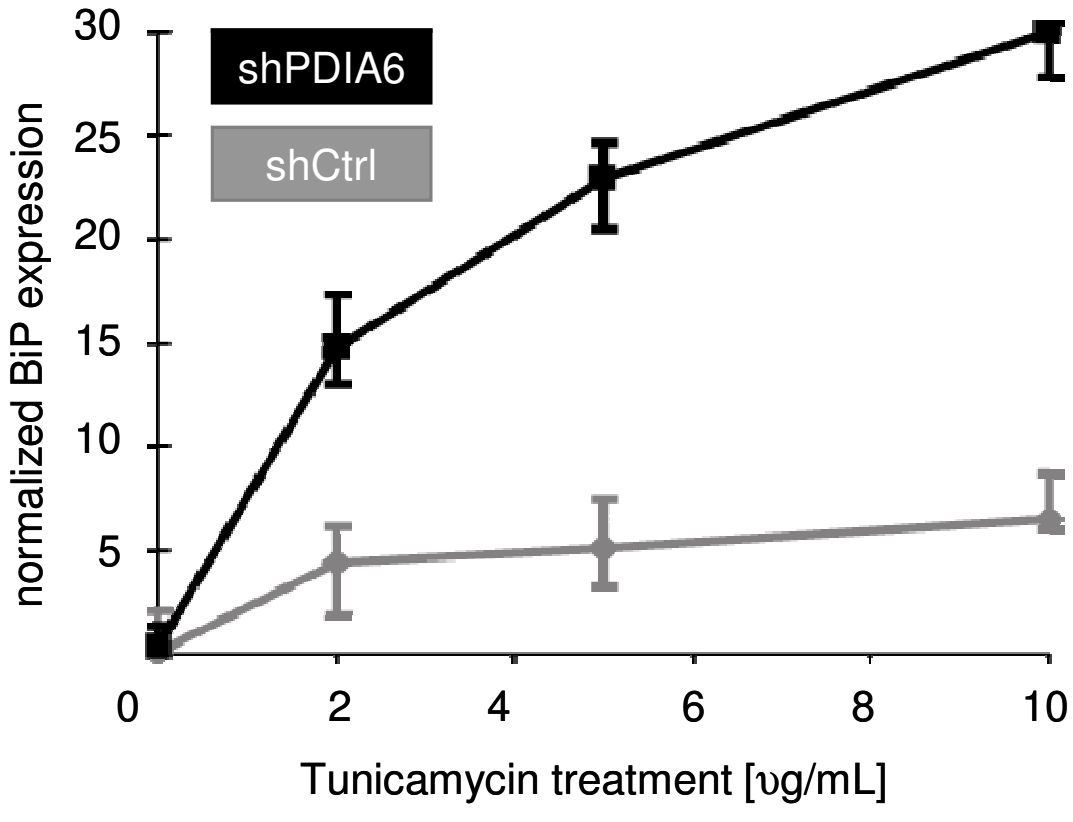

Figure 36: Hypersensitivity to TM of PDIA6 Deficiency in NHI-3T3 cells in dose response experiment: (A) Immunoblot of BiP, PDIA6 and 14.3.3. (a loading control) from Ctrl (grey line) and PDIA6 KD (black line) cells treated with varying doses of TM for 24 h; (B) Dose response change of BiP levels were quantified by densitometry and plotted as normalized BiP expression to TM doses. The means ± SD of 3 independent experiments are shown.

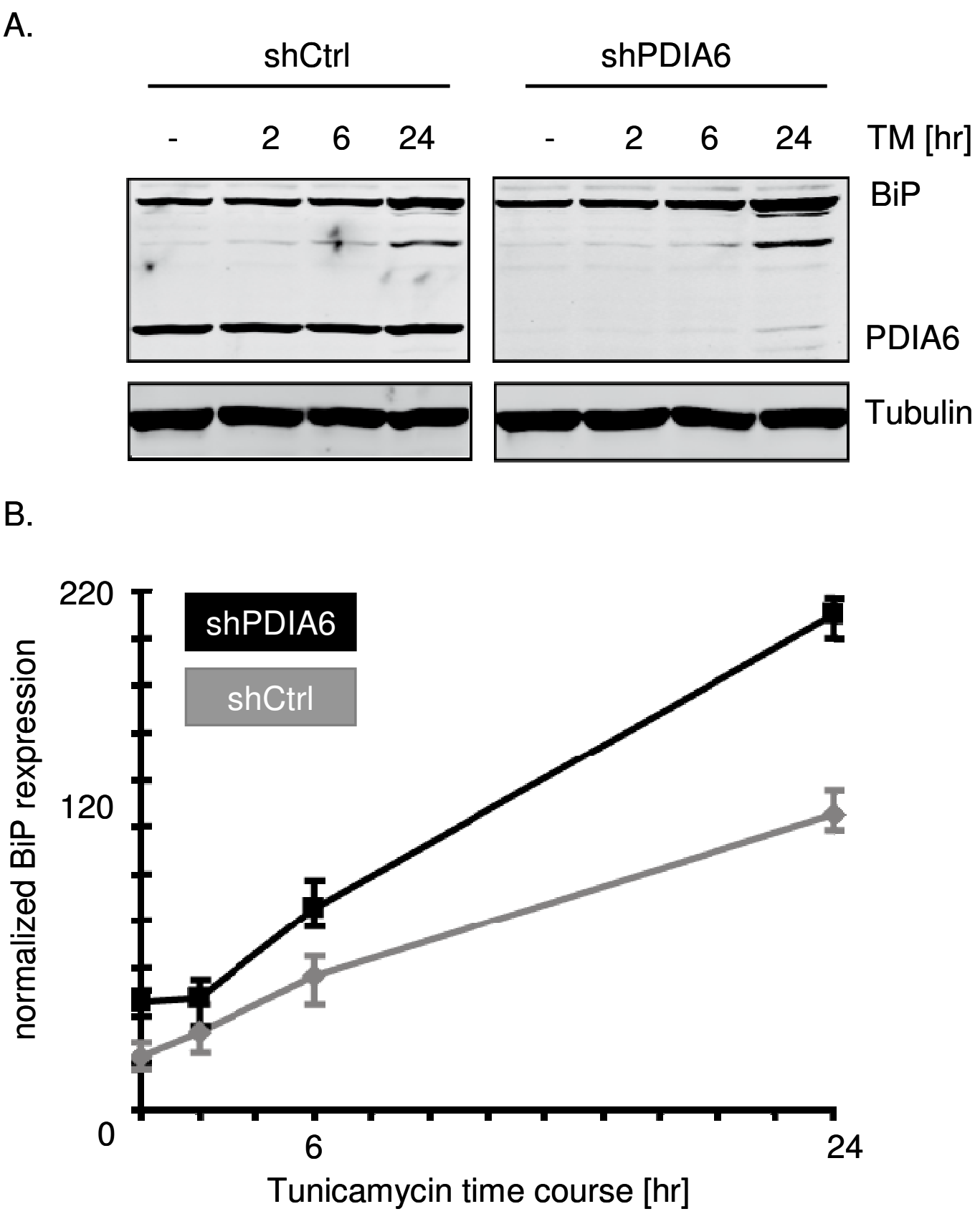

Figure 37: Hypersensitivity to ER stress of PDIA6 Deficiency in NHI-3T3 cells in time course experiment: (A) Immunoblot of BiP, PDIA6 and tubulin. (a loading control) from Ctrl (grey line) and PDIA6 KD (black line) cells treated with 10 µg/mL TM for the indicated period of time; (B) Dose response change in BiP expression levels were plotted in a graph. The means ± SD of 3 independent experiments are shown.

Both experiments (Figure 36-37) revealed a sustained up-regulation of BiP in PDIA6-deficient cells compared to control cells under TM treatment. We confirmed a hypersensitivity of cells to ER stress with a combined deficiency of PDIA6.

To demonstrate that the hypersensitivity was directly due to loss of PDIA6, we tested whether introducing re-expressing exogenously mammalian a PDIA6 cDNA could rescue the effect of PDIA6 knockdown on BiP expression under ER stress.

HEK-293T were transiently transfected with ER-localized green fluorescent protein (ER-GFP) and PDIA6-GFP into control and PDIA6-deficient HEK-293T cells. After 48 hours, the ER-GFP and PDIA6-GFP expressing cells were incubated with 10 µg/mL of TM for 24 hours and analyzed by immunoblot to detect BiP, PDIA6 and 14.3.3 (Figure 38A). Bar graph, reported in Figure 38B, represents quantitative analysis of BiP expression levels (shown in Figure 38A) (n = 3). The results showed a rescue of the observed knockdown phenotype. ER-GFP expression did not affect the hypersensitivity related to PDIA6 knockdown, indeed BiP is over-expressed in PDIA6-deficient cells compared to control cells under TM treatment; but when exogenous PDIA6 was introduced into the cells, the augmented response of PDIA6 KD cells was almost completely rescued and the expression levels of BiP in these cells was similar to control cells. Therefore, we confirmed the specificity of the phenotype which was exclusively related to PDIA6 depletion.

A.

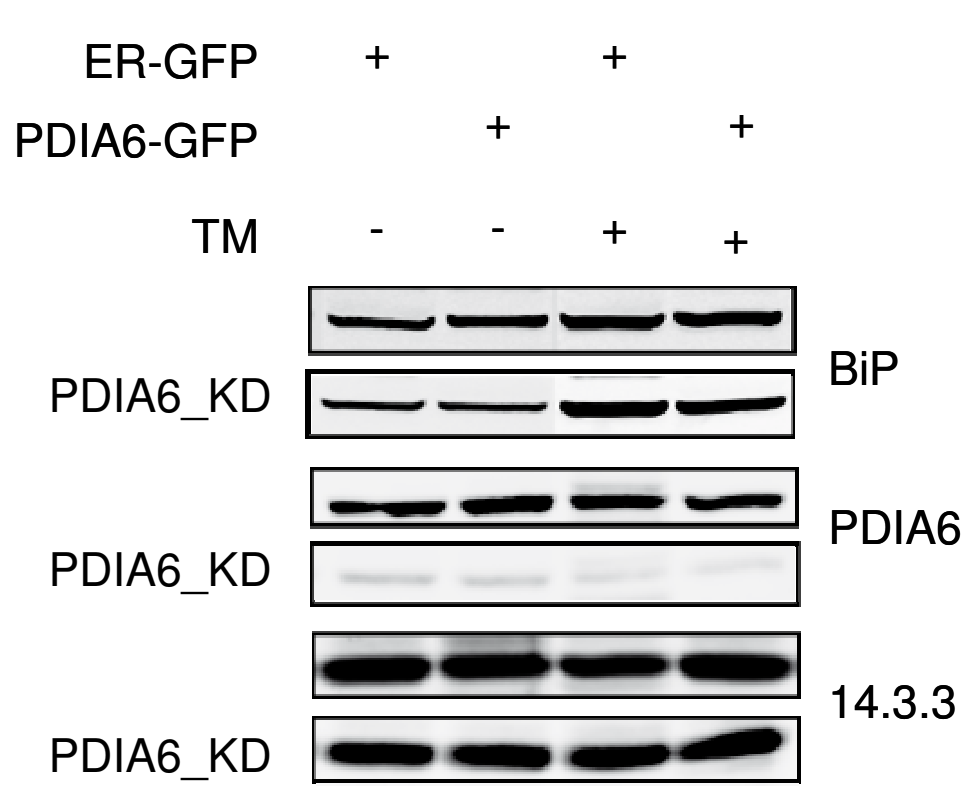

B.

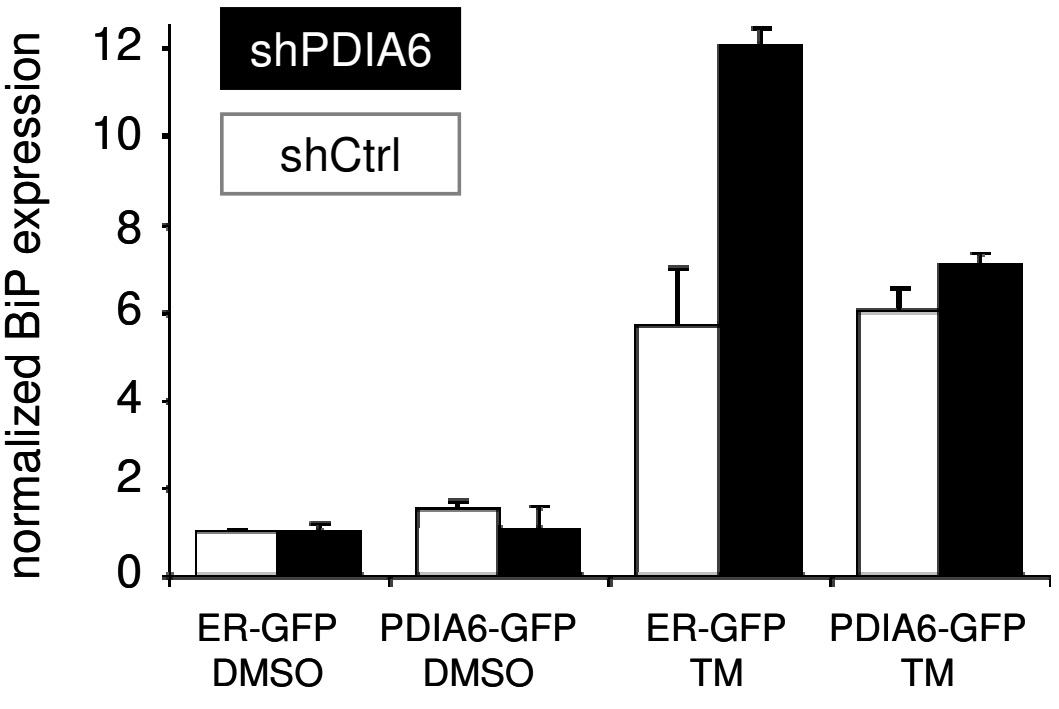

Figure 38: Exogenous PDIA6 rescues the hypersensitivity in PDIA6-knockdown cells exposed to TM: (A) Immunoblot of BiP, PDIA6 and 14.3.3. (a loading control) from Ctrl (white bar) and PDIA6 KD (black) cells treated with 10 µg/mL TM for 24 hours . ER-GFP and PDIA6-GFP were expressed in both cell lines (shCtrl and shPDIA6); (B) Bar graph represents quantitative

analysis of BiP expression levels. The means ± SD of 3 independent experiments are shown.

6.3 PDIA6 Regulates UPR Sensor: IRE1 And PERK.

So far, we saw that RNAi depletion of PDIA6 from fibroblasts and other cell lines significantly increases their sensitivity to ER stress imparted by TM and TG. Then we tried to explore the molecular mechanism by which PDIA6 is involved in the ER-stress.

As described previously, when ER functions are perturbed by various pathological conditions unfolded proteins are accumulated causing ER stress. This accumulation leads to an activation of signaling events known as UPR which should rebalance folding capacity and folding demand within the ER. Imbalances between protein load and folding capacity is monitored by three distinct UPR sensors: IRE1, PERK and ATF6.

We analyzed in detail the activities of two UPR sensor proteins: IRE1 and PERK.

IRE1 is the best characterized UPR signal transduction molecule. As illustrated in Figure 39, once activated by the dissociation of BiP in the ER, it oligomerizes and activates its endoribonucleasic domain that protrudes into the cytoplasm. Then, IRE1 specifically transmits the signal by removing an intron from the messenger RNA XBP1, that as a result of this alternative splicing may be translated into a potent UPR transcription factor. The activation status of IRE1, and

consequently the effect on the maturation, is transient: after an initial activation step, the pathway must return to a silent state. Conditions that disrupt the shutdown of signaling pathways, and therefore cause deregulation of the UPR, can lead to cell death [60].

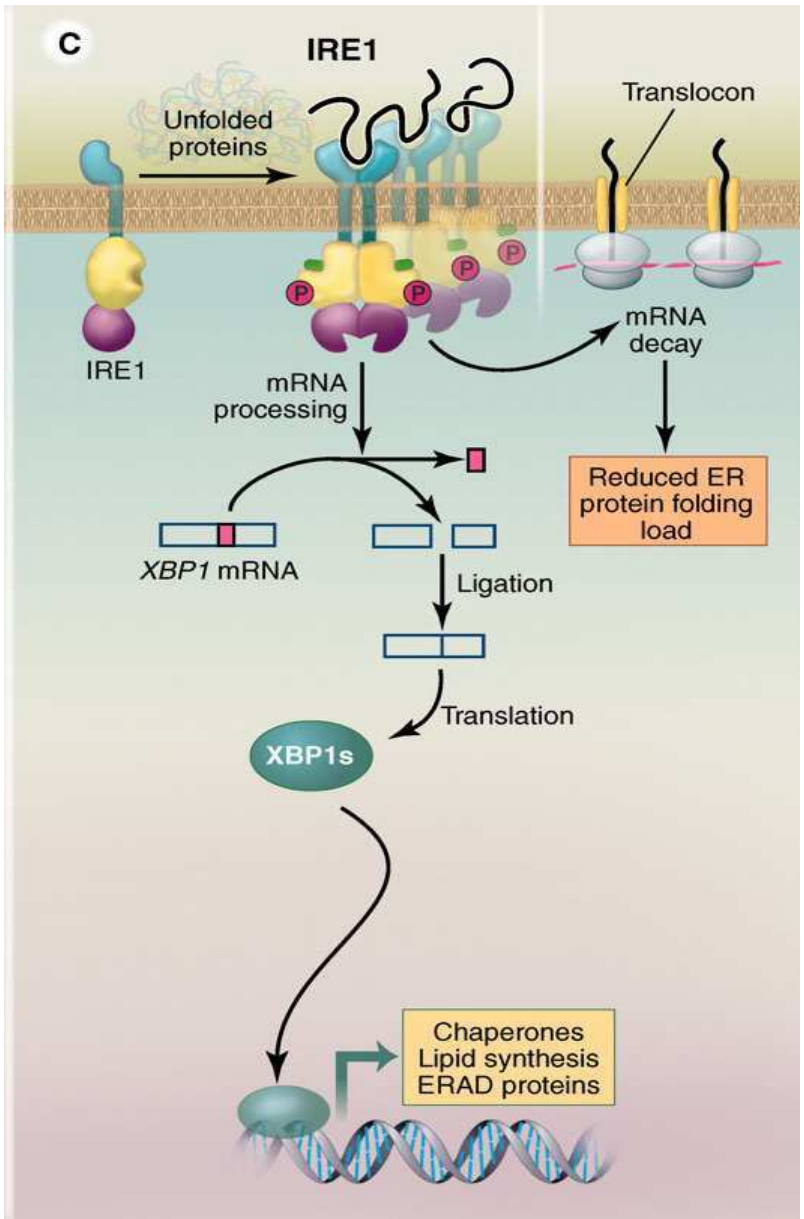

Figure 39: schematic representation of IRE1 signaling.

To test whether PDIA6 lacking in NIH 3T3 cells could affect the XBP-1 splicing event, we determined the levels of XBP-1 mRNA splicing in wild-type and PDIA6 KD cells. Thus, the cells were incubated for 4 h in the presence of increasing doses of TM(0, 2, 5, 10 μg/ml). Total RNA was extracted, and XBP-1

splicing was analyzed by reverse transcription polymerase chain reaction (RT-PCR). PCR products were analyzed by 2 % agarose gel and visualized by ethidium bromide staining. We compared the effects of UPR induction in wild-type and PDIA6-deficient cells (Figure 40). In response to chemically induced ER stress, the wild-type and PDIA6 knockdown cells induced the splicing of XBP-1 in the same way. Comparing the levels of splicing, PDIA6 lacking did not alter the IRE1α activation. We saw only a partial difference in the last point, where cells have been incubated with 10 µg/mL of TM. PDIA6 KD cells displayed pronounced splicing of the XBP1 mRNA, whereas in the control cells the most intense band is the unspliced.

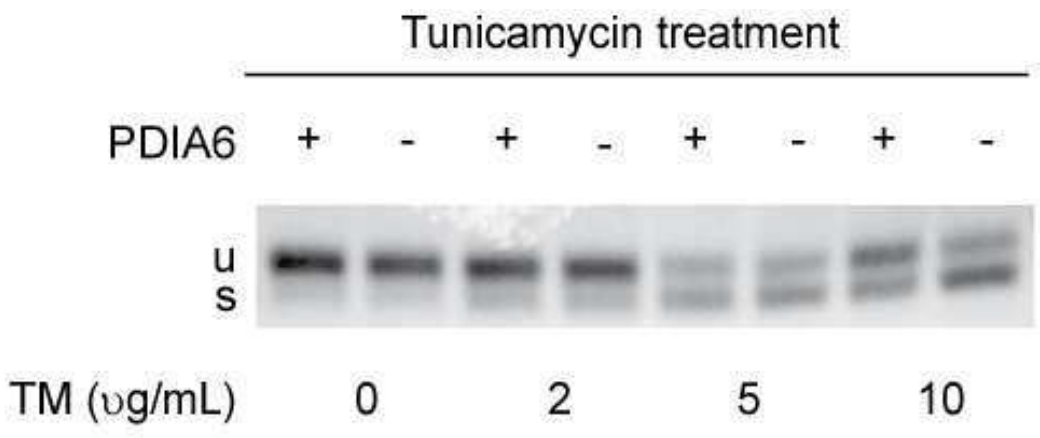

Figure 40: PDIA6 knockdown triggers the UPR: PDIA6 KD and control NIH-3T3 cells were treated with indicated concentrations of TM for 4 hr and the levels of XBP-1 mRNA splicing were determined in total cDNA by RT-PCR. Spliced (s) and unspliced (u) PCR fragments are indicated.

It has been reported by Lin [61] that XBP-1 mRNA splicing levels decline after prolonged ER stress. These observations was confirmed by our experiments. When we incubated cells with 10

µg/ml of TM, we observed in PDIA6 WT cells a decrease in the levels of splicing around 12 hr of TM treatment (Figure 41A). Surprisingly, PDIA6 KD cells showed a sustained maintenance of XBP-1 mRNA splicing, even after 24 hr of treatment, suggesting that PDIA6 may be involved in the inactivation of IRE1 signaling (Figure 41B).

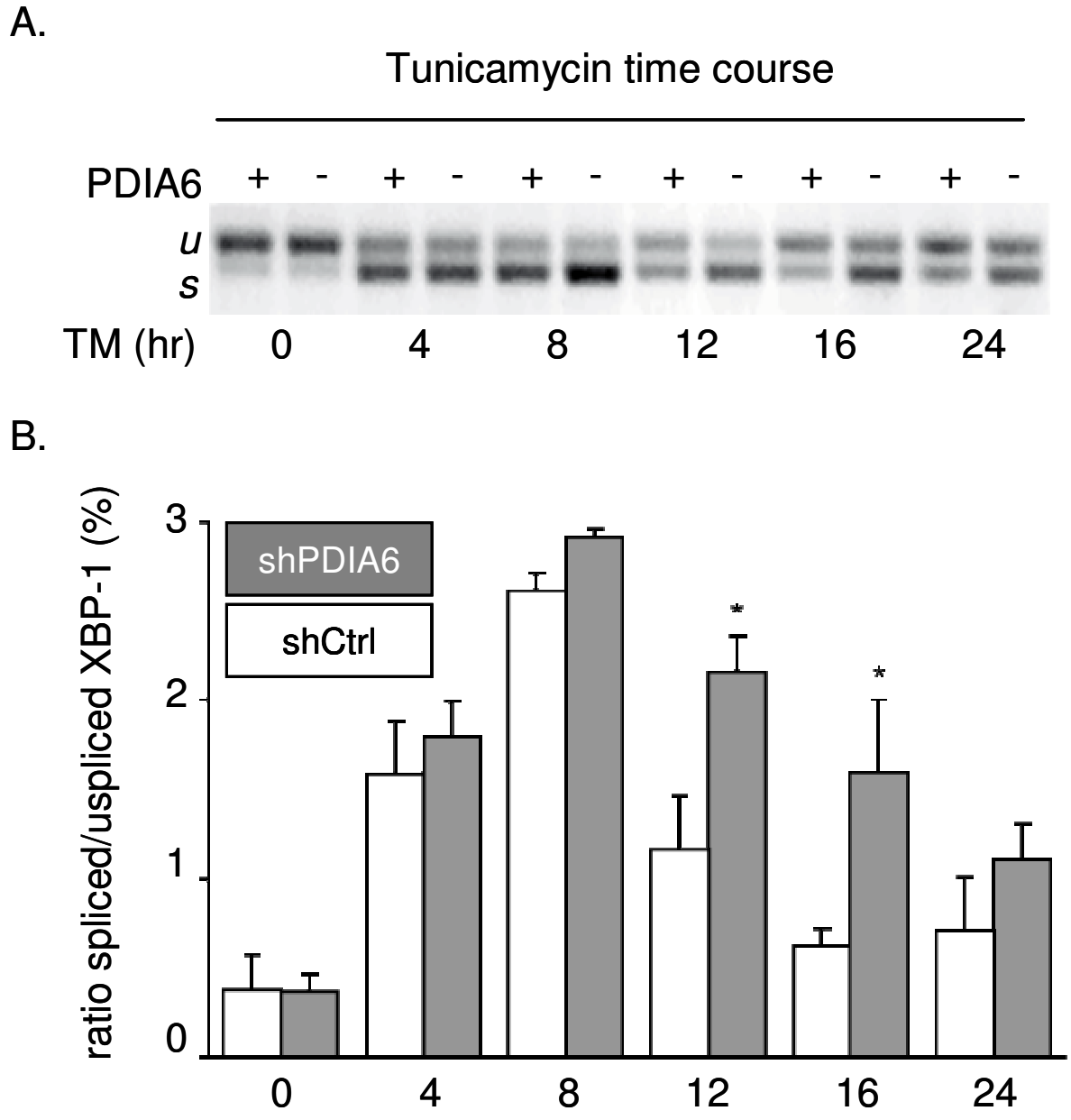

Figure 41: Delayed Inactivation of XBP-1 mRNA Splicing in PDIA6-Deficient NIH-3T3 Cells: (A) XBP-1 mRNA splicing was monitored over time in PDIA6 WT and KD cells treated with 10 µg/ml TM. (B) Percentage of the ratio spliced/unspliced XBP-1 mRNA splicing was determined by densitometric analysis by

ImageJ (National Institutes of Health). The means ± SD of 3 independent experiments are shown.

To further evaluate the potential contribution of PDIA6 in the inactivation of IRE1, we treated PDIA6 WT and KD cells for only 4 hr with high doses of TM to trigger almost full XBP-1 mRNA splicing in both cell types. TM-containing media was then washed out and XBP-1 mRNA splicing monitored during the recovery period: 4, 8 and 24 hours (Figure 42A). After 4 and 8 hr of washout, XBP-1 mRNA levels decreased almost by half in PDIA6 WT cells confirming that the XBP-1 splicing is a transient event. Therefore, compared to the previous experiment the recovery time has been reduced dramatically because of the washout. In addition, a complete retention of XBP-1 splicing was still observed in PDIA6 KD cells after TM washout (Figure 42B). Although both cell types in untreated conditions showed no difference in the ratio spliced/unspliced XBP-1, after washing out the TM-containing media PDIA6 KD cells produced a remarkable delay in the recovery times compared to control cells. The delayed inactivation of XBP-1 splicing in PDIA6 KD cells can be appreciated after 8 hr of washout step (Figure 42B).

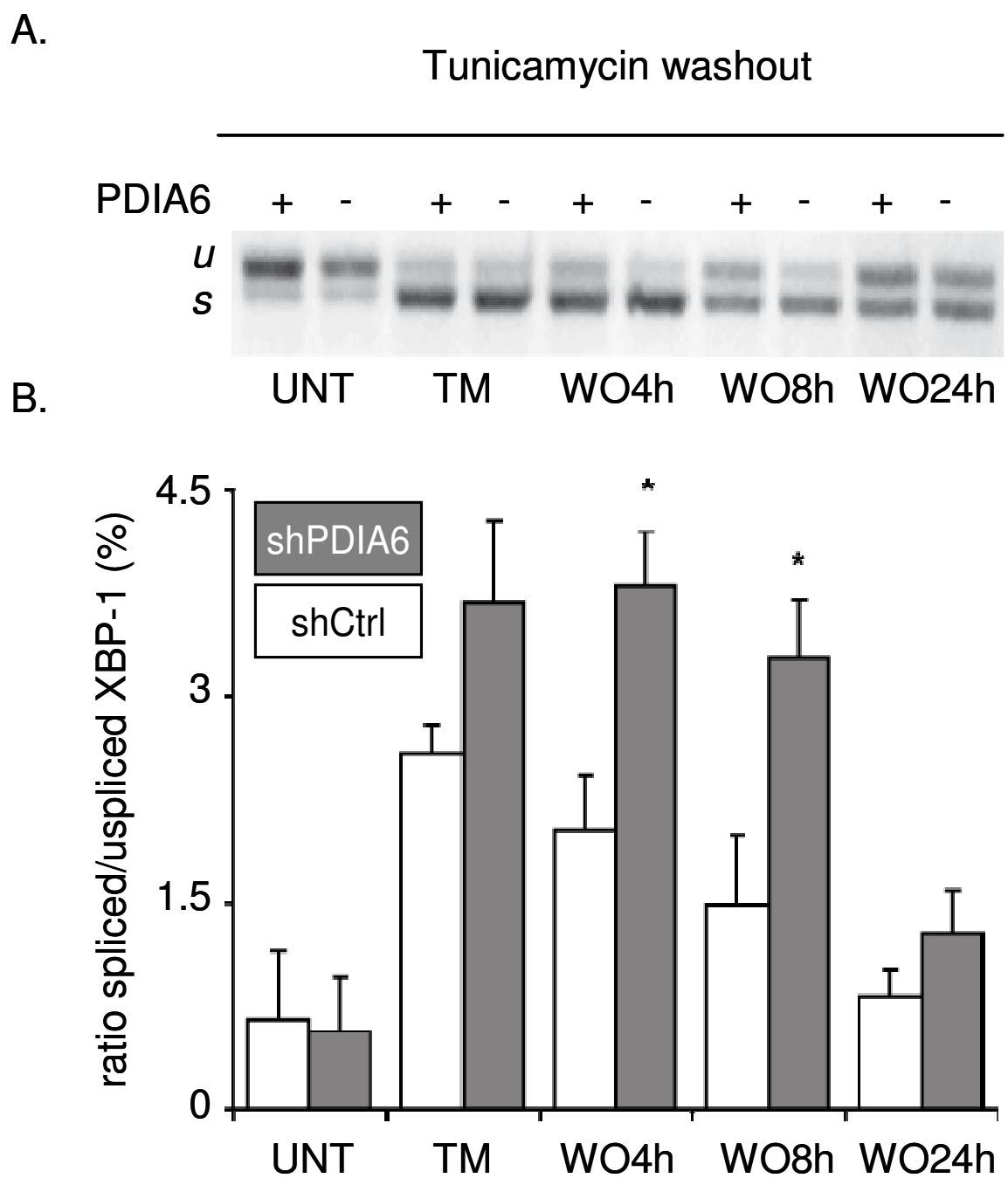

Figure 42: Delayed Inactivation of XBP-1 mRNA Splicing in PDIA6-Deficient NIH-3T3 Cells: (A) XBP-1 mRNA splicing was monitored over time in PDIA6 WT and KD cells treated first with 10 µg/ml Tm and then washed-out for indicated time. (B) Percentage of the ratio spliced/unspliced XBP-1 mRNA splicing was determined after the densitometric analysis by ImageJ (National Institutes of Health). The means ± SD of 3 independent experiments are shown.

Taken together, these results suggest that PDIA6 regulates the amplitude of IRE1a signaling possibly by downregulating its activity.

The other UPR sensor, structurally close to IRE1, is PERK. PERK is a transmembrane kinase that once activated by ER stress, dimerizes through its N-terminal ER luminal domain and promotes PERK trans-autophosphorylation of the C-terminal cytoplasmic kinase domain. This phopshorylated domain phosphorylates the eukaryotic initiation transmembrane factor 2 alpha (eIF2α), which inhibits protein synthesis in the cell, thus relieving the protein load in the ER (Figure 43). Indeed, phosphorylation of eIF2α traps it in an inactive form and thus interferes with the formation of the 43S translation initiation complex [62]; this leads to an overall translational repression and ultimately alleviates protein folding stress by reducing the influx of newly synthesized proteins into the ER.

In addition activated PERK subsequently induces translational upregulation of the transcription factor ATF4. ATF4 is a basic leucine zipper transcriptional activator that belongs to the CREB family of transcription factors. One target of the ATF4 transcription factor is the CHOP promoter, which appears to play a role in the induction of apoptosis during ER stress [63].

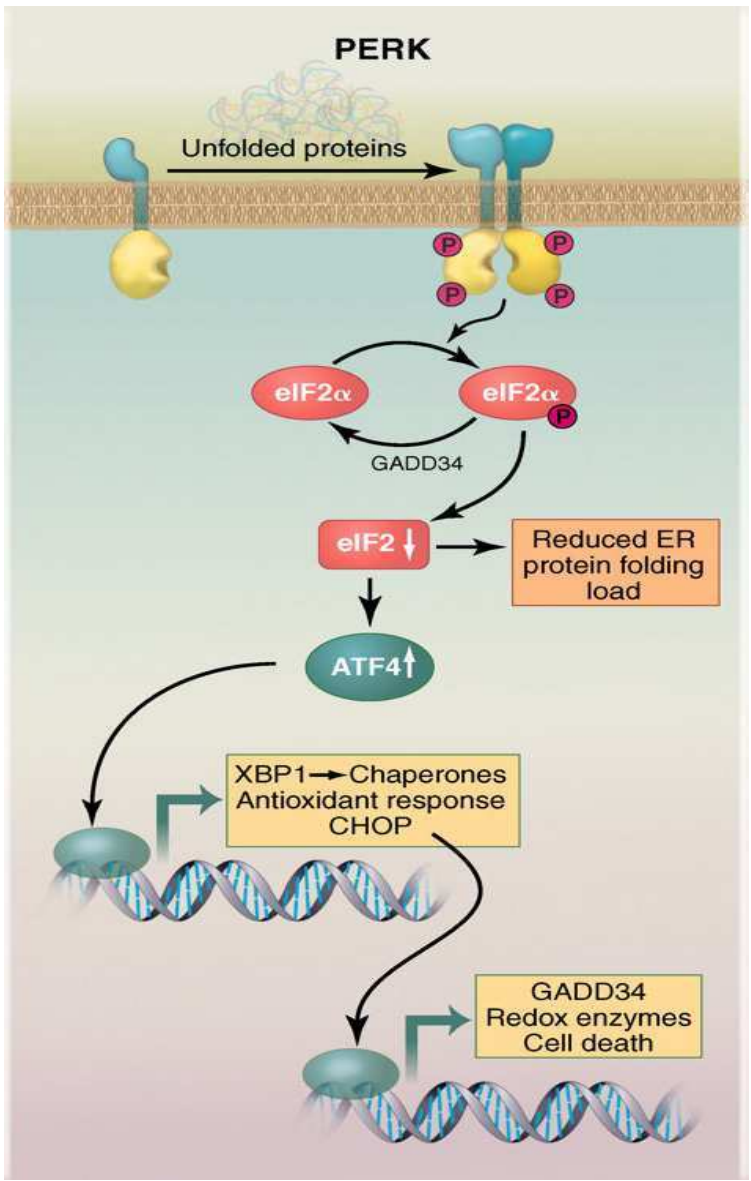

Figure 43: Schematic representation of PERK signaling.

Both IRE1 and PERK contain a remarkably large N-terminal luminal domain (NLD) residing in the ER [64]. Although the primary amino acid sequences of the NLDs show limited homology and have diverged among species, (6% identity/similarity with <12% homology overall), secondary structure shows that they have similar folds and similar mechanism of dimerization. Because of this structural homology, we predicted that PDIA6 could be involved also in the regulation of PERK sensor.

To evaluate the effect of PDIA6 knockdown on towards PERK signaling, we measured the state of phosphorylation of eIF2α over time. PDIA6 WT and KD cells were treated with 2.5 μM

TG for 0, 1, 2 and 4 hours. The peIF2α was analyzed by immunoblot and quantified using total eIF2α as loading control (Figure 44). PDIA6 KD cells show an augmented and prolonged phosphorylation of eIF2α.

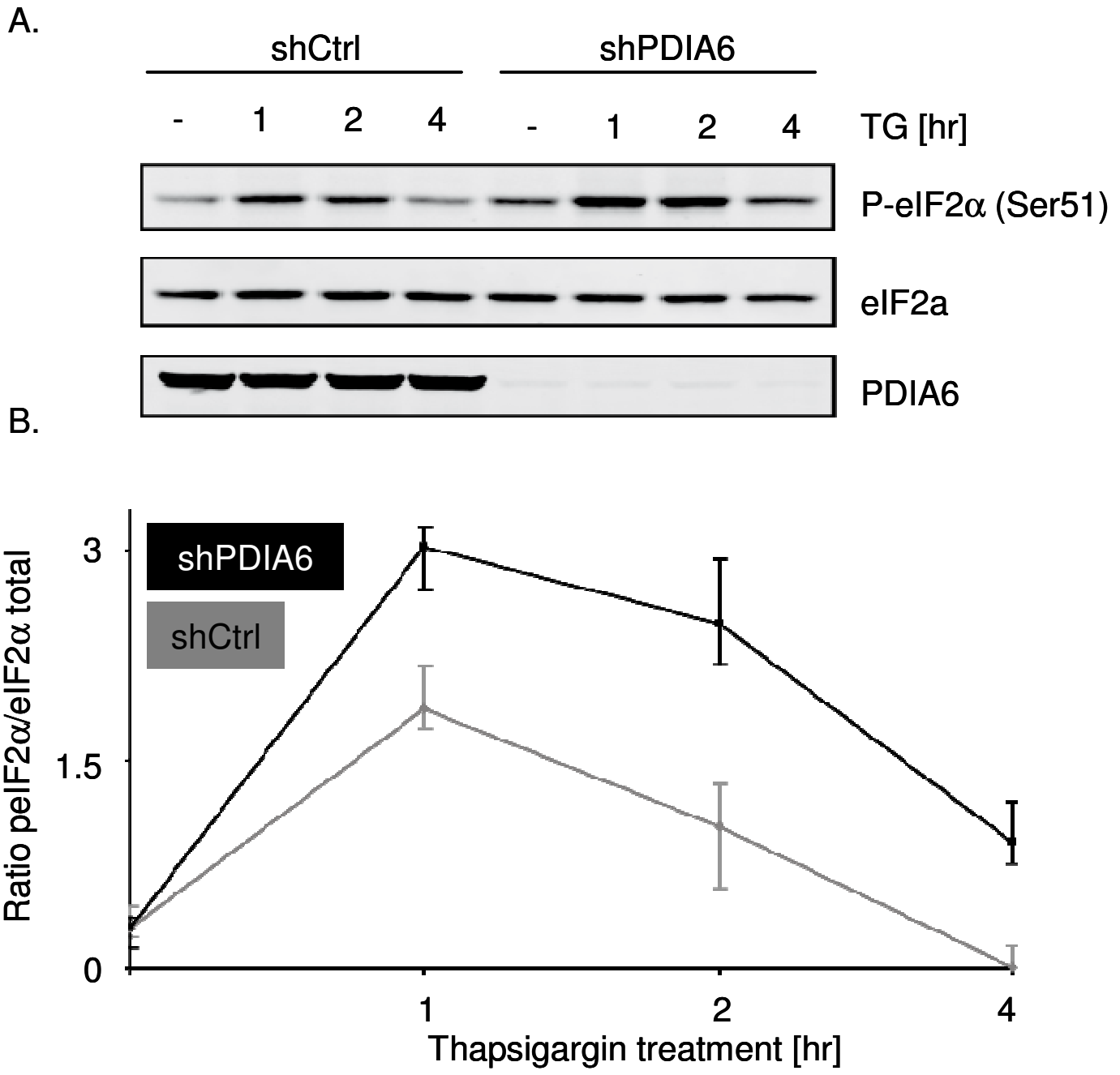

Figure 44: PDIA6 knockdown promotes the eIF2α phosphorylation in NIH-3T3 cells: (A) WT and PDIA6 KD cells were treated with 2.5 μM TG for indicated time. Extracts of cells were subjected to immunoblotting with anti p-eIF2α, total eIF2α and PDIA6 antibodies. (B) the graph shows the ratio of p-eIF2α/total eIF2α quantified by densitometric analysis. The means ± SD of 3 independent experiments are shown.

We have direct data in favor of a stress regulating role of PDIA6: ablation of PDIA6 with shRNA in 3T3 and other cell lines does not induce UPR in of itself, but it does increase the sensitivity to ER stress. In PDIA6-deficient cells, signaling from IRE1 and PERK (XBP-1 splicing and eIF2α phosphorylation) is increased in response to chemical stressors.

6.4 PDIA6-BiP: The Nature of a Protein Complex

Given that PDIA6 has a role in controlling the decay of the UPR signaling, I investigated the mode of action of PDIA6. To answer this question, I explored the nature of the interaction between PDIA6 and BiP, because BiP is an essential component of the UPR.

In the previous experiments we found BiP trapped in complex with mutants PDIA6 that are missing the resolving cysteine of its C-terminal active site. In particular we saw that the double (C38A; C173A)-trapping mutant GFP-tagged human PDIA6 bound BiP stronger than the single trapping mutants or wild-type PDIA6 (Figure 30). These results led us to consider the thioredoxin-like domains of PDIA6 involved in the binding with BiP.

To confirm our hypothesis, we evaluated whether free-cysteines BiP mutant could still bind to PDIA6. Therefore, cysteine was replaced by serine, singly and in combination, in GFP-tagged BiP (Figure 45).

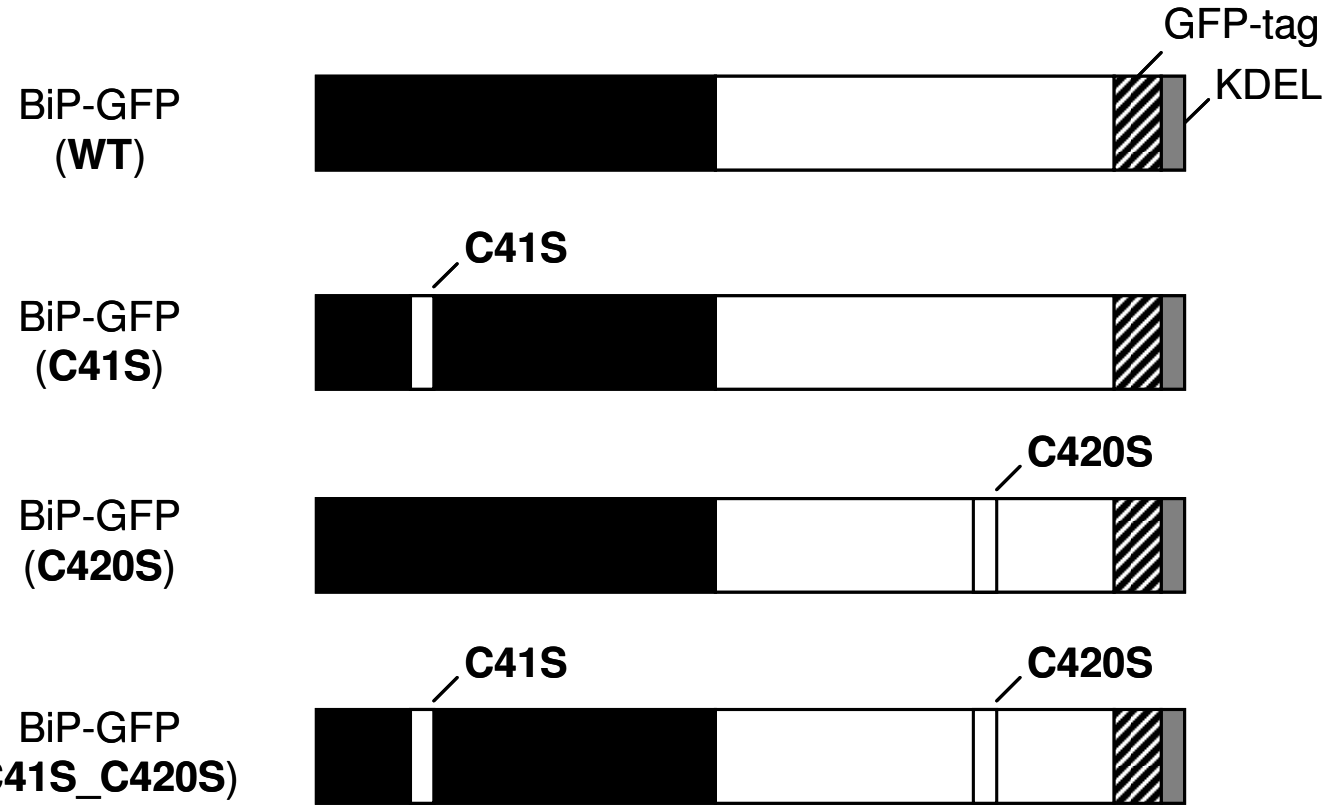

Figure 45: Schematic representation of the GFP-tagged WT and BiP mutants.

We expressed wild-type-, single (C41S)-, (C420S)- and double (C41S; C420S)-trapping mutant GFP-tagged hamster BiP proteins by transient transfection of HEK-293T cells. After 48 hr of transfection, cells were treated with N-Ethylmaleimide (NEM), which is an alkylating reagent that reacts with sulfhydryls to form stable thioether bonds. So, quenching free thiols, it helps to stabilize the disulphide bonds and in our experiment to detect better proteins interacting through cysteines. Protein complexes were immunopurified by the GFP tag through GFP-conjugated beads. The immunoisolate was separated on SDS-PAGE and detected by anti BiP and PDIA6 antibodies (Figure 46).

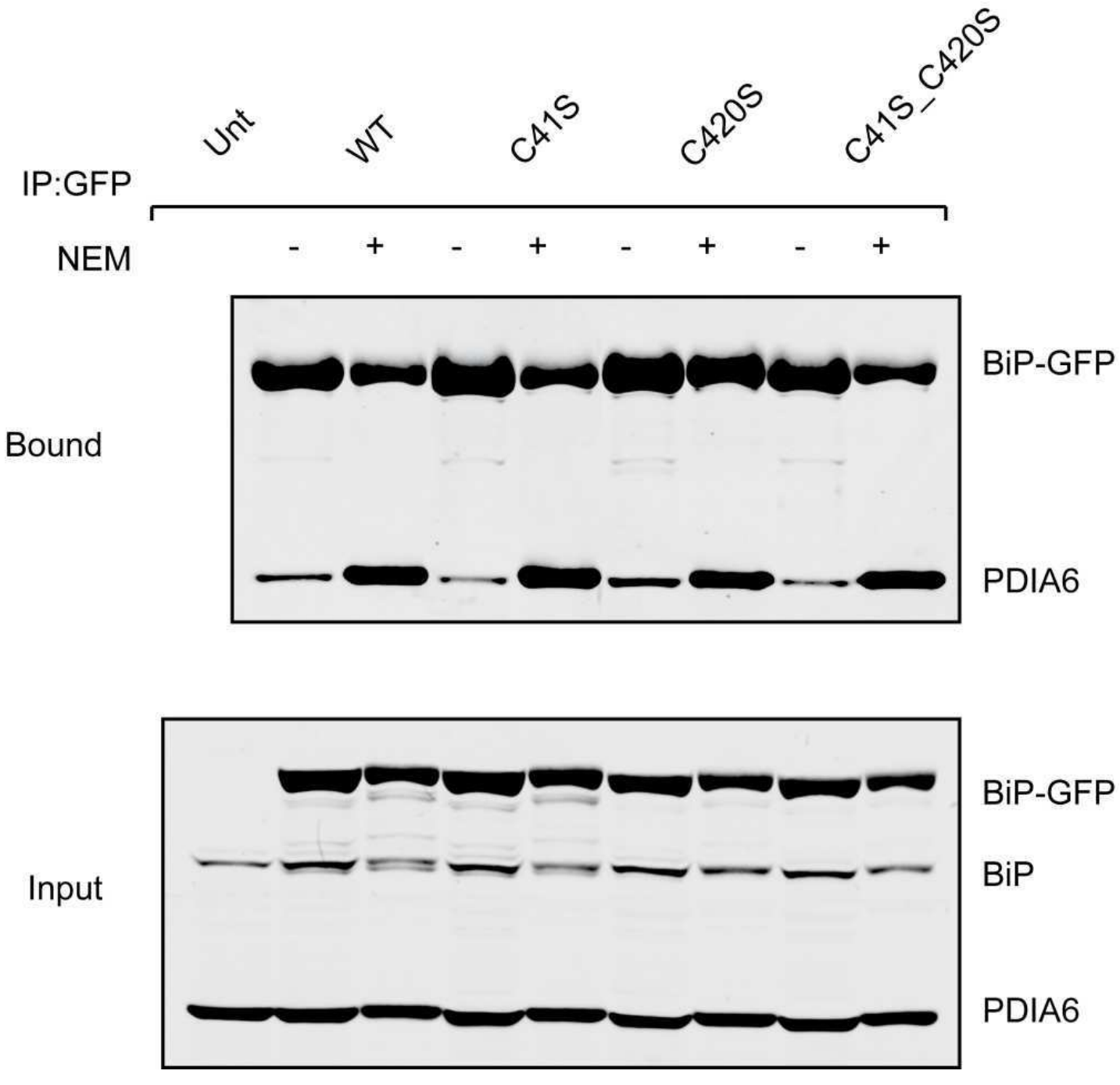

Figure 46: Cysteine-Mutant of BiP Engages endogenous PDIA6 in Mammalian Cells: Immunoblots of GFP-tagged proteins immunopurified with the GFP-conjugated beads from lysates of HEK-293T cells that were untransfected or transfected with expression plasmids of the indicated proteins.

Immunoblot showed that PDIA6 has been co-purified with each of BiP mutant proteins. Even the free-cysteine BiP protein was still able to associate with endogenous PDIA6. Moreover, the interaction between PDIA6 and BiP was significantly increased after NEM treatment. According to these results, the interaction

did not seem to occur via mixed-disulphide bonds, but it was stabilized by an alkylating agent suggesting that the redox state could favour the interaction with BiP.

We were unable to come to a firm conclusion in regard to the nature of the interaction and NEM results. Therefore we hypothesized the presence of a third partner between BiP and PDIA6. Such third protein would bind to BiP through peptide-binding domain and to PDIA6 through a mixed disulphide bonds and it would explain why NEM treatment increased the amount of PDIA6 co-purified with BiP. Thus, we converted in PDIA6 all four cysteine residues from the two thioredoxin-like domains into alanine residues, getting the free-cysteine PDIA6 mutant (that we called *tetra-mutant*), V5 tagged (Figure 47).

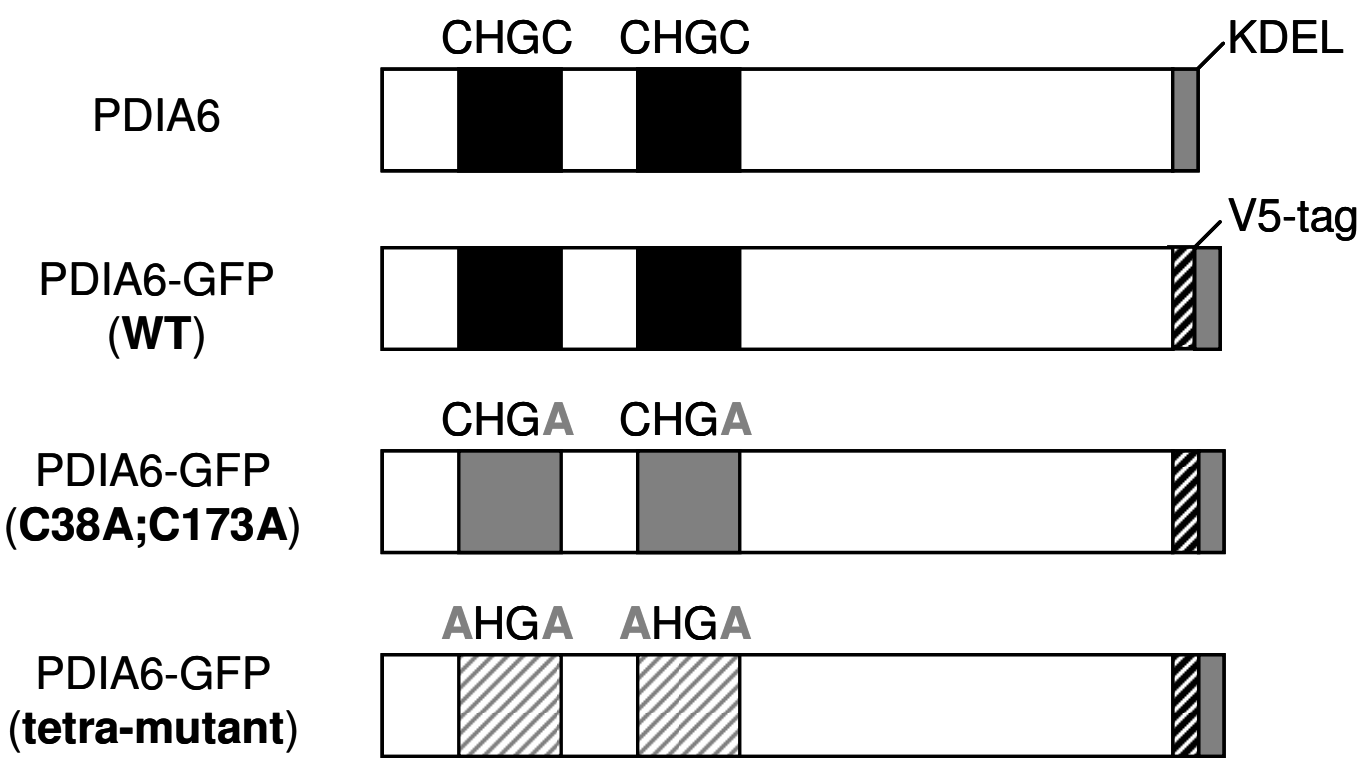

Figure 47: Schematic representation of the V5-tagged Wild-Type (WT), Double- (C38A;C173A) and Tetra-Mutant PDIA6.

According to our hypothesis, the *tetra-mutant* should have not been able to bind the third partner and therefore to be co-purified with BiP the third partner and therefore to be co-purified with BiP. Therefore, we co-transfected HEK-293T cells with GFP-tagged wild-type BiP V5-tagged and alternatively with wild-type, double- and tetra- PDIA6 mutants. Then, the cell lysates were immunoisolated using GFP-conjugated beads and the purified fractions were detected by western blot with anti BiP, PDIA6 and 14.4.4 (loading control) antibodies (Figure 48).

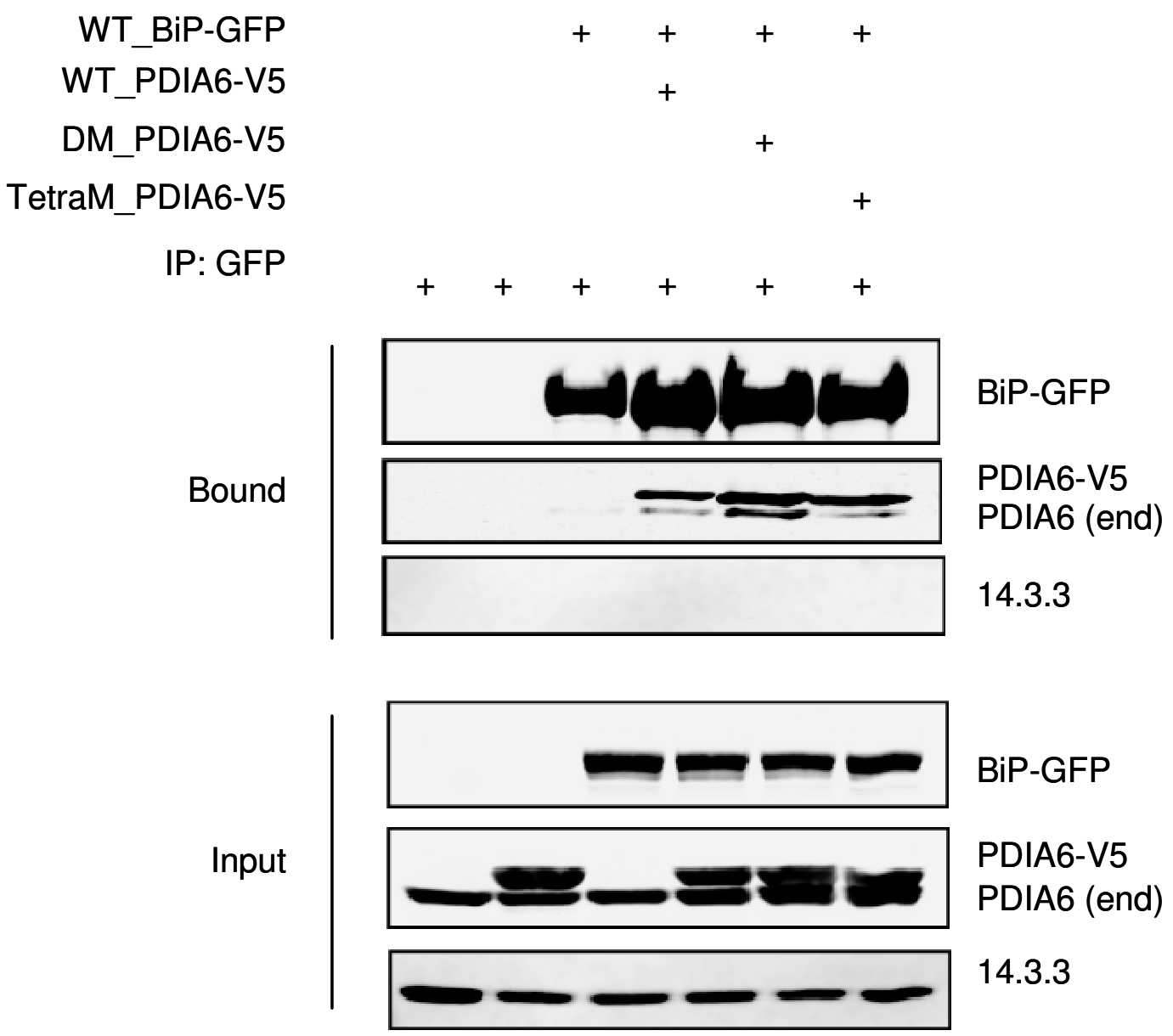

Figure 48: Free-cysteine mutant of PDIA6 still engages exogenous BiP in Mammalian Cells: Immunoblots of GFP-tagged proteins immunopurified with the GFP-conjugated beads

from lysates of HEK-293T cells that were untransfected or transfected with expression plasmids of the indicated proteins.

As seen before, we confirmed the interaction between PDIA6 and BiP because both proteins, wild-type and double PDIA6 mutants, were co-purified with BiP. Surprisingly, free-cysteine PDIA6 mutant protein also was co-immunoisolated with BiP and the intensity of bands between double- and tetra-mutants was comparable. The persistent interaction between BiP and free-cysteine PDIA6 suggested that the binding between the two proteins did not involve a third partner as we supposed. Why the double-mutant PDIA6 trapped more BiP than wild-type PDIA6 can be explain only hypothesizing that the mutation of cysteines probably blocks PDIA6 in a conformational state that favors its interaction with BiP.

So far, we confirmed that the binding is a not via mixed disulphide bonds and involves peptide-binding domain of BiP and a region of PDIA6 away from cysteines.

6.5 PDIA6 Forms a Protein Complex With IRE1α

We know from literature that BiP interacts directly with IRE1 and BiP binding to IRE1 serves to desensitize IRE1 to low levels of stress and promotes its deactivation when favourable folding conditions are restored to the ER [43].

Since we found that PDIA6 knockdown in fibroblast cells produced a delayed inactivation of IRE1, we hypothesized that PDIA6 could act modulating deactivation dynamics of IRE1.

Therefore we searched for a physical interaction between PDIA6 and IRE1. Human wild-type and double- (C38A;C173A) mutant PDIA6 proteins were transiently co-expressed with human IRE1α in human cell line, HEK-293T. As PDIA6 proteins were V5-tagged, we performed a co-immunoprecipitation experiment using V5-conjugated beads and we analyzed the immunoisolate by western blot (Figure 49).

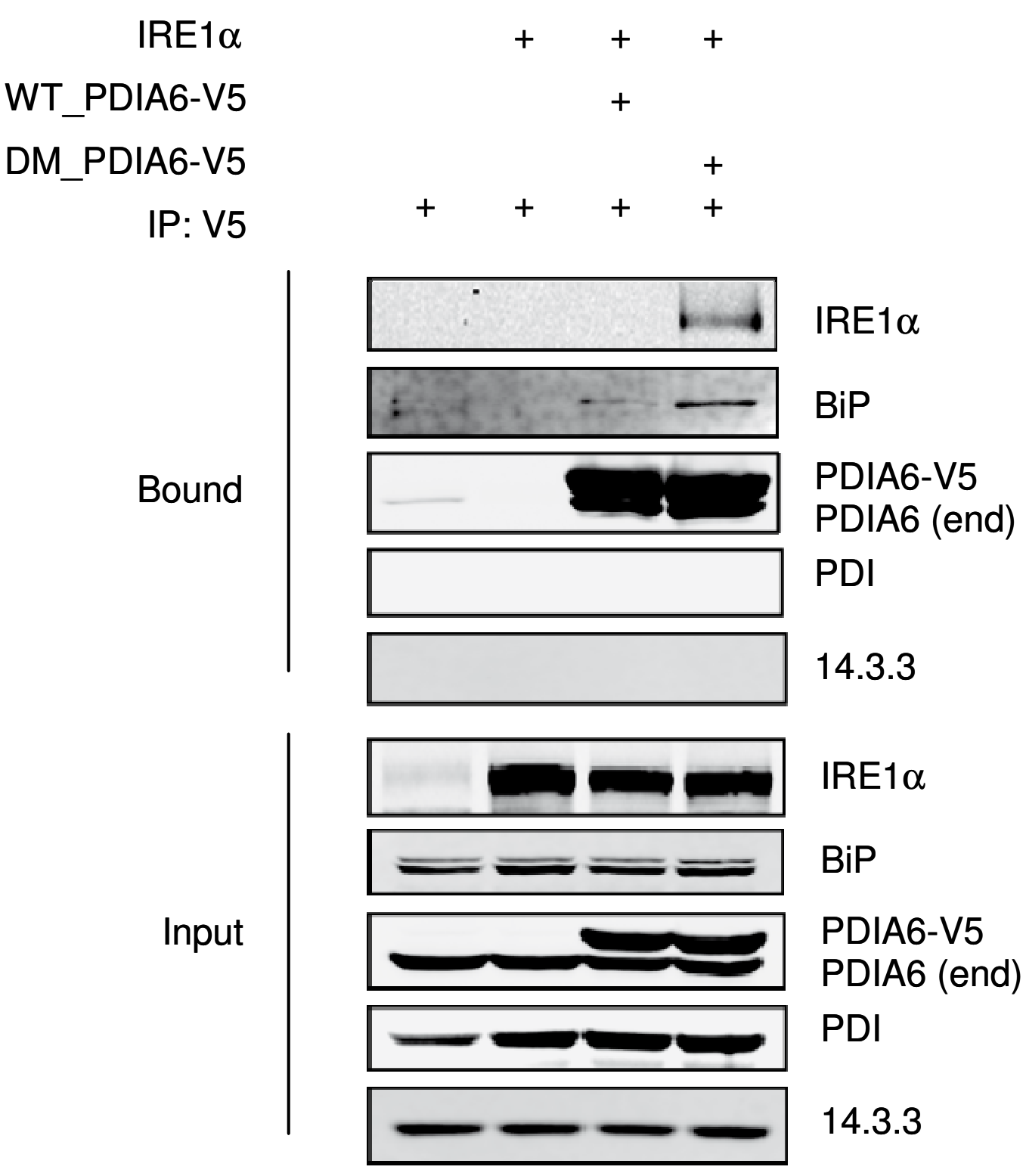

Figure 49: PDIA6 engages exogenous IRE1α in mammalian cells: Immunoblots of V5-tagged proteins immunopurified with the V5-conjugated beads from lysates of HEK-293T cells that were untransfected or transfected with expression plasmids of the indicated proteins. Bound is for co-eluted protein fractions and Input is 5% of total lysate.

The results showed an association between IRE1α and the double-mutant PDIA6 protein. Even increasing the exposition times of the immunoblot, it seems that IRE1α was not co-purified with wild-type PDIA6, probably because of detection limit. In addition, we confirmed the binding between PDIA6 and BiP (as positive control) and the specificity of the interaction because PDI (known as PDIA1) and 14.3.3 did not co-eluted with PDIA6 (as negative controls).

According to these results, the two thioredoxin-like domains could have a role in the interaction with IRE1α and to confirm the results we thought to use the free-cysteine PDIA6 mutant. Therefore, we co-transfected transiently HEK-293T cells with human IRE1α and respectively with human V5-tagged wild-type (WT), double- (CGHA; CGHA, known also as DM) and tetra- (AHGA;AHGA, known also as 4-M) PDIA6 mutants and ER-GFP (as negative control). After 48 hr of transfection, the lysates were analyzed by immunoblot and detected by anti-PDIA6, IRE1, BiP and 14.3.3 antibodies (Figure 50).

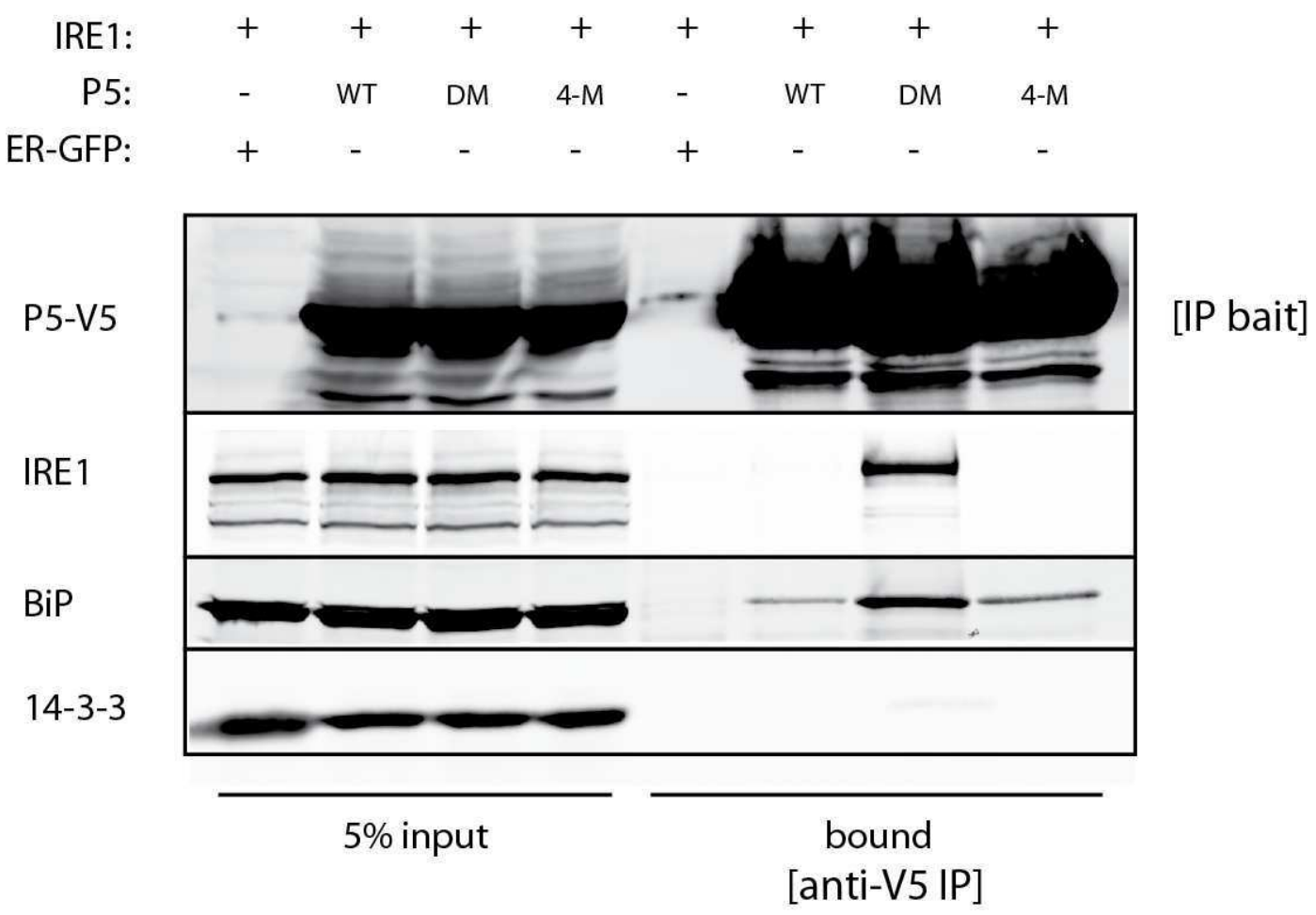

Figure 50: *Thioredoxin-like domains of PDIA6 are essential for the interaction with IRE1α in Mammalian Cells: Immunoblots of V5-tagged proteins immunopurified with the V5-conjugated beads from lysates of HEK-293T cells that were transfected with expression plasmids of the indicated proteins. Bound is for co-eluted protein fractions and Input is 5% of total lysate.*

To overcome the detection limits observed in the previous experiment (Figure 49), we used more transfected cells than before. Although we had more starting material, the immunoblot reported in Figure 50 seems to confirm the same result: IRE1 interacts with double-mutant PDIA6 and does not with wild-type and tetra-mutant PDIA6. But surprisingly, when we overexposed the same immunoblot membrane, we were able to see a faint signal coming from IRE1α co-purified with wild-type PDIA6 and no signal from free-cysteines PDIA6 mutant (4-M or

tetra-mutant) (Figure 51). In addition, we detected endogenous BiP and 14.3.3 that we used respectively as positive and negative controls. And from the cells co-transfected with IRE1α and ER-GFP, we did get any protein eluted with PDIA6, proving that any kind of interaction is real and specific.

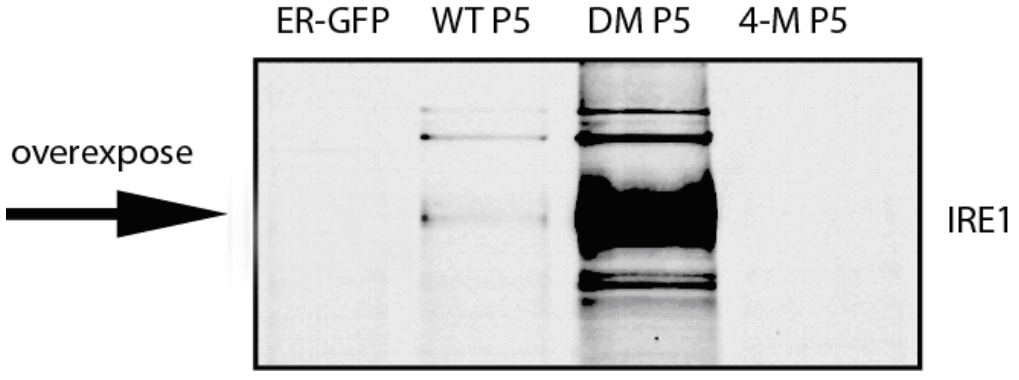

Figure 51: over-exposition of a zoomed immunoblot reported in Figure 26.

Therefore we proved that PDIA6 interacts physically with IRE1α and the association occurs through the two thioredoxin-like domains.

According to the results, they should associate in a high-molecular-disulfide-bonded complex in non-reducing conditions. Thus, the same samples from the previous experiment have been analyzed by a non-reducing gel (Figure 52) and detected by dual-color immunoblot with a mouse antibody against V5 (red) (Figure 52A) and a rabbit antibody against IRE1 (green) (Figure 52B). The sizes of molecular weight markers (MW), which are visible in red channel using the LI-COR Odyssey scanner, are indicated in kDa.

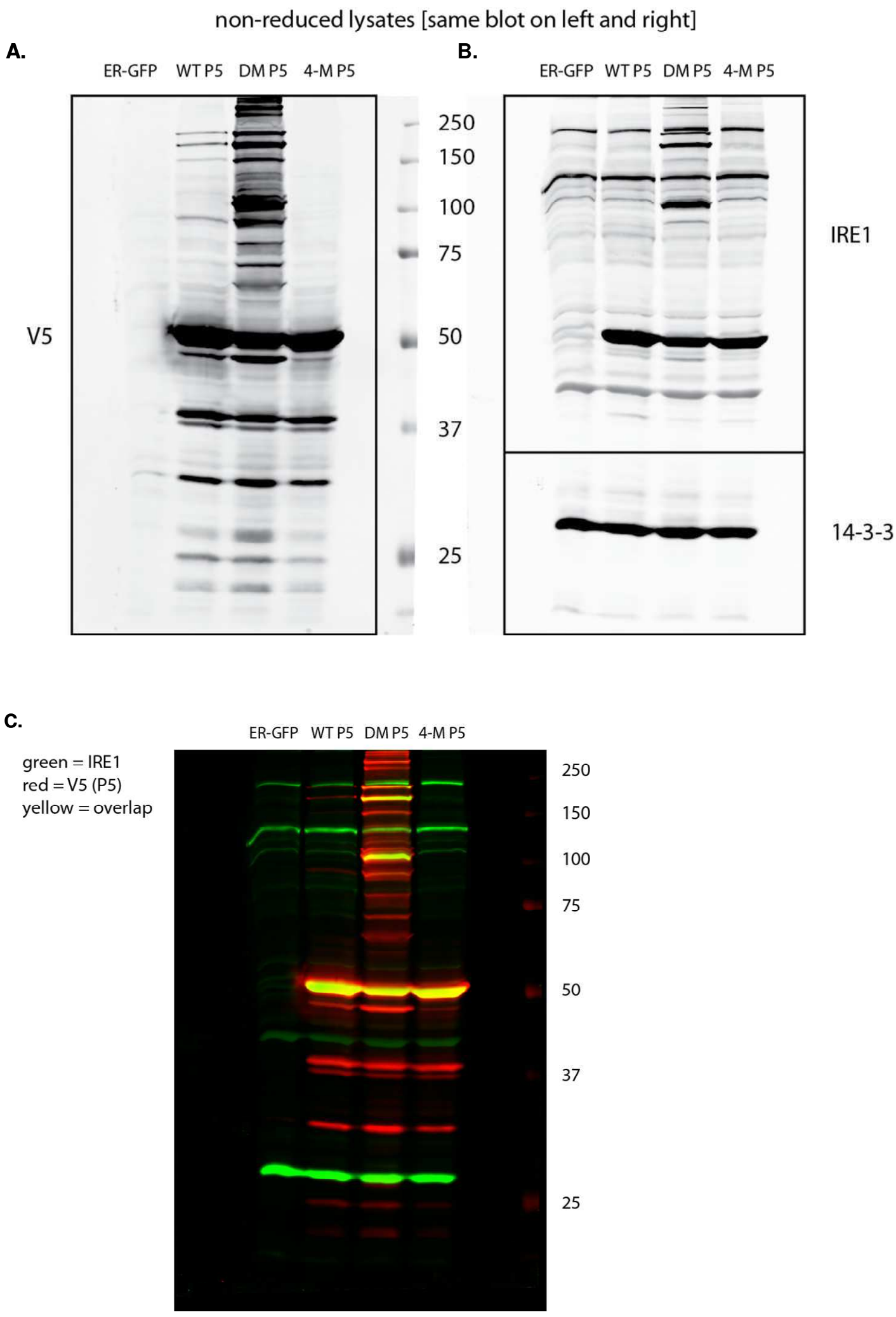

Figure 52: PDIA6:IREα association form a mixed-disulphide complex : immunoblots of lysates analyzed in Figure 25 in non-reducing conditions. PDIA6 has been detected by anti-V5

antibody (red channel)(a) and IRE1α by antiIRE1 antibody (green channel) (b). The overlapping of the two channels is illustrated in c.

By overlapping the two channels we found only in the DM PDIA6 mutant lane a co-localization of the two antibodies represented by yellow bands whose molecular weight should correspond to the sum of the two proteins (Figure 52C).

CONCLUSIONS

-CHAPTER 7-

7.1 Conclusions

The Unfolded Protein Response (UPR) is a homeostatic response to any of the numerous stress conditions that impact the function of the endoplasmic reticulum (ER). The purpose of the UPR is to cope with stress by increasing the folding capacity of chaperones and enzymes in the ER lumen, targeting misfolded proteins to disposal via ER-associated degradation and decreasing the influx of newly synthesized proteins into the ER. If the stress can be mitigated, homeostasis is restored, but if not - the outcome of the UPR is activation of cell-death pathways [65].

Because the outcome of UPR signaling determines cell fate, a key unresolved molecular question is how UPR signaling is attenuated. Indeed, it is often under-appreciated that UPR signaling in response to stress is transient and is attenuated. Pincus et al. showed recently that yeast UPR matches its output to the magnitude of the stress by regulating the duration of IRE1 signaling [43]. BiP binding to IRE1 serves to desensitize IRE1 and facilitates de-oligomerization and deactivation. Since the signaling is transient the duration of signaling is supposed to be a key regulatory aspect of this stress response. Yet, little is known about the decay of IRE1 and PERK signaling and to the best of our knowledge the only available data shows that interactions with cytosolic factors attenuate the activity of UPR transducers xx. Such interactions, of course do not explain how the signaling responds to altered conditions within the lumen of the ER. Research of this question largely focuses on the binding of BiP to IRE1 and PERK, that has been mapped to a 50 amino

acid region of the luminal domain of IRE1 [44] and whose function, at least in yeast, is to sequester inactive IRE1 molecules [43]. In this PhD work we found that there is another luminal ER factor, which interacts with IRE1 and PERK and is involved in attenuation of their activities. This factor is PDIA6 (also known as P5), a poorly understood member of the protein disulfide isomerase (PDI) family. We found that PDIA6 absence confers hypersensitivity to ER stress because one of its main *action is tied to the sensing of UPR, rather than to the consequences of UPR signaling*. We hypothesize that PDIA6 uses its protein disulfide isomerase activity to interact specifically with IRE1 and PERK in the ER lumen and attenuate their activities, thus regulating the duration of ER stress signaling (see model in Figure 53). We propose that this activity is complementary to BiP action, targeting the active population of the UPR transducers We have direct data in favor of a stress regulating role of PDIA6: ablation of PDIA6 with shRNA in 3T3 and other cell lines does not induce UPR in of itself, but it does increase the sensitivity to ER stress. In PDIA6-deficient cells (knockdown, "KD"), signaling from IRE1 and PERK (XBP-1 splicing and eIF2α phosphorylation) is increased in response to chemical stressors. This increase is due to direct cysteine-dependent interaction of PDIA6 with at least IRE1, affecting not the onset of signaling but its duration and integrated strength. Take together, all data suggest that PDIA6 binds to the activated, phosphorylated forms of IRE1 and PERK and shifts the equilibrium from the oligomeric to the monomeric state. Thus, we hypothesize that PDIA6 is a prototype of physiological ER stress down-regulators.

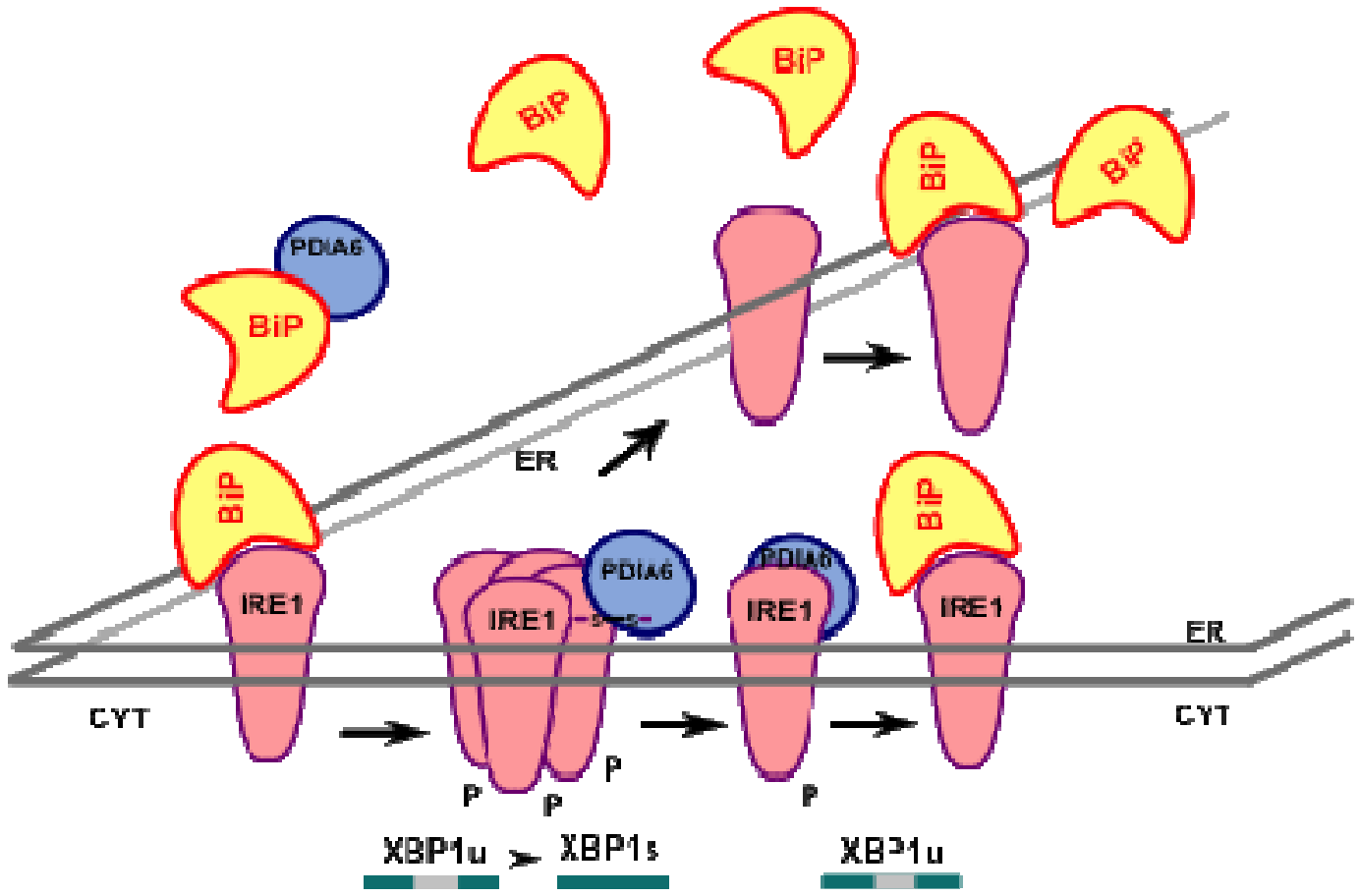

Figure 53: Hypothetical model for the role of PDIA6 in attenuating the IRE1 signaling.

EXPERIMENTAL SECTION

-CHAPTER 8-

8.1 Materials

Tunicamycin and thapsigargin were purchased from Sigma Chemicals (St. Louis, MO). Lipofectamine 2000 transfection reagent was from Invitrogen (Carlsbad, CA). Puromycin and G418 were from InvivoGen (San Diego, CA); DMEM was from Mediatech, Inc. (Manassess, VA), fetal bovine serum was from Gemini (West Sacramento, CA). Glutamine, penicillin/streptomycin supplement was from Gibco-Invitrogen (Grand Island, NY. A GFP-tagged and V5-tagged PDIA6 expressed into the N1 Vector (Clontech, Mountain View, CA) and GFP-tagged BiP expressed into N1 Vector were subjected to site-directed mutagenesis using the QuickChange Kit (Agilent, Santa Clara, CA) to generate the single (C38A or C173A) or double-mutant (C38A;C173A) PDIA6 or T19G BiP mutant, which is ATPase deficient mutant.

8.2 Cell culture

C2C12, 10T1/2, NIH-3T3, 293T, and HeLa cells were from the ATCC. These cell lines were grown in DMEM in the presence of 10% FBS and Gln/Pen/Strept, and, when needed, the proper eukaryotic selection agent (puromycin or G418).

8.3 Immunoprecipitation

Cells were lysed with NP-40 as in Melnick et al. [18]. Detergent lysates representing known cell equivalents were incubated with anti-GFP (ChromoTek), anti-V5 (Sigma) or anti-IRE1. The immune complexes were isolated using protein A-Sepharose for anti-IRE1. The beads were washed and eluted with Sample Buffer 2X. The eluted material was separated using 10% SDS-PAGE.

8.4 Immunoblotting

Images were recorded using an Alpha Innotech (Santa Clara, CA) or Odyssey (Li-Cor, Lincoln, NE) imagers. Antibodies: rabbit anti-14-3-3 (C16) was purchased from Santa Cruz, Biotechnology, Santa Cruz, CA. MAb anti-KDEL was from StressGen (Vancouver, BC); rabbit anti-BiP was from Cell Signaling; rabbit anti-PDIA6 polyclonal antibody (ab11432) and rabbit anti-IRE1 polyclonal antibody (ab37073) were purchased from Abcam (Cambridge, UK). The monoclonal anti-V5 antibody was obtained from Invitrogen Corporation (Carlsbad, CA); mouse anti-PDI Monoclonal Antibody (RL90) was from Thermo Fisher Scientific Inc. (Rockford, IL). Secondary antibodies conjugated to HRP were from Jackson ImmunoResearch Laboratories (West Grove, PA), secondary antibodies conjugated to near-infrared fluorophores were from Li-Cor.

8.5 RNAi silencing

GRP94, BiP, PDIA6 were knocked-down, using the following shRNAs from Sigma Life Science (Saint Louis, MO): SHCLNG-NM_011631, SHCLNG-NM_022310, SHCLNG-NM_027959, respectively. For plasmid-based RNAi, the cells were transfected using Lipofectamine 2000 according to the manufacturer's guidelines. After 48 h they were selected with 2 μg/ml puromycin and maintained under selection. For viral-based RNAi, the cells were cultured in 6-well plates and transduced with lentiviral particles encoding the same shRNA sequences, packaged using the VeraPower kit (Invitrogen)..

8.6 Statistical Analysis

Statistical analysis was performed using a one-way analysis of variance followed by Student's Newman-Keul's post hoc analysis of variance (*, $p < 0.05$, unless otherwise stated in the figure legends).

8.7 Analysis of XBP1 mRNA splicing

XBP1 and β-actin were PCR amplified from total RNA as in [66].

Bibliography

[28] Alberts B, Johnson A, Lewis J, et al. Molecular Biology of the Cell. 4th edition. New York: Garland Science; 2002.

[29] Gething, M.-J. and Sambrook, J. (1992) Nature 355, 33-45

[30] Kaufman, R.J., 1999. Stress signaling from the lumen of the endoplasmic reticulum: coordination of gene transcriptional and translational controls. Genes Dev. 13, 1211–1233.

[31] Prostko, C.R., Brostrom, M.A., Brostrom, C.O., 1993. Reversible phosphorylation of eukaryotic initiation factor 2 alpha in response to endoplasmic reticular signaling. Mol. Cell. Biochem. 127–128, 255–265.

[32] Hampton, R.Y., 2000. ER stress response: getting the UPR hand on misfolded proteins. Curr. Biol. 10, R518–R521.

[33] Xu, C., Bailly-Maitre, B., Reed, J.C., 2005. Endoplasmic reticulum stress: cell life and death decisions. J. Clin. Invest. 115, 2656–2664.

[34] Szegezdi, E., Logue, S.E., Gorman, A.M., Samali, A., 2006. Mediators of endoplasmic reticulum stress-induced apoptosis. EMBO Rep. 7, 880–885.

[35] Ron D, Walter P. Signal integration in the endoplasmic reticulum unfolded protein response. Nat Rev Mol Cell Biol. 2007 Jul;8(7):519-29.

[36] Cox, J. S. & Walter, P. A novel mechanism for regulating activity of a transcription factor that controls the unfolded protein response. Cell 87, 391–404 (1996).

[37] Mori, K., Kawahara, T., Yoshida, H., Yanagi, H. & Yura, T. Signalling from endoplasmic reticulum to nucleus: transcription factor with a basic-leucine zipper motif is required for the unfolded protein-response pathway. Genes Cells 1, 803–817 (1996).

[38] Yoshida, H., Matsui, T., Yamamoto, A., Okada, T. & Mori, K. XBP1 mRNA is induced by ATF6 and spliced by IRE1 in response to ER stress to produce a highly active transcription factor. Cell 107, 881–891 (2001).

[39] Calfon, M. et al. IRE1 couples endoplasmic reticulum load to secretory capacity by processing the XBP-1 mRNA. Nature 415, 92–96 (2002).

[40] Haze, K., Yoshida, H., Yanagi, H., Yura, T. & Mori, K. Mammalian transcription factor ATF6 is synthesized as a transmembrane protein and activated by proteolysis in response to endoplasmic reticulum stress. Mol. Biol. Cell 10, 3787–3799 (1999).

[41] Harding, H., Zhang, Y. & Ron, D. Translation and protein folding are coupled by an endoplasmic reticulum resident kinase. Nature 397, 271–274 (1999).

[42] Harding, H. et al. An integrated stress response regulates amino acid metabolism and resistance to oxidative stress. Mol. Cell 11, 619–633 (2003).

[43] Pincus D, Chevalier MW, Aragón T, van Anken E, Vidal SE, El-Samad H, Walter P. BiP binding to the ER-stress sensor Ire1 tunes the homeostatic behavior of the unfolded protein response. PLoS Biol. 2010 Jul 6;8(7):e1000415.

[44] Kimata Y, Ishiwata-Kimata Y, Ito T, Hirata A, Suzuki T, et al. (2007) Two regulatory steps of ER-stress sensor Ire1 involving its cluster formation and interaction with unfolded proteins. J Cell Biol 179: 75–86.

[45] Melnick J, Dul JL, Argon Y. Sequential interaction of the chaperones BiP and GRP94 with immunoglobulin chains in the endoplasmic reticulum. Nature. 1994 Aug 4;370(6488):373-5.

[46] Ostrovsky O, Ahmed NT, Argon Y. The chaperone activity of GRP94 towards of insulin-like growth factor II is necessary for the stress response to serum deprivation. Mol Biol Cell 2009;20:1855–64.

[47] Eletto D, Dersh D, Argon Y. GRP94 in ER quality control and stress responses. Semin Cell Dev Biol. 2010 Jul;21(5):479-85. Epub 2010 Mar 16. Review.

[48] Meunier L, Usherwood YK, Chung KT, Hendershot LM. A subset of chaperones and folding enzymes form multiprotein complexes in endoplasmic reticulum to bind nascent proteins. Mol Biol Cell 2002;13:4456–69.

[49] Kapulkin V, Hiester BG, Link CD. Compensatory regulation among ER chaperones in C. elegans. FEBS Lett 2005;579:3063–8.

[50] Ferrari DM, Söling HD (1999) The protein disulphide-isomerase family: unraveling a string of folds. Biochem J 339: 1–10.

[51] Schwaller M, Wilkinson B, Gilbert HF (2003) Reduction–reoxidation cycles contribute to catalysis of disulfide isomerisation by protein-disulfide isomerase. J Biol Chem 278: 7154–7159.

[52] Koivu, J., Myllyla, R., Helaakoski, T., Pihlajaniemi, T., Tasanen, K. and Kivirikko, K. I. (1987). A single polypeptide acts both as the beta subunit of prolyl 4-hydroxylase and as a protein disulfide-isomerase. J. Biol. Chem. 262, 6447-6449.

[53] Wetterau, J. R., Combs, K. A., McLean, L. R., Spinner, S. N. and Aggerbeck, L. P. (1991). Protein disulfide isomerase

appears necessary to maintain the catalytically active structure of the microsomal triglyceride transfer protein. Biochemistry 30, 9728- 9735.

[54] Jessop CE, Watkins RH, Simmons JJ, Tasab M, Bulleid NJ. Protein disulphide isomerase family members show distinct substrate specificity: P5 is targeted to BiP client proteins. J Cell Sci. 2009 Dec 1;122(Pt 23):4287-95. Epub 2009 Nov 3.

[55] Kikuchi M, Doi E, Tsujimoto I, Horibe T, Tsujimoto Y. Functional analysis of human P5, a protein disulfide isomerase homologue. J Biochem. 2002 Sep;132(3):451-5.

[56] Zito E, Melo EP, Yang Y, Wahlander Å, Neubert TA, Ron D. Oxidative protein folding by an endoplasmic reticulum-localized peroxiredoxin. Mol Cell. 2010 Dec 10;40(5):787-97.

[57] Hendershot L, Wei J, Gaut J, Melnick J, Aviel S, Argon Y. Inhibition of immunoglobulin folding and secretion by dominant negative BiP ATPase mutants. Proc Natl Acad Sci U S A. 1996 May 28;93(11):5269-74.

[58] Kaufman, R.J., 2002. Orchestrating the unfolded protein response in health and disease. J. Clin. Invest. 110, 1389–1398.

[59] Ron D, Walter P. Signal integration in the endoplasmic reticulum unfolded protein response. Nat Rev Mol Cell Biol. 2007 Jul;8(7):519-29.

[60] Lin JH, Li H, Zhang Y, Ron D, Walter P., Divergent effects of PERK and IRE1 signaling on cell viability. PLoS One. 2009;4(1):e4170. Epub 2009 Jan 12.

[61] Lin, J.H., Li, H., Yasumura, D., Cohen, H.R., Zhang, C., Panning, B., Shokat, K.M., Lavail, M.M., and Walter, P. (2007). IRE1 signaling affects cell fate during the unfolded protein response. Science 318, 944–949.

[62] Algire MA, Maag D, Savio P, Acker MG, Tarun SZ Jr, Sachs AB, Asano K, Nielsen KH, Olsen DS, Phan L, Hinnebusch AG, Lorsch JR. Development and characterization of a reconstituted yeast translation initiation system. RNA. 2002 Mar;8(3):382-97.

[63] Ma Y, Hendershot LM. Delineation of a negative feedback regulatory loop that controls protein translation during endoplasmic reticulum stress. J Biol Chem. 2003 Sep 12;278(37):34864-73. Epub 2003 Jul 1.

[64] Liu CY, Xu Z, Kaufman RJ., Structure and intermolecular interactions of the luminal dimerization domain of human IRE1alpha. J Biol Chem. 2003 May 16;278(20):17680-7. Epub 2003 Mar 13.

[65] Walter P, Ron D. The unfolded protein response: from stress pathway to homeostatic regulation. Science. 2011 Nov 25;334(6059):1081-6.

[66] Calfon M, Zeng H, Urano F, Till JH, Hubbard SR, et al. (2002) IRE1 couples endoplasmic reticulum load to secretory capacity by processing the XBP-1 mRNA. Nature 415: 92-96.

Acknowledgements

First and foremost I want to thank my brother **Davide Eletto**. It would not have been possible to write this doctoral thesis without his help and support. I appreciated all his contributions of time, ideas, and life to make my Ph.D. experience productive and stimulating. The joy and enthusiasm he had for his research was contagious and motivational for me, even during tough times in the Ph.D. pursuit. I am also thankful for the excellent example he has provided as a successful man scientist.

I also thank my supervisor Cosimo Pizza for all the hope he has put on me. I would like to acknowledge the members of the Pizza group who have contributed immensely to my personal and professional time at University of Salerno (ITALY). The group has been a source of friendships as well as good advice and collaboration.

I specially thank the Argon Group of the Children's Hospital of Philadelphia – CHOP (USA) for the wonderful experience of being a visiting student. I would like to express my deep and sincere gratitude to my supervisor in that time, Professor Yair Argon, M.D., Ph.D., Professor in the University of Pennsylvania, Chief of Dept. Pathology and Lab Medicine, Division of Cell Pathology, The Children's Hospital of Philadelphia. His wide knowledge and his logical way of thinking have been of great value and helpful for me. His patience, understanding, encouraging and personal guidance have provided a good basis for my research carrier. I will never

forget that time. A special thanks to Jalpa Modi, Devin Dersh, Michal Marzec and all the guys that I met in the CHOP. Moreover, I thank Professor Elisabeth R. Barton, Ph.D, Anatomy and Cell Biology School of Dental Medicine, University of Pennsylvania, for her scientific support and much more.

I thank Professor Rosa Siciliano and Fiorella Mazzeo, National Research Council (CNR) Avellino (ITALY), for their contribution to my Ph.D. work.

I also thank other people I met along the way, I do not need make a list of names. They know who are. We had a great time together.

Thanks also to my parents who always believed in me.
And thank you "Nina"…your presence has been essential for me.

Last but not least, a big thank you to **Emilio**. Without him I would be a very different person today, and it would have been certainly much harder to finish a Ph.D. Thank you for supporting me with your smile and your daily presence even at a distance of many many kilometres.

I finish with a final silence of gratitude for the life.